DEVELOPMENT OF AN EXPERIMENTAL APPARATUS WITH THE CAPABILITY TO TEST SEMI-MONOCOQUE UAS WINGS

By

RANDY PHUC HO

Bachelor of Science in Aerospace Engineering

Bachelor of Science in Mechanical Engineering

Oklahoma State University

Stillwater, Oklahoma

2020

Submitted to the Faculty of the
Graduate College of the
Oklahoma State University
in partial fulfillment of
the requirements for
the Degree of
MASTER OF SCIENCE
May, 2022

DEVELOPMENT OF AN EXPERIMENTAL APPARATUS WITH THE CAPABILITY TO TEST SEMI-MONOCOQUE UAS WINGS

Thesis Approved

Dr. Andy Arena

_____

Thesis Adviser

Dr. Robert Taylor

_____

Dr. Ryan Paul

_____

ACKNOWLEDGEMENTS

I would like to first thank my fiancé, Makayla, and my family for the love and support they provided me throughout the long journey of completing this thesis. Along with them, I would also like to thank my committee Dr. Arena, Dr. Paul, and Dr. Taylor; without their support and advice, this would not have been possible. Finally, I would like to thank my lab for their support and giving of motivation, especially Jeffrey Sandwell for all the late-night engineering talks.

Name: RANDY PHUC HO

Date of Degree: MAY, 2022

Title of Study: DEVELOPMENT OF AN EXPERIMENTAL APPARATUS WITH THE CAPABILITY TO TEST SEMI-MONOCOQUE WINGS

Major Field: MECHANICAL AND AEROSPACE ENGINEERING

Abstract: In many aircraft, manned or unmanned, proof loading and failure tests for the wing structure are required to understand the structural characteristics. These are carried out for required certifications and to check if the aircraft can handle the expected flight loads. Theoretical analysis is not generally sufficient enough in certifying aircraft; therefore, physical tests must be conducted. This research is planned to develop a static testing apparatus capable of testing Group I and Group II unmanned aerial vehicle (UAV) wings up to at least 5 G's and modular for all wing planforms. This apparatus is designed to handle the semi-monocoque composite wings and will use a small-scale whiffletree for simulating the spanwise-lift distribution over the wing. The whiffletree is highly regarded in industry for its ability to best match the shear and bending moment created by lift. Three experiments are conducted after the design and fabrication of the apparatus are completed. Two of these experiments are carried out with the use of an aluminum beam to validate the apparatus's loading characteristics in a repeatable proof loading case and failure case. Along with the theoretical calculations for these two experiments, an overall complete uncertainty analysis was conducted for the entire apparatus. The final experiment conducted is the test of a fiberglass composite wing designed and fabricated at Oklahoma State University. The results of these experiments yield that the apparatus does transfer loads up to an accuracy of ±5% of the theoretical analyses and that the apparatus can be applied to a composite semi-monocoque wing as intended. Some of the interesting discoveries found in this research were the uncertainty found in the whiffletree design and the failure mode of the wing spar. Due to the construction and requirement to be modular, the whiffletree was found to have a 3% uncertainty in transferring loads. While favorable for its intended purpose at Oklahoma State University, it may require more research to be conducted for more precision in transferring loads for other research. Finally, the failure mode of the wing used in experiment three was found to be a shear failure; however, due to debonding of epoxy on the shear web and skin, it is not possible to decisively say whether the wing failure in normal shear or transverse shear. This experiment also sparks future work and research to be done in studying shear failure in these composite wings.

TABLE OF CONTENTS

Chapter Page

Chapter Page

LIST OF TABLES

Table Page

LIST OF FIGURES

Figure Page

Figure Page

Figure Page

Figure Page

CHAPTER I

INTRODUCTION

Motivation

In the composite aerospace assembly research lab at Oklahoma State University (OSU), composite UAV airframes are being designed, fabricated, integrated, and prototyped every day. This lab is used for graduate and undergraduate students and generally creates a range of UAVs from 2 lbs. to 55 lbs. However, there have been cases where the lab has designed and fabricated aircraft over 55 lbs. such as a one-eighth scale of the Cessna Citation Longitude. This can be viewed below in Figure 1.

Figure 1: OSU Cessna Citation Longitude

Currently, graduate students generally work on research and development projects while undergraduates work on their senior design vehicles to compete in SpeedFest. A few examples of

previous research and development projects conducted at the composite assembly lab are the low acoustic signature reconnaissance UAV, Noctua, the long-endurance UAV, Dragonfly [1], and the short takeoff and landing UAV, Locust. These UAVs were all under 55 lbs. and were designed, fabricated, and prototyped at OSU. These UAVs can be viewed below in Figure 2, Figure 3, and Figure 4.

Figure 2: Low Acoustic Signature UAV Noctua

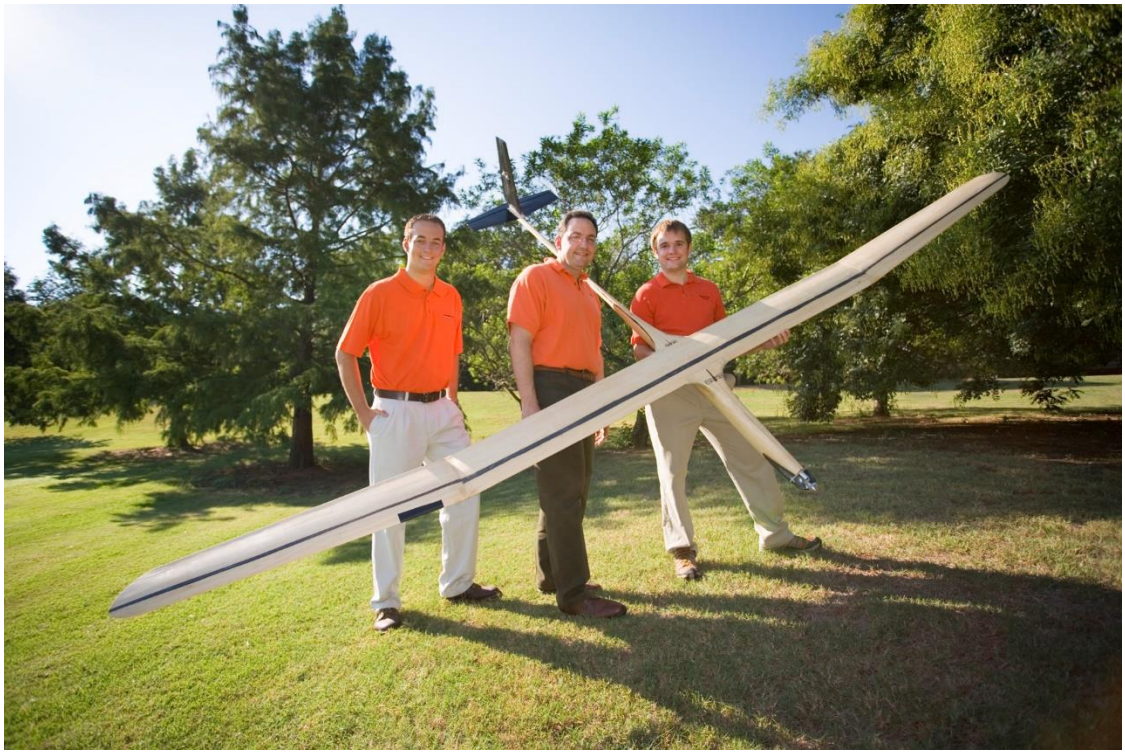

Figure 3: Long-Endurance UAV Dragonfly

Figure 4: Short Takeoff And Landing UAV Locust

Finally, many academic institutions, including OSU, design and build UAVs for competitions. These students are usually either doing UAS research, part of a student club, or students completing an undergraduate degree requirement with a senior design. A couple of the competitions these students would work to compete in are the AIAA Design/Build/Fly competition and SpeedFest. Design/Build/Fly began in 1996, while SpeedFest began in 2011 [1] [2]. Both competitions have a new statement of work every year for students to follow as they design and fabricate an unmanned aircraft to compete for first prize. Design/Build/Fly takes place every year in Wichita, KS, while SpeedFest takes place at OSU's flight field just outside of Stillwater, OK. These UAVs generally range from 2 lbs. to 20 lbs. and sometimes can be seen flying over 150 mph. Below, in Figure 5 and Figure 6, are two UAVs designed and fabricated at Oklahoma State University, one for Design/Build/Fly and the other for SpeedFest [1] [2].

Figure 5: OSpray - Design/Build/Fly 2004

Figure 6: Scorpion - SpeedFest 2016

The composite airframes constructed in this lab typically start from a statement of work that then translates to the designing of an airframe assembly using Solidworks. Once the design of the airframe is finished, the fabrication process begins, and composite molds are created. With these molds, the composite skin for the airframes can be manufactured. Then, the integration of structural components such as bulkheads, ribs, and shear webs will begin. Once the assembly of the structure of the airframe is done, the electrical components can be integrated. Finally, with all of the integration finished, the airframes are ready to have final structural tests done before flying. This is where more research is required. For the composite airframes fabricated in this lab, the structural testing is generally done to the wing where a spanwise loading using a method called the “tip test” is used. The test is a rough simulation of about 2.5 G’s and can be seen in the required structural tests for Design/Build/Fly [2]. Another method that is occasionally used at OSU is the sandbag method which can be viewed below, in Figure 7, testing the wing of the aforementioned Cessna Citation Longitude.

Figure 7: Sandbag Test Of Cessna Citation Longitude Wing

These methods will be expanded upon further in Chapter II.

UAVs are typically smaller than their manned counterparts but do share many standard requirements. One of these standard requirements is the ability to verify expected flight loads carried by the structure. Even though UAVs don't carry human life, it is still a flight risk if the aircraft loses control or fails in flight. One complication for verifying structural load requirements for many UAS platforms is the use of composite materials, such as fiberglass and carbon fiber. Material properties and, more importantly, overall bending stiffness and torsional rigidity for composite assemblies featuring sandwich-type layups and bonded interfaces remain challenging to ascertain. Generally, for the wing design of fixed-wing aircraft, the max bending and shear loading is designed around the main spar. This is because the main spar is usually placed near the quarter chord of the wing, where generally, the highest magnitude of lift is created. By designing the wing's max loading around the main spar, this gives an extra factor of safety on top of the typical designed factor of safety for the spar. This extra factor of safety is due to the design not taking into account the strength of the skin due to its material properties and curvature of the skin. For composite

aircraft, the curvature of the skin also plays a significant role in its strength and stiffness. This added strength from just geometry has not been heavily studied as of yet and cannot be predicted with very high accuracy. Along with the main spar, there are many components that go into composite wings that interact with one another to give the wing its full strength. Figure 8 shows some of these components in a wing section, along with what materials that are used for each. This wing section also shows a common structural design for the composite wings fabricated and developed at OSU.

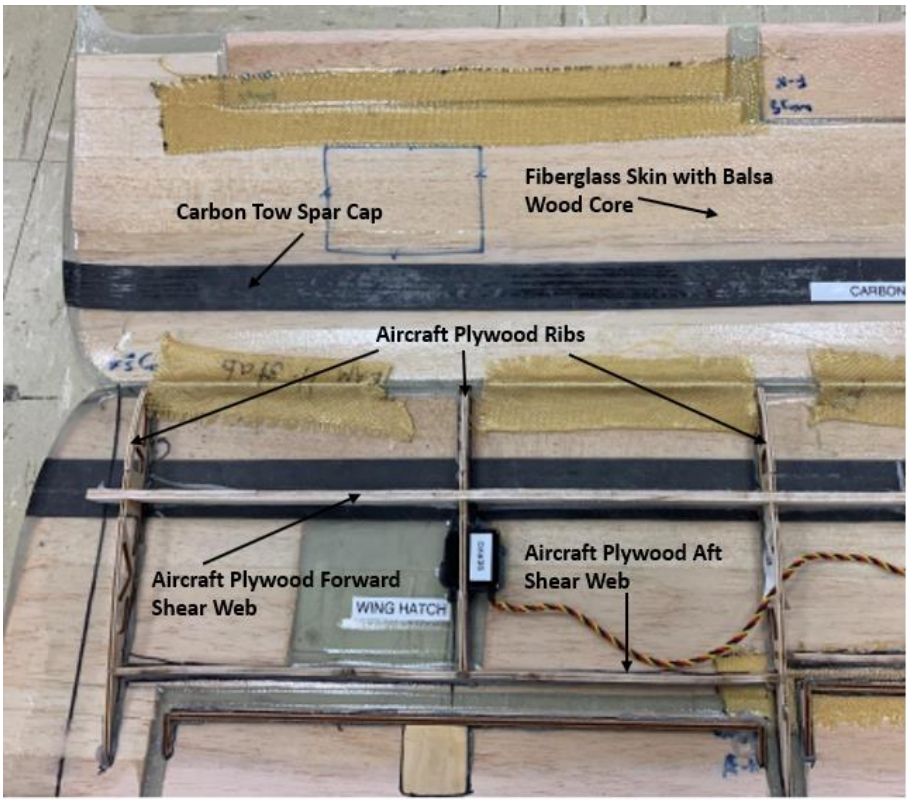

Figure 8: Wing Structural Components

Some of the components shown above are the main spar, aft spar, ribs, and skin, which can be made up of many different materials such as balsa wood, aircraft plywood, fiberglass, epoxy, and carbon fiber. With all the components and various types of materials interacting with one another, many people in the industry are led to do full wing tests to know the true strength, stiffness, and failure modes of the wing. Furthermore, part quality control, especially outside of production facilities with skilled artisans performing the layups and industrial-grade autoclaves, leaves room for

structural property variation within a part among a group of the same part. Alternatively, compared to their metal companions, composite UAVs have a greater difficulty in predicting where/when failure will occur. Thus, confidence in analysis methods to verify important structural components can handle the flight loads they were designed for is low. Because of this, along with the current method of testing lacking in adequately simulating the load distribution down the span of the wing and testing for high G cases. This research is motivated by the standard practice in the aerospace industry to validate structural analyses for flight-critical parts. This thesis aims to document the development of an experimental apparatus that can replicate flight loads on primary wing structure to test the corners of the design envelope and verify ultimate loads, where appropriate.

As previously stated, the research presented in this thesis is the development of an experimental static load testing apparatus for composite wings of UAVs. The goal of this apparatus is to be able to accurately distribute loads through a wing to simulate the wing loading created due to aerodynamic lift. The apparatus will be sized to be able to handle Group I and II UAVs for up to a minimum of 5 G's. This paper will go through the current literature on static testing composite UAVs, the design and development of the apparatus, validation of the loading characteristics, and how this can be used for future work and experiments.

Goals & Objectives

As previously stated, the goal of this thesis is to develop an experimental testing apparatus for static testing composite wings. The following list will give the objectives to meet this goal.

1. Conduct an extensive literature review of how composite wings are currently being statically tested.
2. Design testing apparatus for static wing testing
    a. Be able to withstand simulating a wing loading for Group I and II UAS to at least 5 G's
    b. Have the ability to adjust load distribution for different wing planforms
    c. Be able to test large and small UAV wings

3. Manufacture and assemble testing apparatus
4. Conduct theoretical analysis to be compared to experimental data to validate the apparatus simulates loads as expected
5. Show how apparatus would be applied to different wing planforms

CHAPTER II

REVIEW OF LITERATURE

Because of the complexity and interaction of components, full-scale airframe wing testing has always been essential for all aircraft. Testing wings to their expected ultimate loading is critical to understanding their failure modes and strength and stiffness characteristics. Static tests are also required for many certifications, such as the Far 23 airworthiness standard and ASTM F3298-19 standard specification for the design, construction, and verification of lightweight UAS [3] [4]. There have been many different techniques used to do static wing testing. One of the main goals of static wing tests is to be able to simulate the lift distribution the wing is subjected to during flight. Figure 9 shows a generic visualization of the lift distribution for different wing planforms [5]. As shown in Figure 9, the lift distribution is not the same for each wing. Geometry plays a large role in how the lift distribution curve will look and therefore gives the requirement for the testing apparatus to be able to adapt to different wing planforms. This literature review will now go through three common techniques for static wing testing.

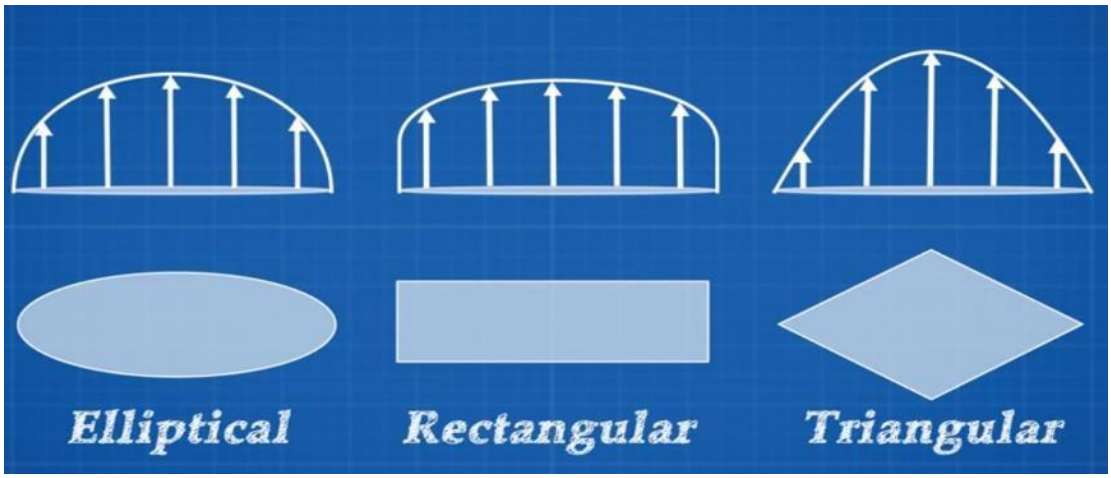

Figure 9: Lift Distribution for Different Wing Planforms

The Tip Test

Some test engineers who do not have the means of large testing apparatuses and are not required to meet as rigorous static test certifications have used a method called the "tip test." As mentioned earlier, this method comes from the structural testing requirements for Design/Build/Fly [2]. The "tip test" is a method in which the wing would be held at the wingtips, and force would be applied at the root due to the weight of the aircraft to test the bending and shear strength at the root. This technique is shown below in Figure 10, while Figure 11 and Figure 12 display the shear and bending moment diagrams for the UAV in Figure 10. In Figure 10, the UAV being tested was a UAV designed and fabricated at OSU by undergraduate students for Speedfest in 2016. This UAV was named Obsidian and was a jet UAV with a gross takeoff weight of 15 lbs. [1]. In the Design/Build/Fly rules, this test is said to be roughly 2.5 G's in bending. This method is a good quick qualitative test of a UAV; it is not a quantitative test that simulates for a realistic wing loading. While this method is effective in testing the wing root chord and has the ability to work for all wing planforms, as mentioned, it does not accurately simulate the true load distribution and, therefore, would not have the ability to test the entire span of the wing to the loads it would realistically be subjected to due to lift.

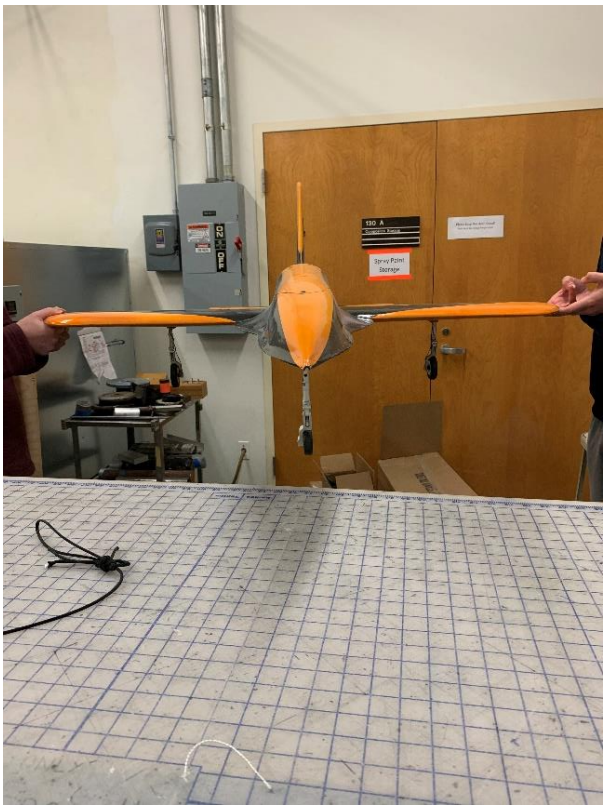

Figure 10: Tip Test On Obsidian UAV

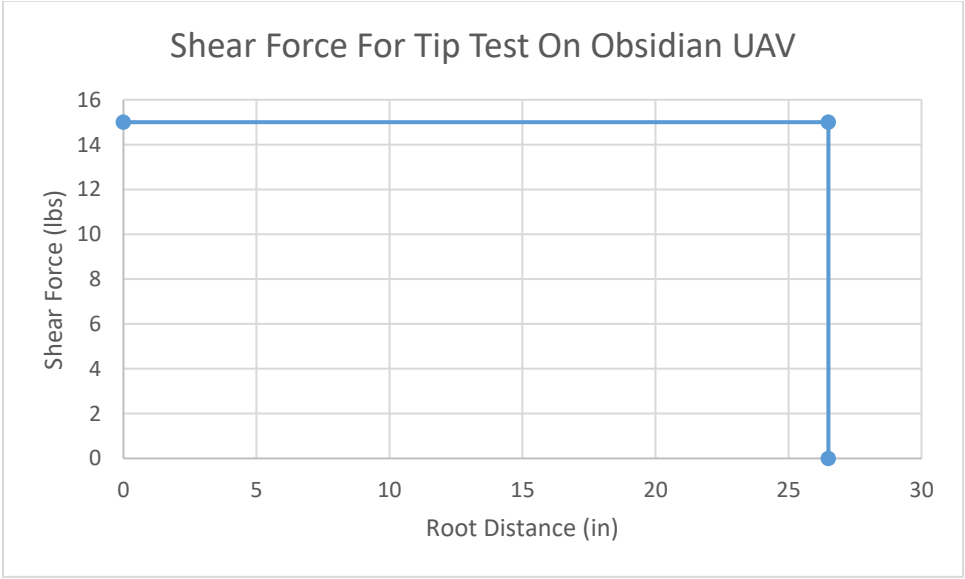

Figure 11: Shear Diagram For Tip Test On Obsidian UAV

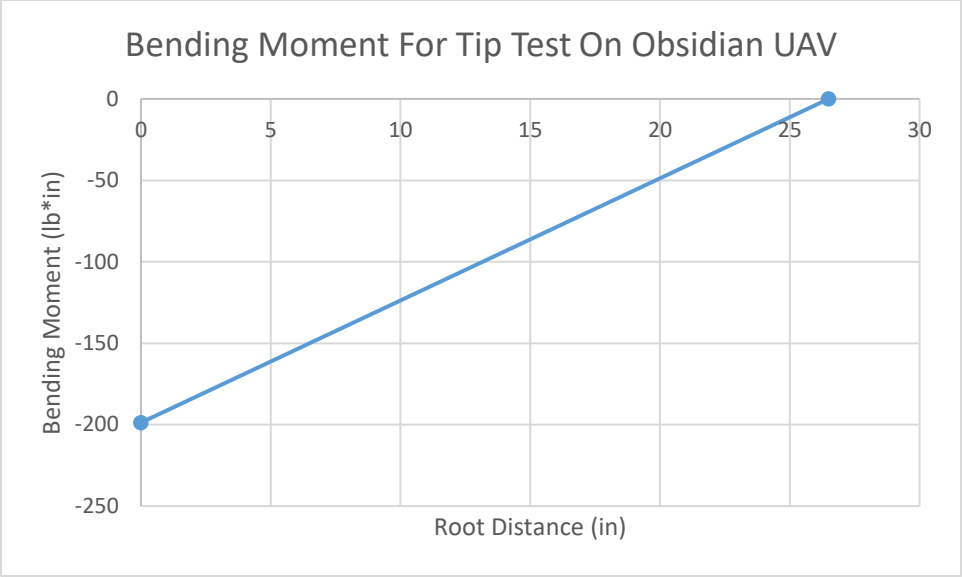

Figure 12: Bending Moment Diagram For Tip Test On Obsidian UAV

The Sandbag Method

Another method used in static wing testing is the "sandbag method." In this method, the test engineer takes a wing and holds it at the root chord, and begins adding sandbags from the root to the tip to simulate the wing loading [6] [7] [8] [9]. As previously shown in the motivation for this research in Figure 7, the sandbag method was conducted at OSU on the Cessna Citation Longitude. Another example of the sandbag method can be viewed below, where Figure 13 shows a static test conducted by Sonex Aircraft [6]. This method can be used for any wing planform and is a more accurate way of simulating the lift distribution in the wing as opposed to the "tip test." However, this method can become less practical for larger wings, high G loading tests, and ease of changing from a range of smaller to larger wings.

Figure 13: Sandbag Method

The Whiffletree

Finally, another widespread technique for simulating the load distribution in static testing is the whiffletree [10] [11] [12] [13]. The whiffletree has been used in industry for years because of its high accuracy in simulating aerodynamic loads and variability for load placement. This technique for static structural testing is commonly used by many aerospace designers, such as The Boeing Company, Airbus, and NASA [14] [15] [16]. The Boeing Company and Airbus both have used the whiffletree method on their large commercial aircraft, while NASA used it to test the F/A-18 Hornet [14] [15] [16]. These static tests can be seen in the figures below.

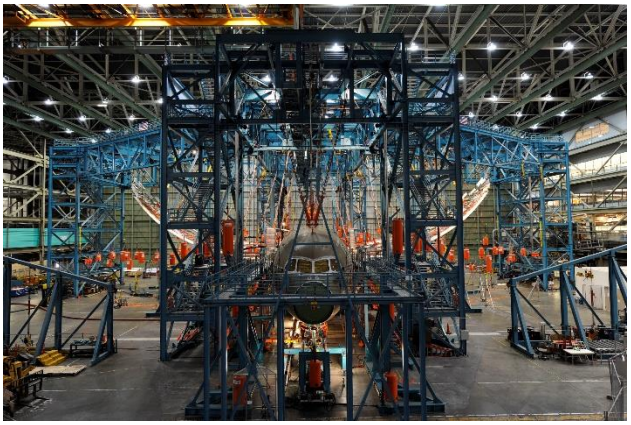

Figure 14: Boeing 787 Static Wing Test

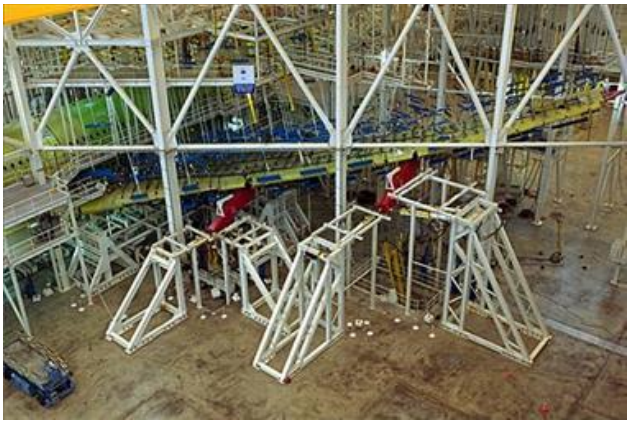

Figure 15: Airbus A-380 Static Wing Test

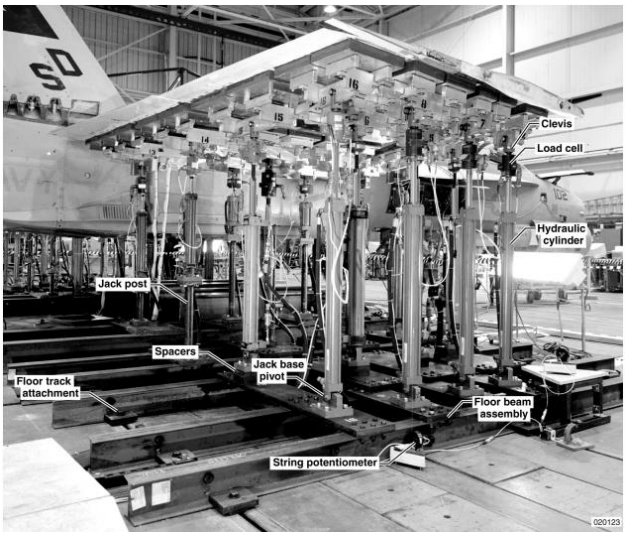

Figure 16: F/A-18 Static Wing Test

This method of testing is seen in applications for smaller aircraft as well, such as four and two-seater aircraft and UAVs [17] [18] [19]. Although there have been many whiffletree designs for smaller aircraft and UAVs, there have not been many found for smaller-scale UAVs in the aforementioned Group I and Group II class. These tests are generally done for ultimate load testing for airworthiness certifications. Even though these static tests are usually used for the entire wing, it is not limited to only static testing full-scale wings; there have also been cases where test engineers have used a whiffletree to test control surfaces [16] [20].

The whiffletree method is used to simulate the wing loading due to the aerodynamic and ground forces. One of the advantages of using the whiffletree method is its variability of adjusting for different wing planforms. The whiffletree method uses a series of strategically placed point loads, shown in Figure 17, that can be moved along the span to simulate the shear and bending loading on the wing that is due to lift. Figure 17 is an example of a four-tier whiffletree due to there being four levels of beams used to apply the load to the wing. More complex whiffletrees can have more tiers and tiers that span the chord to be more precise on loading along the wing.

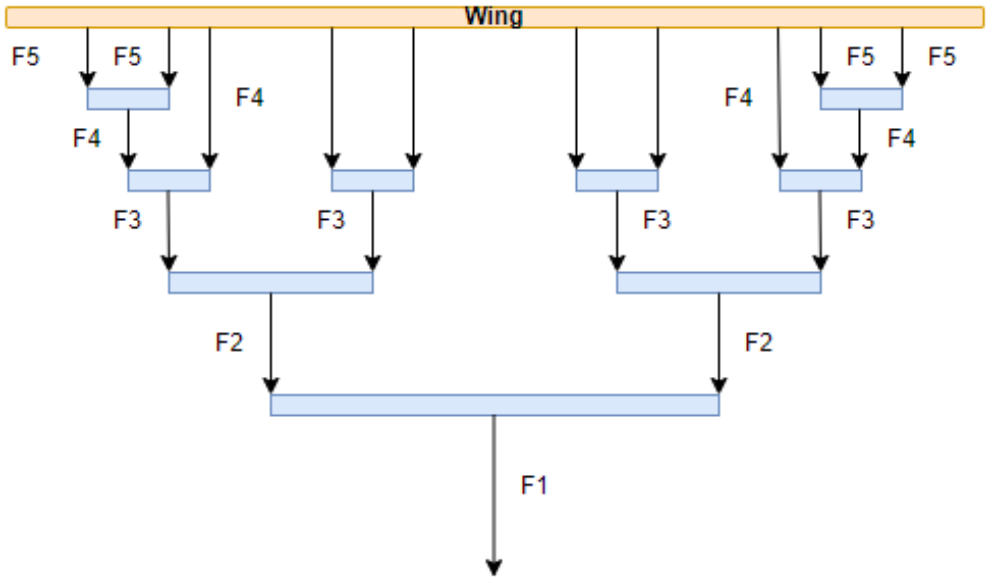

Figure 17: Four-Tier Whiffletree Diagram

An example of what a four-tier whiffletree being analytically applied can be seen can be first started with Figure 18, Figure 19, and Figure 20 below. While Figure 18 shows the lift distribution on a rectangular wing from the wing root to the wingtip and is followed by the shear and moment diagrams. Note: the development of these figures will be addressed in the next chapter.

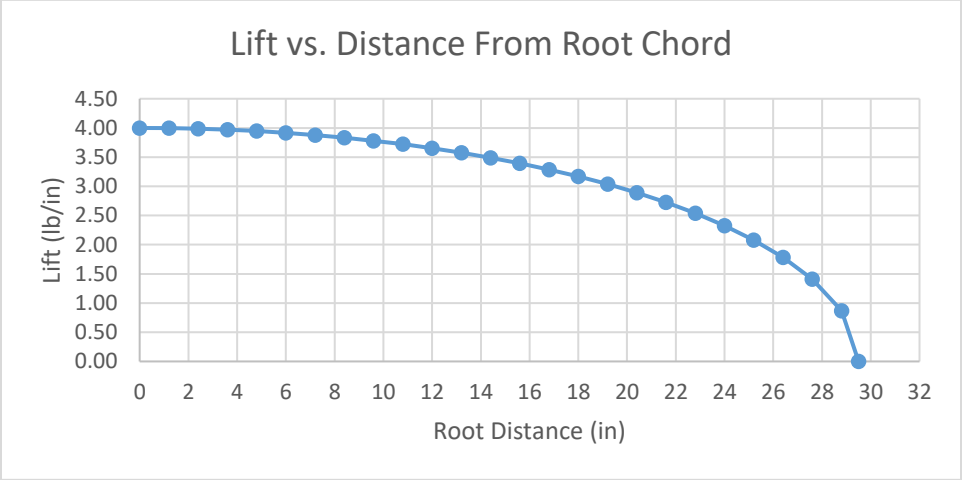

Figure 18: Lift vs. Distance from Root Chord

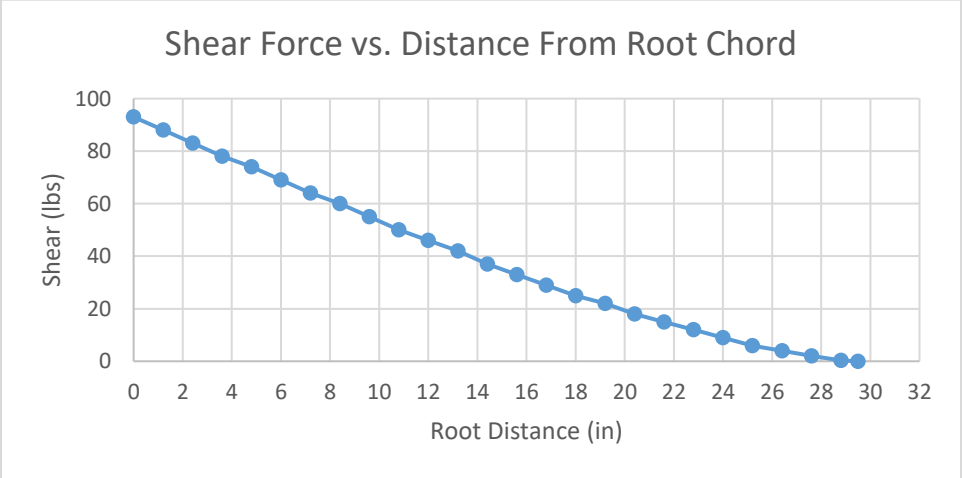

Figure 19: Shear Force vs. Distance from Root Chord

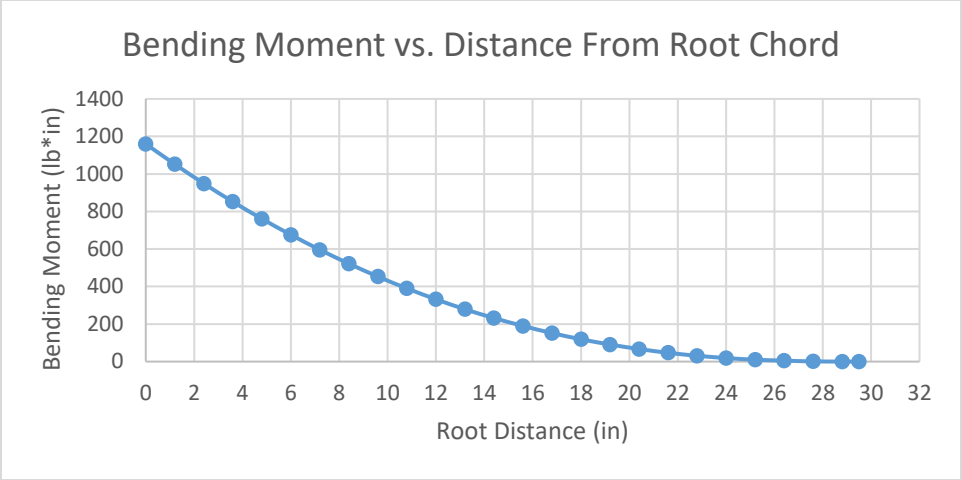

Figure 20: Bending Moment vs. Distance from Root Chord

By applying the whiffletree to this wing, it can be seen in Figure 21 and Figure 22 how the theoretical shear and bending moment of the wing compares to the shear and bending moment done by the whiffletree. As shown below, the shear done by the whiffletree is a slight overestimate until it reaches the root, where the root shear is equivalent to the theoretical root shear. While the bending moment below follows closely to the theoretical, it becomes a slight overestimate at the root.

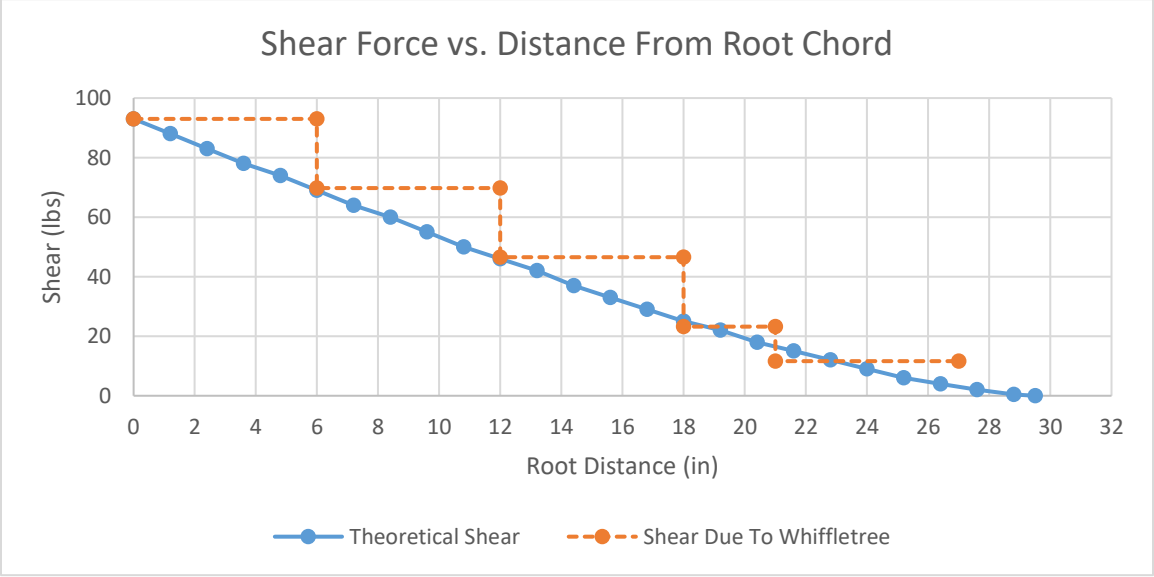

Figure 21: Shear Force With Applied Whiffletree

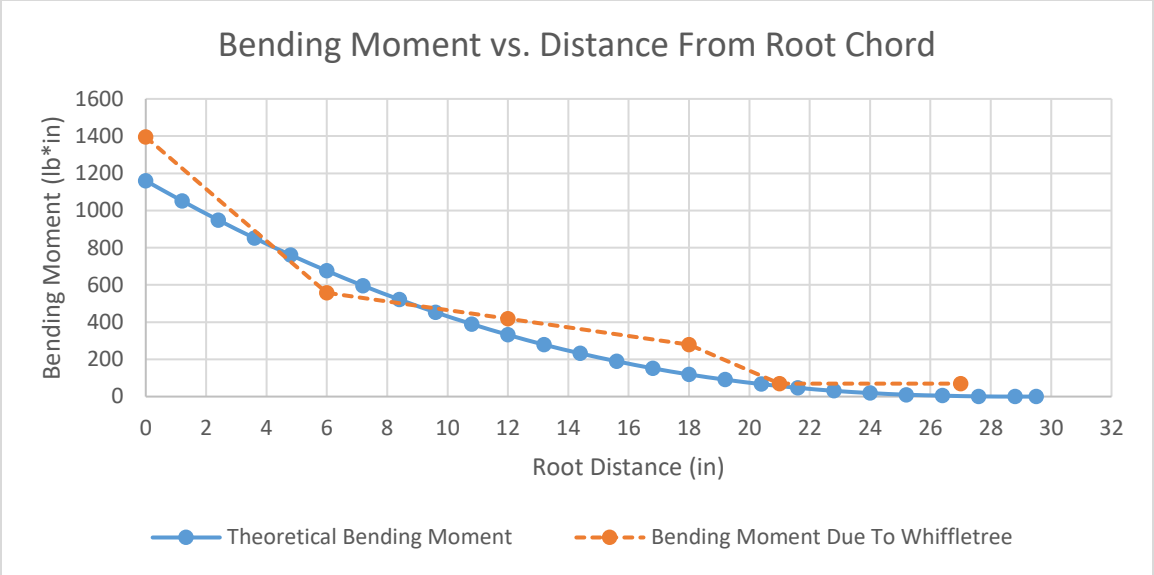

Figure 22: Bending Moment With Applied Whiffletree

This example would be for a case in which the test engineer wanted to test this wing to the expected ultimate load, in this case, 93 lbs. Generally, it is believed that the failure mode of a wing will be at the root chord, where the shear and bending moment is at its highest. However, as seen in other composite wing tests done by the whiffletree method, the wing can have failures in other areas such as control surfaces. This was observed in a static test done at Mississippi State University on an ultralight UAV, where the wing went under a compressive failure at the point where the composite wing was open cut for the aileron [21]. This is why it is essential for the load to be as accurate as possible to show failure modes that are not typically considered in general analyses. Because the whiffletree is the most practical and accurate as opposed to other methods of static testing, the research here will focus on developing a testing apparatus that uses a whiffletree system.

CHAPTER III

DEVELOPMENT AND DESIGN OF STATIC TESTING APPARATUS

This chapter will go through the development and design of the static testing apparatus. It will start with a refresher of the requirements of the apparatus, then proceed to the initial analysis done to begin the design and rationale for component sizing, to finally, the design of the apparatus. The structural and power limits are displayed below in Table 1 and will be justified throughout the chapter.

Table 1: Apparatus Structural And Power Limits

Structural Limit	670 lbs.
Power Input Limit	AC 110/220 ±15%V
Power Output Limit	12V 50A

This design will be dependent on the use of the 80/20 T-Slot Aluminum Building System [22] decided upon due to its adaptability, variety of parts, strength, and proven use in industry. Therefore, a great deal of analysis will be done on 80/20 shafts throughout this design. Finally, with the thought in mind of having as minimal of an amount possible of parts being interchanged from wing to wing, this design only requires occasionally the top mounting plate in the central structure, the foam inserts in the wing clamp assembly, and the tension spring for the winch to be changed

from wing to wing. The reasoning for these needing to occasionally change and/or be modified will become more apparent as this chapter continues on.

Requirements

The goal of this apparatus is to be able to statically test a variety of composite wings for Group I and Group II UAVs to a minimum of 5 G's, simulate their wing loading, and be able to adjust to various planforms. The Group II UAS weight class is defined by the Department of Defense (DoD) to be 21 lbs. to 55 lbs. [23]. This drives the structure for this apparatus to be able to handle at least 550 lbs. From the literature review conducted, the whiffletree is the superior method for simulating wing loading for this particular design. Also, due to the high amount of force being used in the apparatus, the ability to test from a safe distance is required. Finally, for the design to be able to adjust for a wide variety of wing planforms, the whiffletree will need a design that allows it to be modular.

Preliminary Design

In Figure 23 and Figure 24, the full assembly can be seen with the overall dimensions of the apparatus. The size of this apparatus is based on a wing that had a root chord of 24 inches and a wingspan of 102 in. These dimensions were based on a 55 lb. UAV, which, as stated before, is the maxima of Group II UAVs. This apparatus was sized for this wing size; however, the original wing used to develop the location of the point loads along the wingspan was a rectangular wing with a 7.5 in. chord and 59 in. wingspan. This wing is the one modeled as the test wing in Figure 23 and Figure 24, along with the shear and moment diagrams from chapter II.

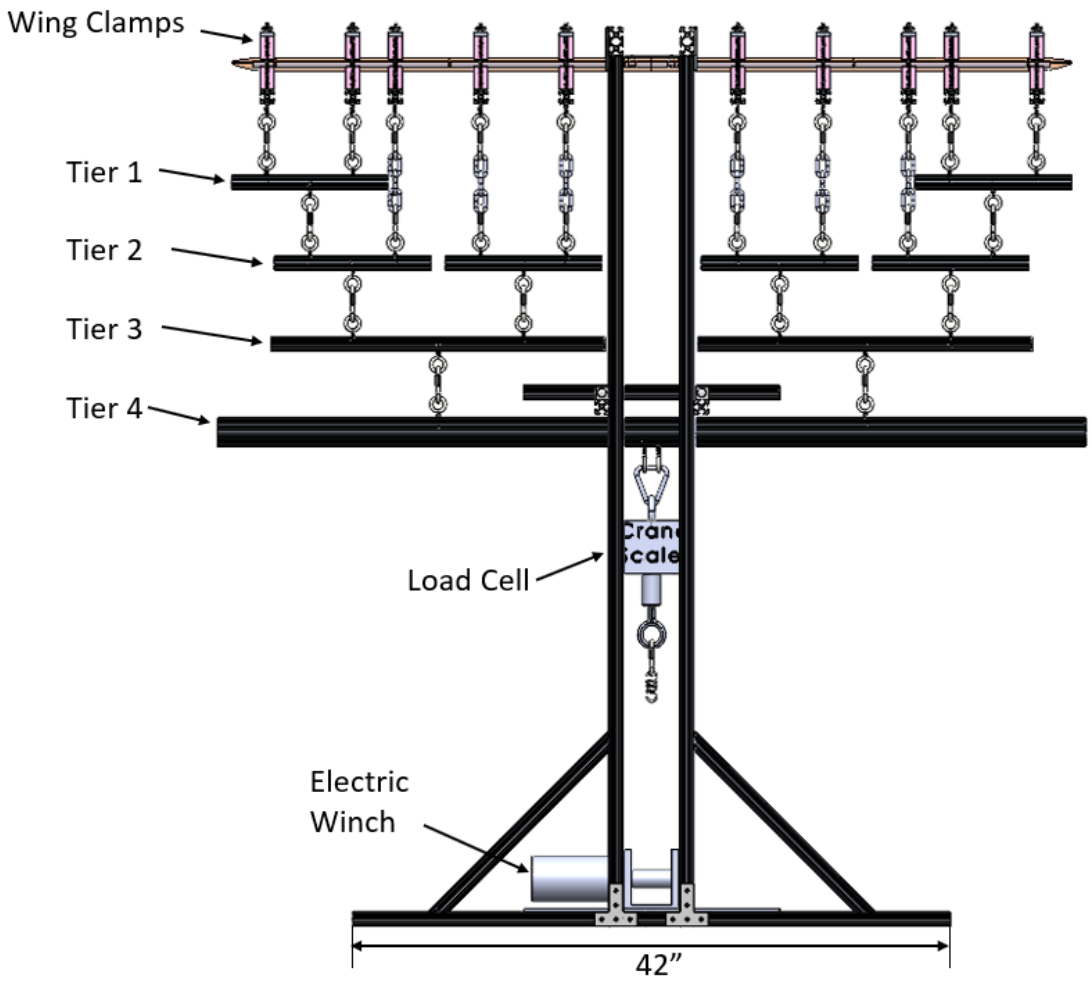

Figure 23: Testing Apparatus Full Assembly Front View

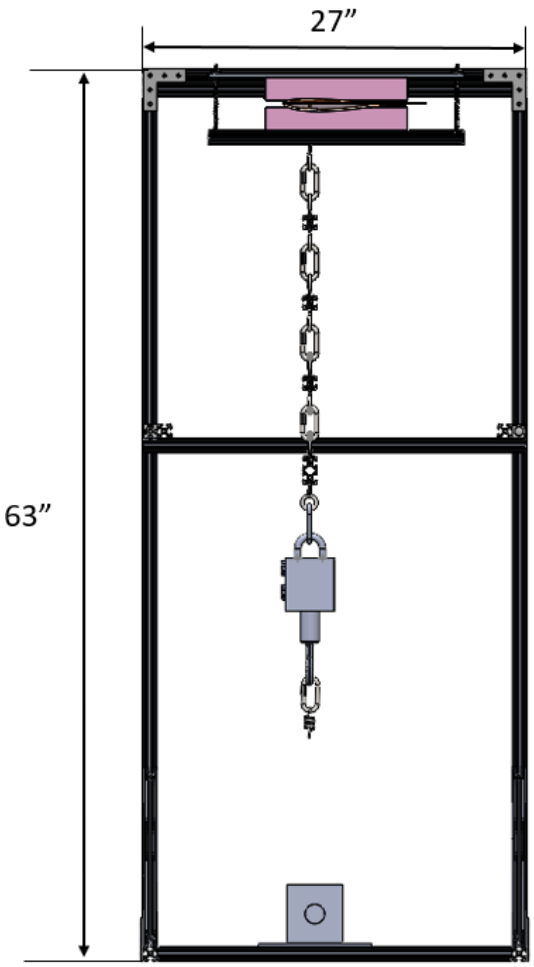

Figure 24: Testing Apparatus Full Assembly Side View

To start this design, an estimation of lift over a wing planform needed to be developed to understand what the shear and moment on a wing are. There are a few ways of approximating the spanwise lift distribution for a wing. A couple of reasonable methods are Schrenk’s method [24] and Prandtl’s lifting-line theory. The method chosen to estimate the spanwise lift was Prandtl’s lifting-line theory. Equations (1) and (2) were the equations used for finding the elliptical lift distribution along the span of the wing. Where Γ(y) is the circulation distribution and L’(y) is the elliptical lift distribution.

$$\Gamma(y) = \Gamma_0 \sqrt{1 - \frac{4y^2}{b^2}} \tag{1}$$

$$L'(y) = \rho_\infty V_\infty \Gamma(y) \tag{2}$$

These equations were applied to the formerly mentioned rectangular wing and referred from Anderson's Fifth Edition Fundamentals of Aerodynamics Textbook [25]. With the lift distribution now approximated, the shear and moment along the span of the wing could then be solved. The shear and moment along the span can be found by taking the integral and double integral of the lift distribution. Equations (3) and (4) show the equations required for this calculation.

$$Shear = \int -L'(y)dy \tag{3}$$

$$Bending\ Moment = \iint L'(y)dy \tag{4}$$

With these equations applied, Figure 18, Figure 19, and Figure 20, from chapter II, were developed to better understand what the shear and bending moment was at any point on the span. These calculations can be viewed in the Appendix Section. Now that the shear and moment along the wing have been developed, the application of the whiffletree can now be made.

As mentioned before, the whiffletree uses a series of point loads to simulate the shear and bending moment. For a preliminary placement of loads, it was desired to match the max shear at the root. Knowing the max shear at the root and the number of point loads being applied, statics could be used to decide what the theoretical force at each point is. This drove the placement of the point loads along the span to be as exact of the shear as possible. Once the placement of each point load was decided, the shear and moments could be solved. Figure 21 and Figure 22 were developed to show where the locations of the point loads along the span. Finally, with the design structure so heavily dependent on the 80/20 shaft, an initial analysis for the max bending moment was done to ensure that deflections that occur during the wing loading process do not exceed the 80/20's yield

point and permanently deform. Equation (5) [26] displays the max bending moment equation where σ_{max} is the maximum bending stress, I is the second area moment of inertia, and c is the max distance from the neutral axis.

$$M_{max} = \frac{\sigma_{max} I}{c} \tag{5}$$

This analysis was done on a 1 in. by 1 in. 80/20 shaft and found a max bending moment of approximately 2981 lb.-in. Now with an approximation of where the point loads will be placed and the max bending moment limit for each structure, the detailed design and sizing could begin.

Detail Design and Sizing

This section will now go over the components of the design in more detail, along with their sizing and reasoning behind it. This will first go through understanding 80/20 because it is part of all subassemblies of the design. Then to the individual subassemblies, the central structure, the wing clamps, the electrical system, and finally, the whiffletree. All of the analyses in this section can be found in the Appendix section.

As mentioned earlier in this chapter, one of the main components that allow this design to be possible is 80/20, along with its end feed fastener. Figure 25 displays an Isometric and cross-sectional view of an 80/20 member.

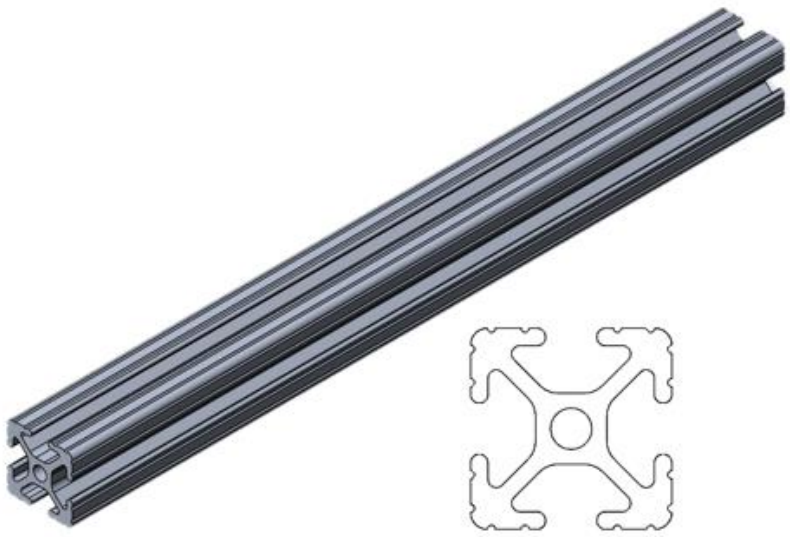

Figure 25: Isometric and Cross-Section View of 80/20

As seen above, 80/20 shafts give a significant amount of modularity with their patented T-slot design. 80/20 is made from 6105-T5 aluminum, which makes it have great strength, corrosion resistance, and low weight. Most of the design is made from 80/20, from the central mounting structure to part of the wing clamps to the beams for the whiffletree assembly. Nearly all of the 80/20 used in this design has a 1 in. by 1 in. cross-section, except for the Tier 4 beam and top structure, where the analysis will later be discussed and show that the beams would not be stiff enough for the application.

The end feed faster made for 80/20 T-slotting was the first analyzed component due to its use for nearly all the hardware used in the design. The analysis was done on the surface area interaction between the 80/20 beam and 80/20 end feed fastener. The yield stress of 80/20 is 35,000 psi. This was compared to the interaction surface area at 550 lbs. and yielded a result of a factor of safety to be a little above 10. This calculation can be seen in the Appendix section. Figure 26 displays the end feed nut with the area that interacts with the 80/20 shaft shaded.

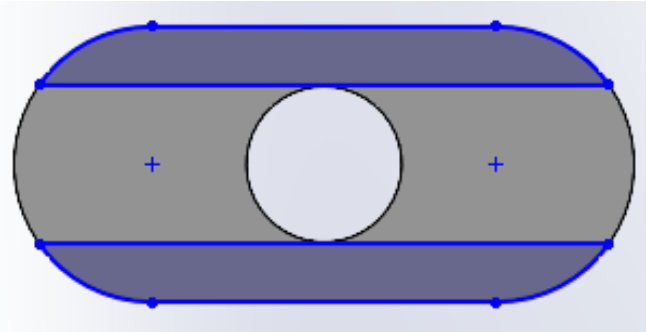

Figure 26: End Feed 80/20 Nut

Central Structure

The central structure of this design is the subassembly that the wing and winch mount to. This structure handles all of the loadings that come from pulling with the winch to the loading that goes through the fastening points on the wing. Figure 27 and Figure 28 display a Front, Side, and Isometric view of the central structure.

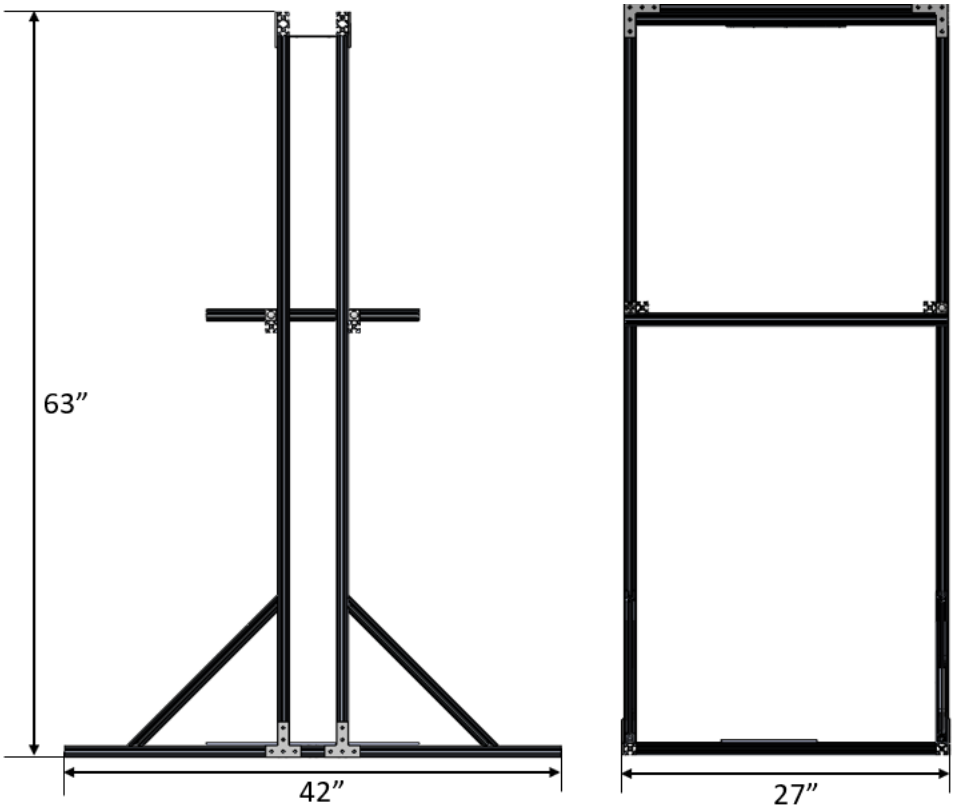

Figure 27: Central Structure Front and Side Views

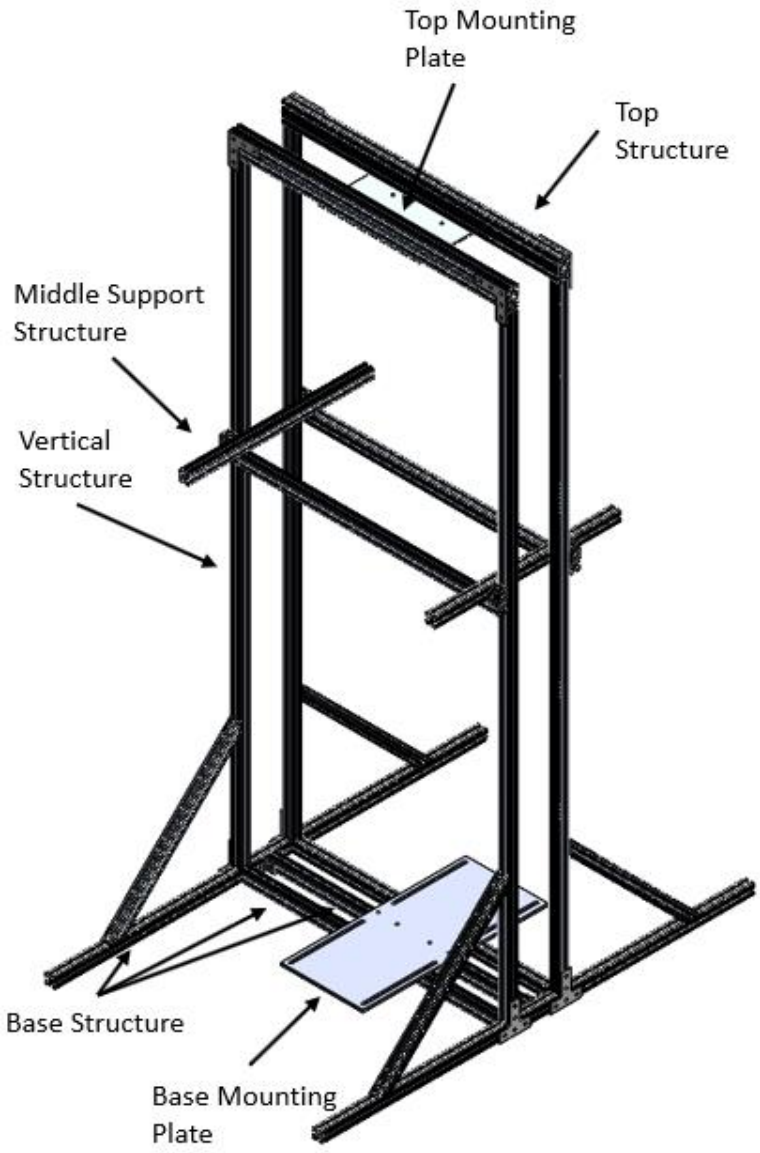

Figure 28: Isometric Central Structure View

Because the loading starts at the base of the structure, it was designed first and built from the base up. The first analysis was done on the three beams that attach to the base mounting plate. The length of these beams was decided on due to the requirements of a max root chord length of 25 in. There are six attachment points to the plate, two for each beam. The analysis is done for each beam with both ends fixed with twin point loads on the beam. A free-body diagram (FBD) of one beam with twin loads can be seen below.

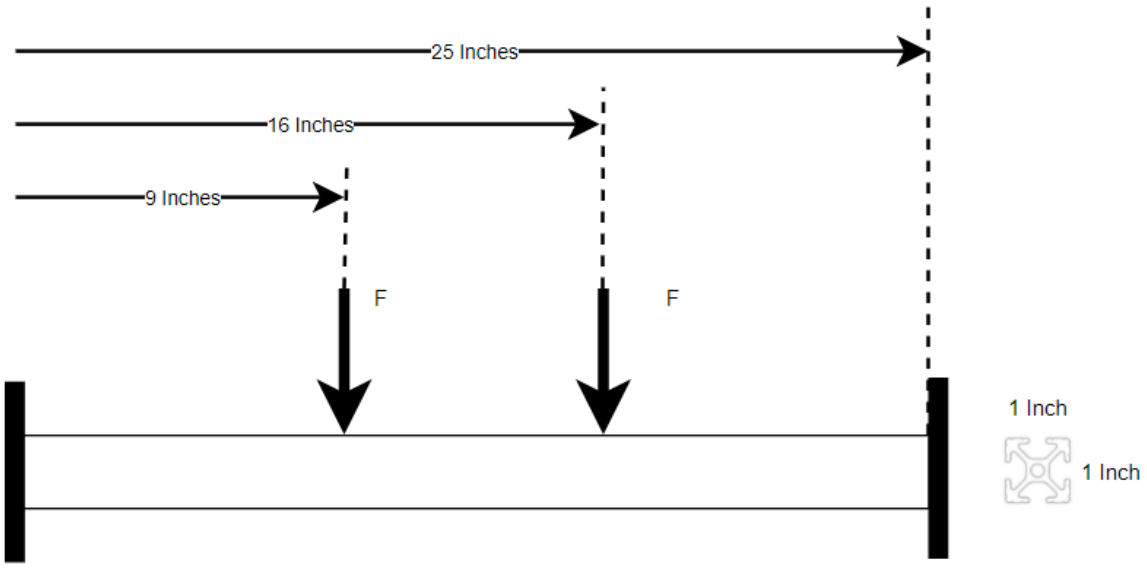

Figure 29: Bottom Base Twin Loaded Beam FBD

The analysis done on these members was for the deflection of the beams at the design load of 550 lbs. The calculation for deflection was decided because it was believed that the first mode of failure would be the stiffness of the beam. The analysis yielded a deflection of .027 in. or about .3% of the available vertical distance above the winch, which deemed the 1 in. by 1 in. cross-section stiff enough for this application. The equation referred to for this calculation was found in the tenth edition of Shigley's Mechanical Design textbook [26] and is displayed below. In equation (6), F is the point load force, x is the distance from the datum, in this case, the left fixed point, l is the length of the beam, E is the elastic modulus, and I is the inertia of the beam. In these 80/20 calculations, both E and I were provided from 80/20's online site [22].

$$y = \frac{Fx^2}{48EI}(4x - 3l) \tag{6}$$

Next, the vertical structure was analyzed. This structure's expected first mode of failure was thought to be a buckling failure. Thus, the calculation for maximum allowable force before

buckling was conducted. The equation used for this calculation was Euler's column buckling formula, shown in equation (7) [26] [27]. In this equation, n is a factor that is for accounting for end conditions, while L is the column length, and E and I are the same as for equation (6).

$$F = \frac{n\pi^2 EI}{L^2} \tag{7}$$

With a safety factor of almost ten, there was no need to make any inertial changes to the vertical structure. However, the length of the vertical structure was not able to be finalized until the end of the design of the wing clamps, electrical system, and whiffletree. This was because the overall height of the apparatus was based on the required lengths of the hardware used for connecting all of the subassemblies. Once the other subassemblies were designed, the vertical structure length could be solidified at 60 in.

Next, the top structure for the apparatus was initially planned to be 1 in. by 1 in. 80/20 shaft. However, after applying equation (8) [26] for the deflection of the beam, it was found that even though the beam does not yield under the load, its deflection of nearly .17 in. was not favorable and would affect the wingtip deflection data gathered from a test at the higher loads. This analysis led to the decision to increase the stiffness. To increase the stiffness of the beam, it was decided to take an inertial approach, as opposed to a material change, and exchange the 1 in. by 1 in. 80/20 shaft for a 2 in. by 1 in. 80/20 shaft. This decision was highly favorable as it resulted in an 82% decrease in overall beam deflection. The overall deflection of the beam at 550lbs. after the change came to be .03 in. The FBD for the beam analyzed before the cross-section change to the new change can be viewed in Figure 30 and Figure 31.

$$y = \frac{F(l-x)x}{6EIl}(x^2 + (l-x)^2 - l^2) \tag{8}$$

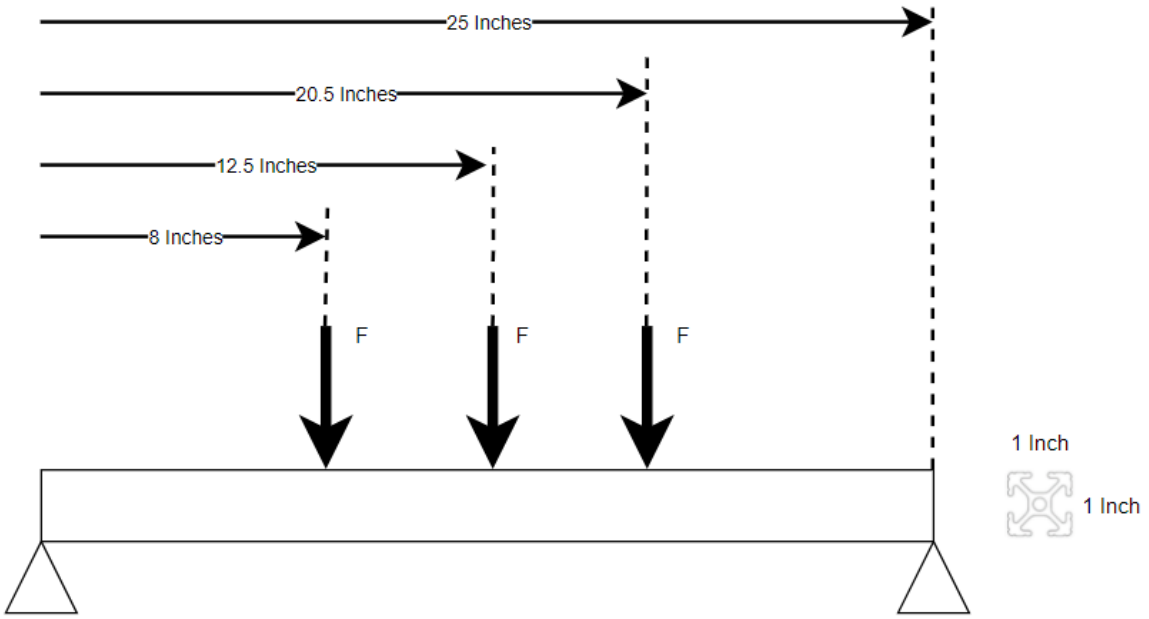

Figure 30: Initial Top Structure FBD

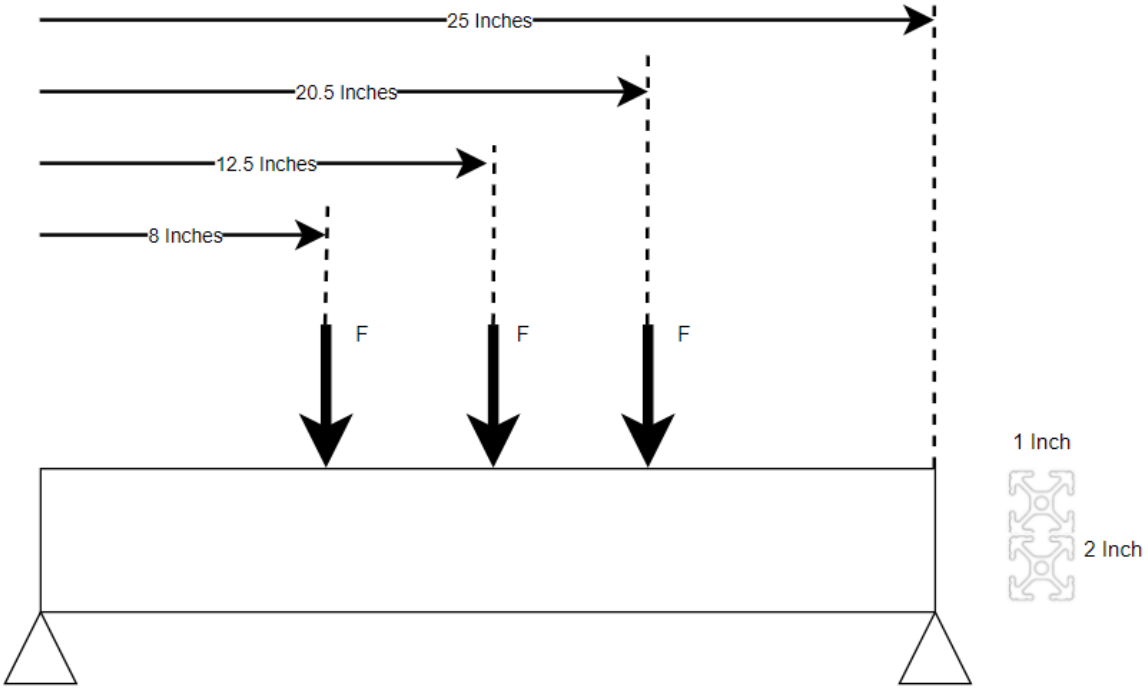

Figure 31: Final Top Structure FBD

Finally, although all the structures discussed had been designed to handle the max expected loadings, it was still desired to have additional structure to have better load distribution throughout

the central structure. Therefore, the middle support structure was added to help with the alignment of the vertical structure and to give a little more support due to the structure being so tall. Then by adding the braces, it gave another avenue to relay the loads from the vertical structure to the base structure and to lower the stress concentrations between the vertical and base structures.

Wing Clamps

The wing clamps in this design are the clamps used to clamp around the wing to transfer the loads from the whiffletree to the wing. A side and isometric view, along with overall dimensions, of the wing clamps can be viewed in Figure 32 and Figure 33

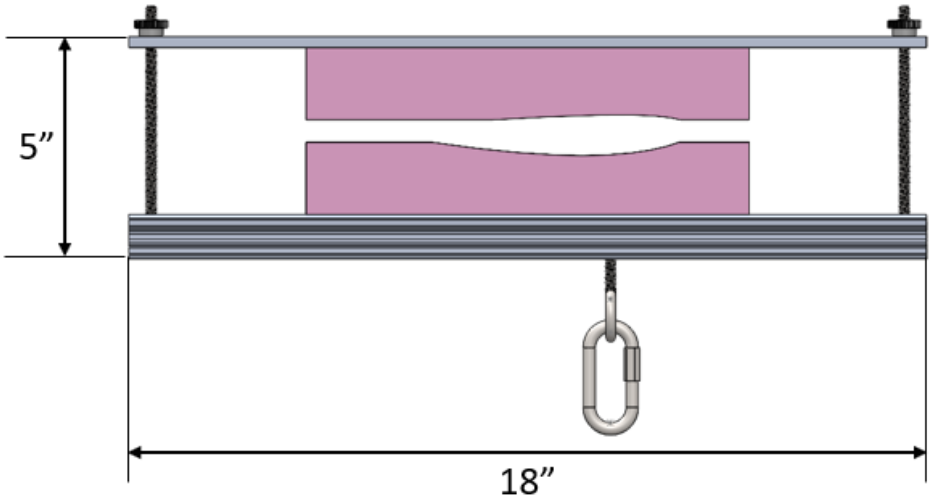

Figure 32: Wing Clamp Side View

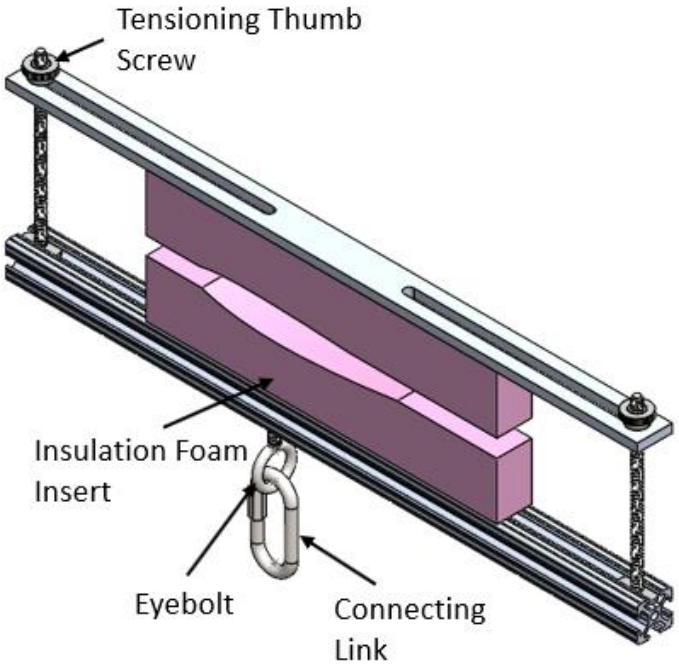

Figure 33: Wing Clamp Isometric View

The wing clamps attach to the whiffletree via the connecting link that is attached to an eyebolt on the 80/20 base. This transfers the load to the wing clamp and from the clamp to the wing. The 80/20 shaft on the base allows the eyebolt to be moved and placed at the quarter chord of each wing, where the magnitude of the lift down the chord line is at its highest to simulate the lift along the chord. The overall height and width of these clamps are 5 in. by 18 in. As mentioned earlier, the root chord of the wing this apparatus was designed around was 24 in. The expectation for a wing of that size root chord would not be rectangular, and so the clamps could be a little shorter in length to save on weight and overall size for when they are applied to wings with smaller chords. However, specialty clamps were also made that are 24 in. in width.

In the wing clamp design, the largest concern was how to apply the load without crushing the wing. In wings made from aluminum, whiffletrees have been directly attached to the wing itself, or the clamps used were made from metal or wood [10] [13] [17] [18]. However, because composites are not as strong or as stiff as aluminum wings, they are more susceptible to skin-

crushing failures. Aluminum wings also tend to have more ribs in a place where these clamps could possibly be placed, whereas composites tend to have very few ribs, if any at all sometimes. Therefore, the material pushing against the wing needs to be stiff enough to apply the load but also soft enough to not damage the composite skin. In Niu's Composite Airframe Structures textbook [28], a diagram using rubber pads that are located on top of the forward and aft shear webs is shown. This diagram can be seen below in Figure 34.

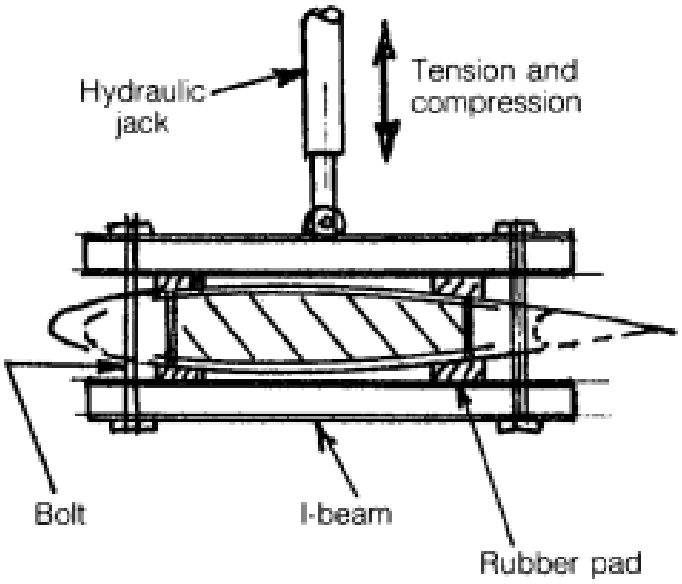

Figure 34: Wing Loading Clamp From Niu [19]

While this method could be viable, the concern for some smaller UAVs not having aft shear webs and the small area that can create large stress concentrations at the two points of contact led to the decision to try something different. Hence, the insulation foam was thought to be a viable option due to its ease of cutting to airfoil shapes, affordability, ease of access, and ability to be soft on the wing but still effective in transferring the load from the whiffletree apparatus. The foam used for this design is 1 in. thick Owens Corning foam board.

As shown in Figure 33, the remaining components of the wing clamp design are the slotted aluminum bar and the hardware used. The aluminum bar was slotted to decrease the bending stress on the bar when it's in use for areas where the chord is smaller. Finally, the tensioning thumb

screws were decided for ease for the test engineer to not any specific tools to set up the clamps on the tested wing.

Electrical System

The electrical system is composed of six major components. The electric winch for applying the force, the DC power supply (12v 50A) for supplying the power to the system, the load cell needed to measure what the force is being applied from the winch, the receiver and transmitter for remote control, and finally, the electronic speed controller (ESC) for controlling the rate of pull done by the winch. All of these components can be viewed below in Figure 35.

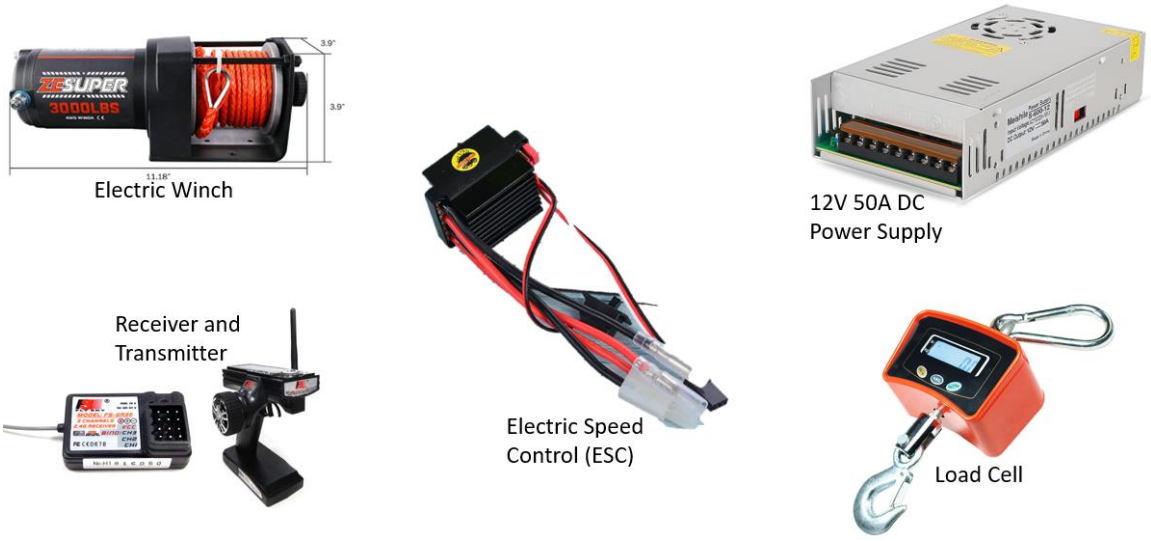

Figure 35: Electrical System

The first design decision made for this electrical system was the electric winch. A mechanical winch was also considered; however, due to the need to be a safe distance from the structure, a mechanical winch would require a secondary mounting point away from the central structure. This was very undesirable because it would limit where the testing apparatus could be used and create a larger area required for testing. Since the mechanical winch was not a feasible solution, other options had to be considered.

Initially deciding how to apply the load, three potential avenues were thought of that differed greatly. These three avenues were hydraulic, pneumatic, and electric. Hydraulic systems are commonly used for larger-scale aircraft such as commercial, space, and fighter aircraft [29]. However, for this application, that kind of loading power is not necessary. Hydraulics also tend to leak constantly, which creates a mess and requires to always have more hydraulic fluid on hand. For these reasons, the hydraulic option was ruled out. A pneumatic solution seemed like a much better option than the hydraulic one. It's not nearly as prone to leaking as hydraulics are, and if it does leak, it typically causes no mess. Its system is also typically much lighter than hydraulic systems. Unfortunately, for a pneumatic system, some of the downsides are that there is always a need for a compressor. And also, the need for multiple parts such as at least two hoses, a regulator, as mentioned, a compressor, power for the compressor, and most likely various fitting to make the hoses, regulator, and compressor all compatible.

Even with some deficiencies in the pneumatic option, it was still believed to be a possible option; however, looking into a fully electric system still needed to be investigated to be completely thorough. Once investigated more, the electric option was believed to be the better option. Initially, with the electric option, it was believed to only need either the DC power supply or a small car battery to go along with the electric winch. This was a very advantageous option due to the need to not have to worry about fittings leaking or extra components. There was also the additional benefit of the range to be further away from the testing apparatus during a test was much higher than the pneumatic option would've been. The electric seemed like the more straightforward option because there were so few parts. However, in testing the electric winch's remote control, the winch was found to have issues with its rate of pull being too fast. So the need for additional components were required. Hence, the need for an ESC, receiver, and transmitter to better control the rate of the winch pulling. Although the addition of the ESC resolved the issue of the pull rate for the winch, there was still one other change required for the winch that was found later in testing. The synthetic rope used for the winch stretched too much and could not hold a steady tension and so the addition

of tensioning spring and replacement of the rope with a steel cable was done to resolve this stretching and tension issue. Both the pneumatic and electrical options seemed viable. And even though the electric option needed a few more components, it still seemed like a more favorable option as opposed to the pneumatic option.

Once the loading system was decided upon, it was now time to fill out what the rest of the electric system required to use the electric winch. The first decision was how to power the electric winch. Generally, electric winches are attached to cars and ATVs and powered by the battery used for the car or ATV. Because a car battery is heavy, bulky, and has to be recharged, a better option needed to be used. This is how the idea of using a DC power supply came to fruition. Using the power supply allowed it to be plugged into an AC 110V/220V wall socket that could be converted to the required 12V 50A output. The 50A specification for the power supply was based on the research done about line pulling capacity versus full load current draw [30]. The estimated line pulling capacity at 50A is roughly 750lbs. The ESC, as mentioned earlier, was added to the system during the fabrication of the apparatus to give better control over the winch's motor. The ESC had a rating for 6v-12V and 320A, along with a 5V 2A Battery Eliminator Circuit (BEC) fitted for a receiver. Next, the receiver and transmitter used were a Flysky three-channel FS-GT3B. Finally, with the electric winch powered and more controllable, the need for measuring the load on the wing was required. The best solution decided was a crane scale type of load cell because of its ability to link the winch cable and whiffletree. The crane scale used in the design has a resolution of .5 lbs. and a maximum loading of 1100 lbs.

Whiffletree

Finally, the last subassembly, the whiffletree is the assembly used for distributing the load from the electric winch along the wing to simulate the shear and bending moment on the wing. Figure 36 displays the assembly and components.

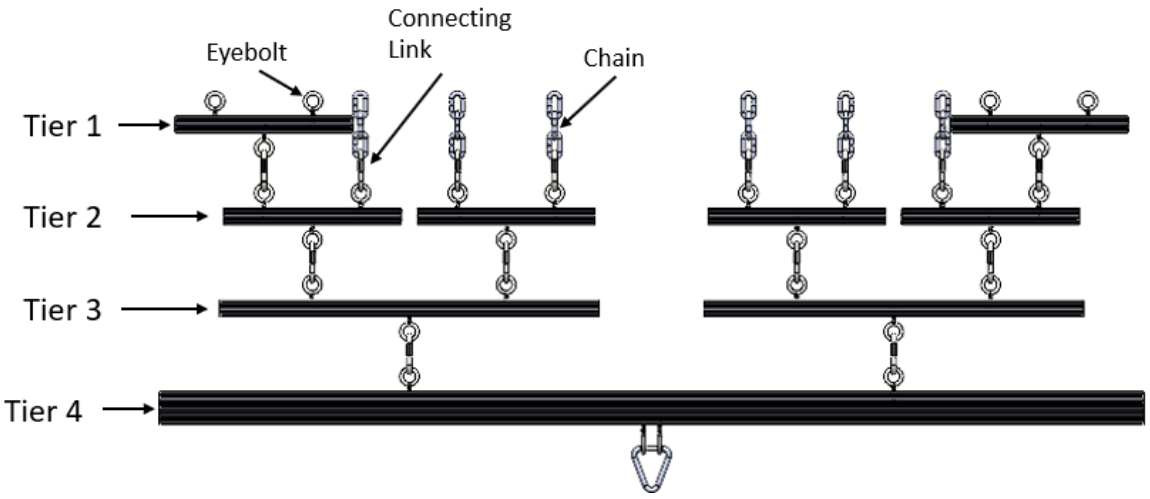

Figure 36: Whiffletree Component Diagram

The initial sizing of each beam is based on the point load placements from the earlier discussed test wing in the full assembly Figure 23 but upscaled for simulating a 102 in. wingspan. All of the beams in Tier 1 and Tier 2 have a length of 11 in. While Tier 3's are 23.5 in. and Tier 4 is 61 in. All were planned to be made from 80/20 shafts. However, an initial analysis needed to be done first to size what the beam cross-sections needed to be. Because all the whiffletree Tiers are under the same loading configuration with differing magnitudes of loading, the analysis for sizing the tiers were all the same. Figure 37 displays the loading FBD for all of the beams in the whiffletree tiers.

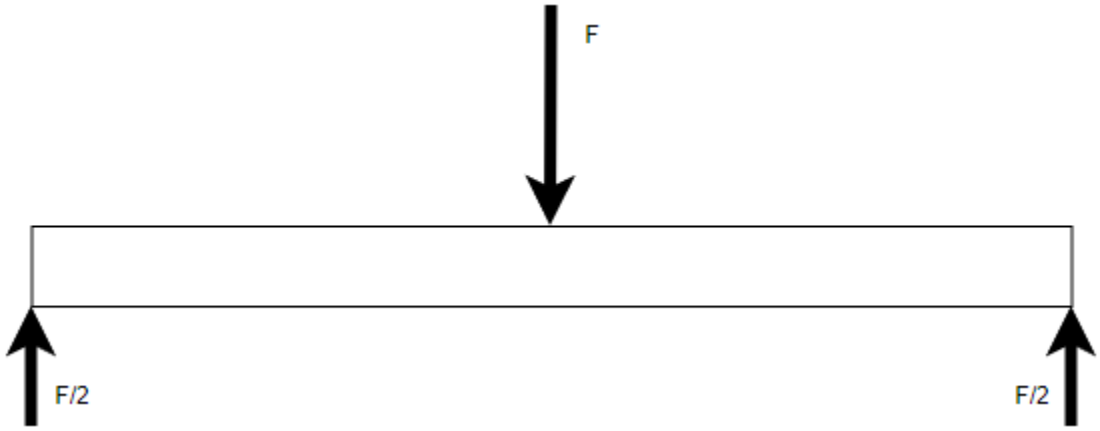

Figure 37: Tier Loading FBD

For the first initial analysis for each 80/20 shaft, a 1 in. by 1 in. cross-section was decided. The analysis would be done at the design load of 550 lbs. The analysis done on each shaft was for max deflection and max bending moment with forces placed as far apart as possible, or worst-case scenario, to check for structural failure. This would be for the case if the apparatus was testing a wing that was at the design's span limit. Equations (9) and (10) below are the equations used for this analysis, while Table 2 shows the results of the analysis.

$$y_{max} = \frac{FL^3}{48EI} \tag{9}$$

$$M_{max} = \frac{FL}{4} \tag{10}$$

Table 2: Whiffletree Initial Analysis Results For Tiers at Span Limit

Tier	Length (in.)	Force (lbs.)	Deflection(in.)	Max Moment (lb.*in.)
4	61	550	5.99	8388
3	23.5	275	0.17	1616
2	11	137.5	0.01	378
1	11	68.75	0.00	189

As shown in the table Tier 4 has a max bending moment of approximately 8388 lb.-in. As previously stated, for a 1 in. by 1 in. 80/20 shaft, the max bending moment before failure is 2981 lb.-in., Tier 4 has too high of a bending moment. Referring to equation (5), the only way to increase the max bending moment, in this case, is by either changing the material altogether or changing the geometry of the beam. The first method chosen to address the issue was changing the geometry. By making the 80/20 shaft a 2 in. by 1 in., as done in the top structure earlier, the max allowable bending stress becomes approximately 10,235 lb.-in. This now allows Tier 4 only to deflect .9 in.

and not to exceed the materials yield stress. Tier 4 will now not begin to yield until it reaches a force of 670 lbs. This is what defines the apparatus's structural limit.

Adaptation for Different Wing Planforms

The ability of the apparatus to adapt to different wing planforms is imperative to its success. Hence, as previously mentioned, 80/20 was found to be the perfect choice due to its patented T-slot. The T-slot in the 80/20 shafts allows members connected to each to slide across one another such as in the central structure, the vertical structure on the base structure can move out to allow for larger wings with wider bolt patterns to only require the need for the top plate to be changed out and for the structure to move to the new sized plate. Figure 38 displays the central structure at its max extension down the base structure.

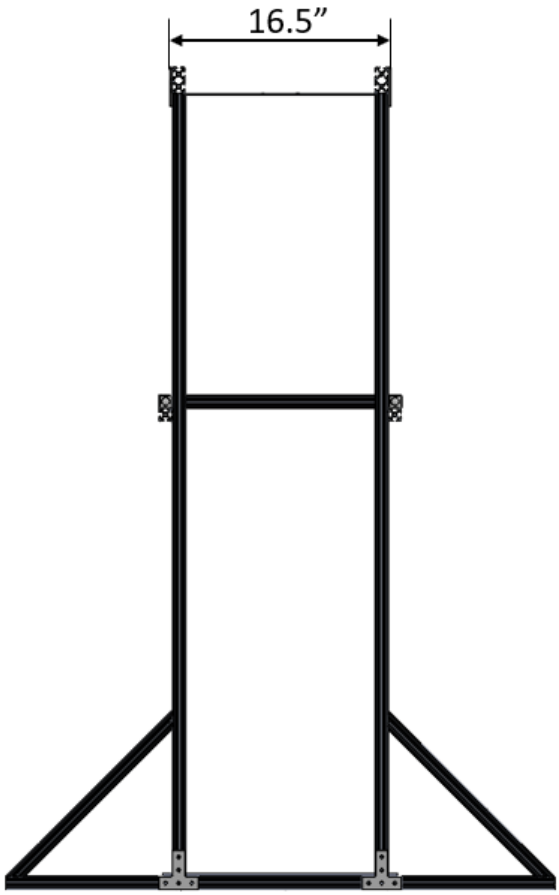

Figure 38: Central Structure at Max Extension

The use of the T-slot isn't only required for the central structure but also for the wing clamps. The point load along the chord is placed at the quarter chord, where generally, the magnitude of lift is at its greatest. Because this point is a function of the chord, the 80/20 shaft provides the required flexibility to account for the different chord lengths. Finally, the most important place for the T-slot is on the whiffletree. As mentioned previously, all tiers of the whiffletree are made from 80/20 shaft. This allows not only for the whiffletree to change for larger wingspans but also for different lift distributions.

With the structure designed to handle the appropriate loads, it is now time to show how this apparatus accounts for different wing planforms. A rectangular, or Hershey bar, wing has been shown, i.e., the wing in Figure 23 and Figure 24, but that wing is the most classic example of a wing. While there are different wing planforms such as elliptical, swept, and tapered, another factor that must be considered is how the wing attaches to the fuselage. Typically for high and low wing configurations, the wing is fastened to the fuselage via some type of hardware such as bolts or quarter-turn locks. Figure 39 shows the top-mounted wing of the UAV, Skyfall, designed and fabricated at OSU by the 2015 Orange Team for Speedfest. As viewed below, the wing has four holes, two in the front and two in the back, where the wing is screwed into the fuselage. This attachment can be viewed below in Figure 40.

Figure 39: Skyfall Top-Mounted Wing

Figure 40: Skyfall Wing Attached To Fuselage

Mid wings, however, tend to be two-piece wings. These wings tend to have a spar that goes through the fuselage that acts as an alignment hole for the wing, along with an anti-rotation pin that can sometimes be the aft spar. Figure 41 displays the port wing for a two-piece wing, while Figure 42 displays an example of that two-piece wing being connected with its fuselage. Notice the wing has a single spar tube and a built-in pin the wing to keep the wing from rotating. In case the anti-rotation pin is also the attachment method for keeping the wing attached to the fuselage. This UAV was also developed at OSU by the Orange Team for Speedfest in 2020.

Figure 41: Port Wing For Two-Piece Wing

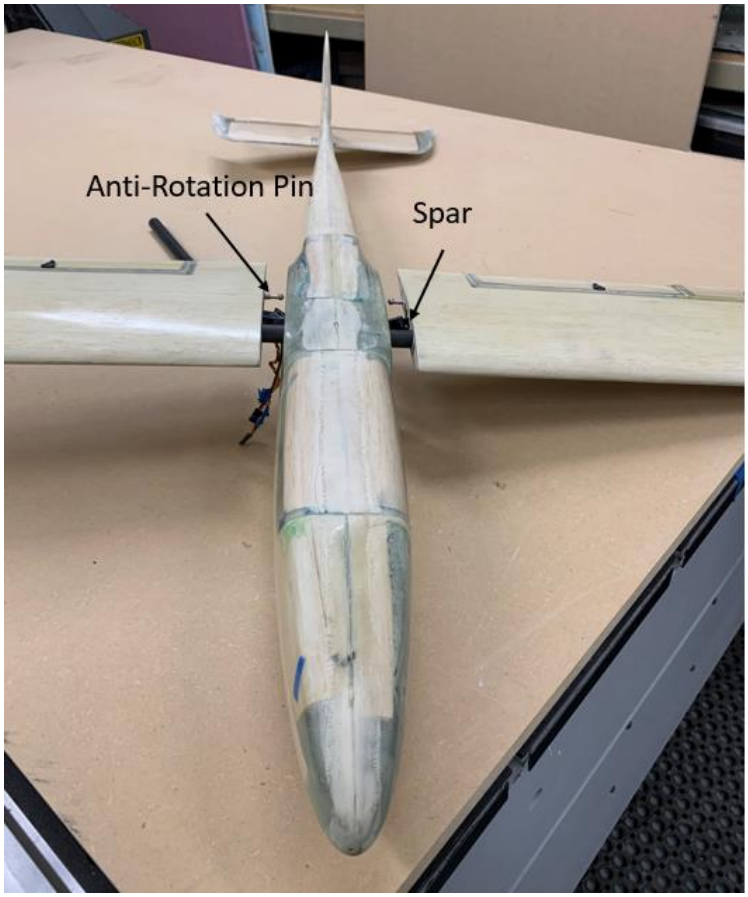

Figure 42: Two-Piece Wing Attachment

To account for these different wing types and attachment methods, there are several options to modify the mounting plate to adjust for these different wing types and mounting methods. As shown previously, the full piece rectangular wing in Figure 23 and Figure 24 is a top-mounted

wing, so the wing in the CAD views actually portrays the wing upside down due to the whiffletree pulling down to the ground. To adjust for a bottom-mounted wing, the mounting plate would simply move from under the top structure to on top of the top structure. The wing would then be fastened to the plate just as it would be to a fuselage. Figure 43 displays how the apparatus would be applied.

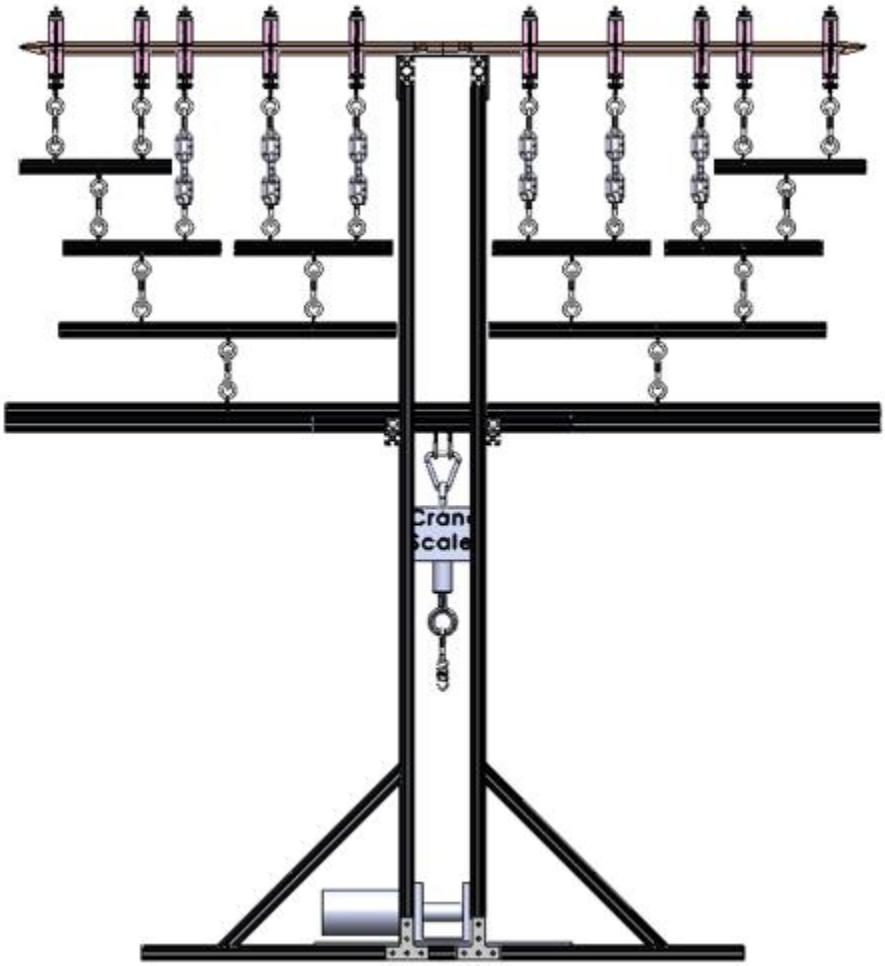

Figure 43: Apparatus With Bottom-Mounted Wing

Next, let's take a look at a two-piece wing. A two-piece wing is a little more tricky for testing but still possible. For a two-piece wing, the mounting plate will require flanges to act as the sides of the fuselage. This can be seen below in Figure 44 and Figure 45.

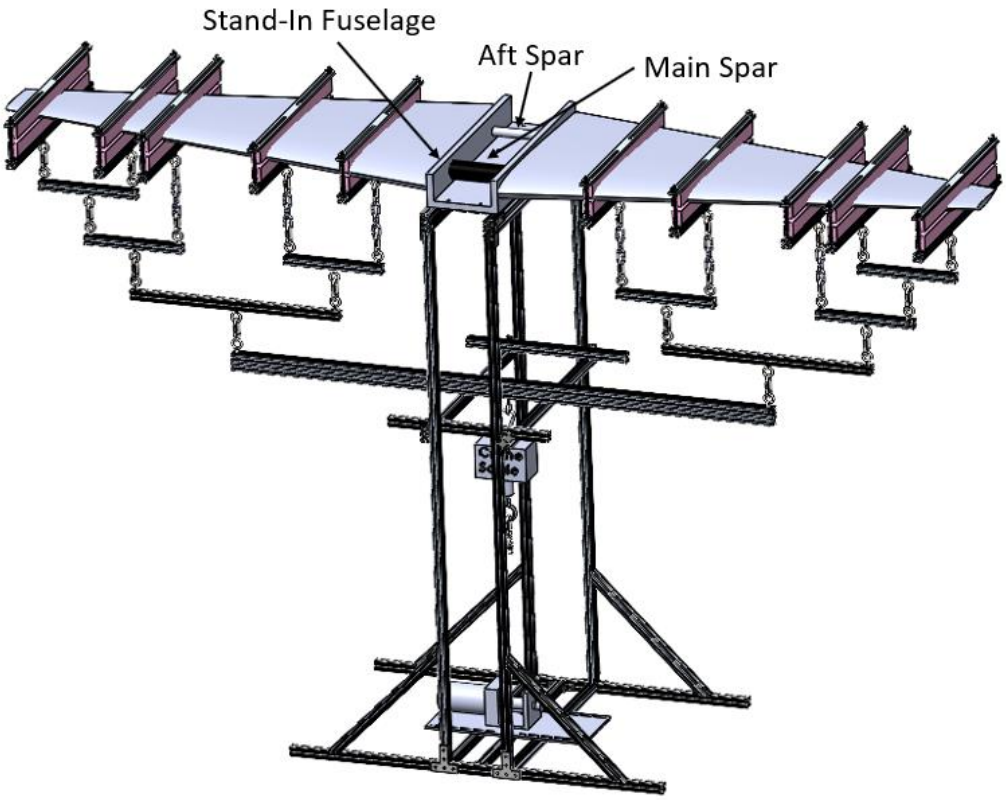

Figure 44: Apparatus With Two-Piece Wing Isometric View

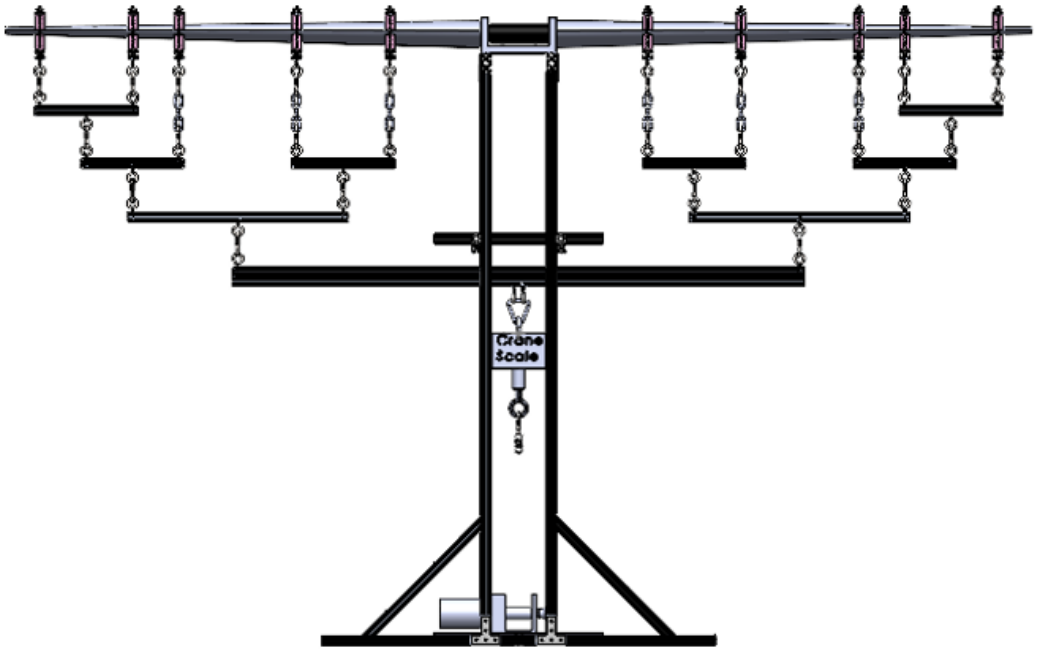

Figure 45: Apparatus With Two-Piece Wing Front View

Figure 44 and Figure 45 display a tapered two-piece wing at the max design wingspan and root chord of 102 in. and 24 in. Finally, another unique aspect of the design to accommodate for a swept wing is that the wing clamp eyebolts can slide down the chord to stay at the quarter chord of the wing so the wing can still be loaded properly. Figure 46, Figure 47, and Figure 48 display a front, side, and isometric view with this application.

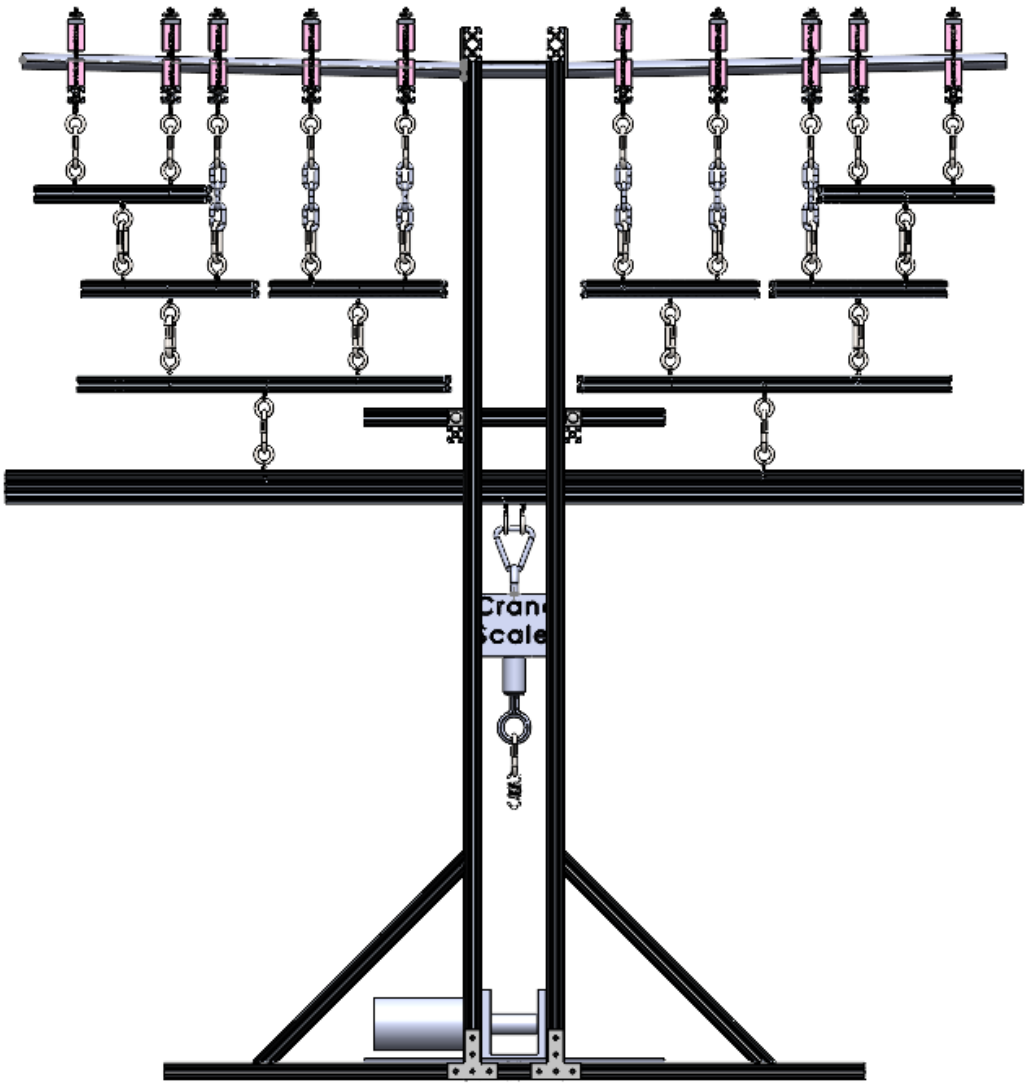

Figure 46: Apparatus With Swept Wing Front View

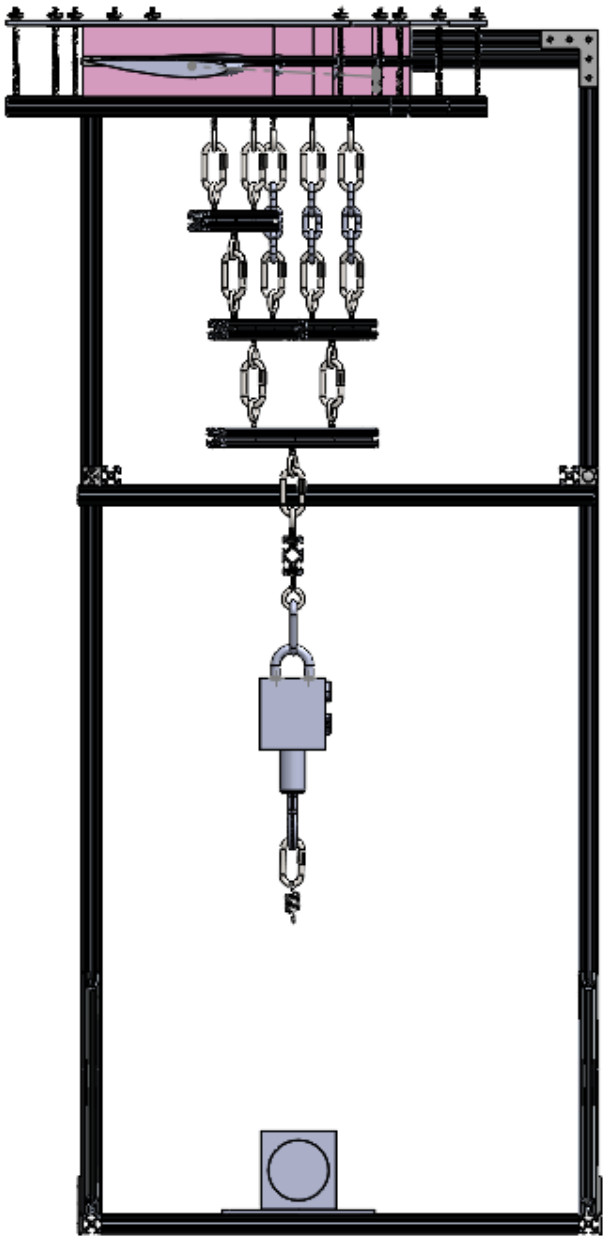

Figure 47: Apparatus With Swept Wing Side View

Figure 48: Apparatus With Swept Wing Isometric View

Now that the design has been designed to meet the apparatus requirements, it is now time to manufacture, assemble and test the apparatus to ensure it works as intended. This will be expanded upon in Chapter IV.

CHAPTER IV

FABRICATION AND PRELIMINARY TESTING ANALYSIS

This chapter will walk through the fabrication of the apparatus, then go through the initial concept decision to decide what a viable test was to do to prove that the apparatus distributes loads as expected. An uncertainty analysis will also be walked through and show why it is so important for an apparatus with so many moving parts working together.

Fabrication

With the design completed, it was now time to fabricate the apparatus. Fabrication of the apparatus first consisted of using a CNC waterjet to cut the slots and holes inside of the top and bottom mounting plates, the brackets used for connecting the 80/20 members, and the top bars for the wing clamps. Then, the 80/20 shafts were bought and cut to their correct lengths via a miter saw. Finally, with everything cut to size, it was time to place hardware where required to assemble the apparatus. The entirely fabricated and fully assembled apparatus can be viewed below in Figure 49 and Figure 50. An aluminum beam to act as the wing is placed on the top mounting plate to display all the subassemblies in use together.

Figure 49: Full Assembly Front View

Figure 50: Full Assembly Side View

Rationale To Validate Loads Distributed By Apparatus

Once fabrication of the apparatus was completed, there was still a need for investigating if the loads from the apparatus would transfer from the whiffletree to the wing clamps as expected. Testing a composite wing or even a metal wing to validate the loading characteristics of the apparatus due to the prediction of failure or tip deflection is much more complicated due to all the

components and complex cross-sections. Because of these reasons, it was decided that something simple and more predictable was required. It was decided that the best way for investigating this was to test a metal beam that has a known/proven deflection. A simple cantilevered aluminum tube with a 1 in. height and width along with a 1/16 in. wall thickness was decided to be the test specimen. Now that a specimen had been decided upon, it was now time to decide how to cantilever the beam in the apparatus and to do a theoretical deflection analysis for the beam to be later compared to the experimental data. To cantilever the beam, a simple bracket that could be bolted to the top mounting structure was decided. This bracket can be viewed and applied below in Figure 51 and Figure 52.

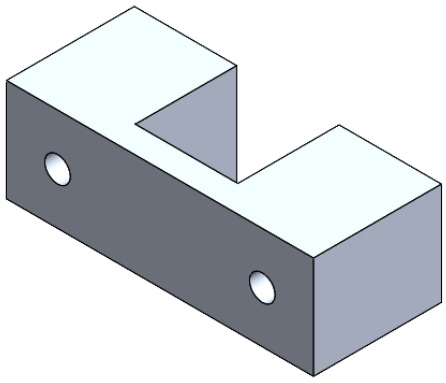

Figure 51: Bracket For Cantilevering Beam

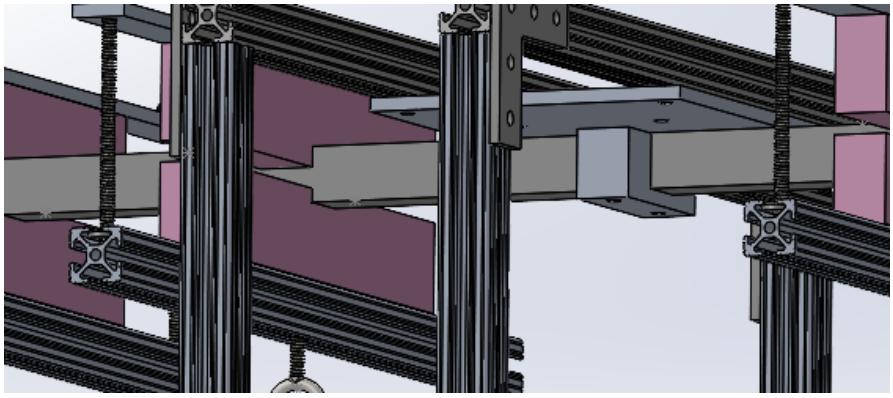

Figure 52: Bracket For Cantilevering Beam Applied

Now with the beam able to be cantilevered, it was time to do the theoretical deflection analysis for the beam. The first step taken was to decide where the loads would be placed along the span of the beam. Using the load placements that were decided for the earlier mentioned rectangular wing's shear diagram in Figure 19, they were applied as the basis for the validation beam analysis. The FBD for this beam with the applied load locations can be viewed below in Figure 53.

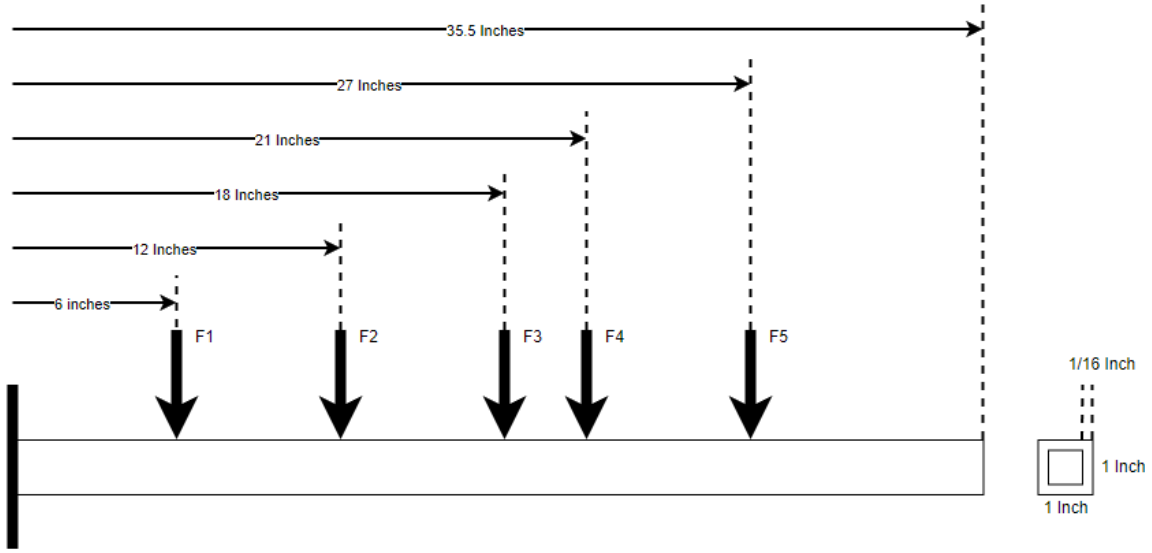

Figure 53: Validation Beam FBD

The length of the beam for the analysis was decided to be 72 in., with the cantilever bracket being applied to the center of the span, as shown in Figure 52. Because the width of the bracket is 1 in., the length of the cantilever beam is 35.5 in. instead of 36 in. Next, the amount of force to be applied to the beam was decided to be 100 lbs. distributed across the whiffletree. Now with the length of the cantilever beam, the placement of the loads, and the force of the loads decided upon, it was now time to begin applying the appropriate equations to find the theoretical deflection at the beam tip. The total tip deflection of the beam is the summation of the deflection at each point load and the deflection of the beam due to its own weight. The deflection equation for a cantilever beam with an intermediate load is displayed by equation (11), while equation (12) is the equation required for finding the max deflection for a uniform load, i.e., the weight of the beam itself. In these equations,

F represents the point load force, a is the force position relative to the cantilevered end, l is the length of the cantilevered beam, E is the elastic modulus, I is the moment of inertia, and w is the loading function spanwise the beam. In this case, w is the uniform distributed load created from the weight of the beam. These equations were derived from Shigley's 10th edition Mechanical Engineering Design [26].

$$y = \frac{Fa^2}{6EI}(a - 3l) \tag{11}$$

$$y = -\frac{wl^4}{8EI} \tag{12}$$

As previously stated, the summation of applying equation (11) to each point load along with the uniform load equation for the weight of the beam gives the theoretical tip deflection. The deflection calculations for each point load were compiled and can be viewed below in Table 3.

Table 3: Validation Beam Point Load Deflections

	F1	F2	F3	F4	F5
a (Force Position) (in)	6	12	18	21	27
Force (lbs)	12.5	12.5	12.5	6.25	6.25
Deflection (in)	-0.02	-0.08	-0.17	-0.11	-0.18

The summation of these deflections, along with the deflection from the weight of the beam, yielded a theoretical deflection of .58 in. Now with theoretical tip deflection solved, an uncertainty analysis must be done before testing can occur. This uncertainty analysis will be expanded upon in the following section.

Uncertainty Analysis

No measurement is perfect, whether it be because of human inaccuracy or the inaccuracy in the measurement device itself. Because of this, a theoretical number is not adequate enough for

an apparatus with so many moving parts that must be so precisely placed. No measurement is perfect and, therefore, will have a level of inaccuracy associated with all methods of measuring. To estimate and quantify a range of these inaccuracies together, an uncertainty analysis is used. In the apparatus developed, there are many areas that affect the final experimental result. In the case of studying the tip deflection of the previously mentioned aluminum beam, there is an overall uncertainty for many components, such as the placement of the wing clamps, the load cell used to track the force, and even the dimensions of the beam itself. Therefore, an understanding of the overall uncertainty in the beam's tip deflection is crucial because of the inaccuracies and local uncertainties of components that propagate to affect the final result. To account for this propagation of uncertainty for the beam's tip deflection, it was decided to use Smith-Kline's method for propagation of uncertainty [31]. Equation (13) shows the general form of this method, where W is the uncertainty, R is the equation of interest, and x_1-x_n is the indicated variable in the equation.

$$W_R = \sqrt{(\frac{\partial R}{\partial x_1} W_{x_1})^2 + (\frac{\partial R}{\partial x_2} W_{x_2})^2 + \cdots (\frac{\partial R}{\partial x_n} W_{x_n})^2} \tag{13}$$

This equation will take into account all of the uncertainties that affect the final result and give the overall uncertainty for the equation of interest. This method is applied by taking the equation of interest and for each variable taking the partial differential of the equation of interest to multiply it by that variable's associated uncertainty and then squaring that value. Doing this for each variable in the equation, summing the values, and taking the square root of the sum, finally gives the overall uncertainty.

To better understand this process, let's look at an example of the Smith-Kline method being applied to an equation. As previously stated, there is uncertainty in the dimensions of the aluminum beam meant for testing. This shows a case for even an object bought "off the shelf," and that is mass-produced, displays that there are still manufacturing errors that much be taken into account.

The moment of inertia is in every calculation for finding the total deflection of the aluminum beam. From the manufacturer, there are uncertainty specifications for the height, width, and wall thickness of the beam cross-section. As viewed below, equation (14) is the equation for solving for the moment of inertia of the square tube used for the experiment.

$$I = \frac{wh^3}{12} - \frac{(w-2t)(h-2t)^3}{12} \tag{14}$$

By applying Smith-Kline's propagation of uncertainty equation to the moment of inertia equation, equation (15) is created.

$$W_I = \sqrt{(\frac{\partial I}{\partial w}W_w)^2 + (\frac{\partial I}{\partial h}W_h)^2 + (\frac{\partial I}{\partial t}W_t)^2} \tag{15}$$

Now using equation (15), the total uncertainty for the moment of inertia can be solved. In this case, the moment of inertia for the square tube was .034 $in.^4$ ± .003 or ± 8.8%.

There are over 20 values that have an uncertainty that propagate to the overall uncertainty of the theoretical deflection value. This means there are over 20 variables that can make the experimental value differ from the theoretical value. This is why a complete uncertainty analysis is imperative because it's impractical to be as perfect in an experimental setting as in a theoretical setting. After doing the complete uncertainty for the deflection equations (11) and (12), the uncertainty of the theoretical beam deflection (.58 in.) was found to be ±.029 in. (±5%). This means that when testing, instead of having an acceptable singular value, there is an acceptable range of values. Below, Figure 54 displays a deflection vs. applied pulling force by the winch chart with uncertainty bars at each point to show the acceptable range values for the aluminum beam. While Figure 55 displays the associated uncertainty percentage vs. applied pulling force by the winch.

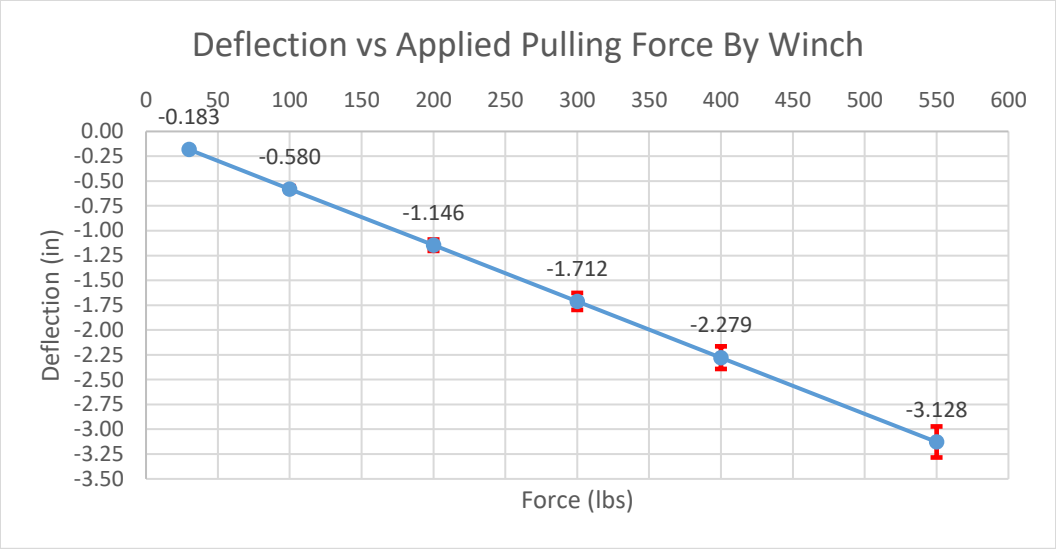

Figure 54: Deflection vs. Applied Pulling Force By Winch For Al Beam

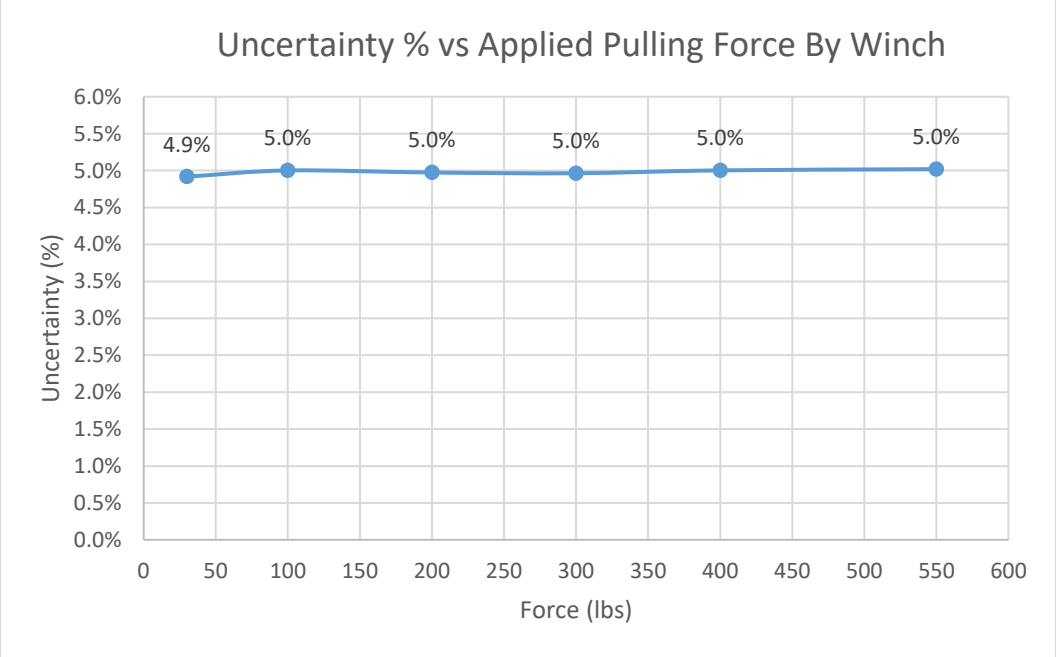

Figure 55: Uncertainty vs. Applied Pulling Force By Winch For Al Beam

As shown above, the uncertainty percentage as a function of force is slightly lower at the lower forces; however, it then converges to 5% at around 100 lbs.

A complete, or at least thought to be complete, uncertainty analysis was done before testing the apparatus. However, an interesting discovery came about when testing the aluminum beam. In

testing, four load cells were added to the four most inboard wing clamps. This was done to check if the values were equivalent. While they were expected to be equivalent, it was found that they were not. This can be viewed below in Figure 56.

Figure 56: Whiffletree With Wing Clamp Load cells

Although they were not equal, the magnitude of the point loads was within 1% of the expected force over that area. This was significant because this meant that the expected load was still being transferred to the beam and that there was little to no loss of force throughout the whiffletree. At first, it was thought to be something to do with the foam inserts used to distribute the force to the beam. This was investigated by using a denser foam that would not deform under the applied loading. This foam can be viewed on the right in Figure 56. However, after testing this initial theory,

it was found that this was not the reason for the load disparity. The next step in investigating the load cell disparity was the possibility of the loads being unequal due to the eyebolts not being perfectly placed on the 80/20 shaft. Originally the uncertainty of the whiffletree subassembly was not adequately factored into the complete uncertainty analysis of the beam deflection. This was because it was incorrectly assumed that the uncertainty for the forces applied to the beam was half of the resolution of the primary load cell for the apparatus. Now that it was recognized that the initial force uncertainty assumption was incorrect, an uncertainty analysis was done on one of the tiers of the whiffletree. A generic FBD for an individual whiffletree member can be viewed below in Figure 57. By using basic statics, equation (16) was developed.

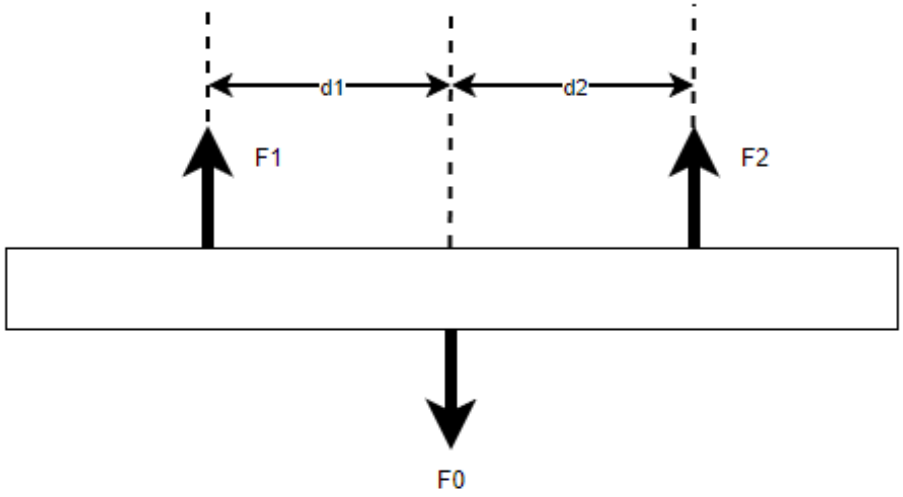

Figure 57: Whiffletree Member FBD

$$F1 = \frac{F0d1}{d1 + d2} \tag{16}$$

With equation (16) developed, by applying the Smith-Kline Uncertainty equation (Eq. (13)) to this equation for tier 1 beams, the uncertainty was found to be approximately ±3%. This approximation

is most sensitive to the distances of d1 and d2. This was later tested as a practical exercise on the apparatus and proved that moving the eyebolts does change the load at the point. Having this uncertainty approximation is very important because force is the second strongest driving factor of overall uncertainty after the inertia of the beam. While a ±5% overall uncertainty is favorable for the planned application in OSU's composite fabrication lab, this, however, may not be for future research and, therefore, may require another user to look into limiting the uncertainty in the whiffletree.

CHAPTER V

TESTING AND RESULTS

With the apparatus fully assembled, a defined experiment, and the preliminary analysis completed, it was now time to begin testing. This chapter will go through the initial flaws found in the design, how those flaws were addressed and fixed, procedures for setting up the apparatus for testing, the experimental setup for the three experiments conducted with the apparatus, and finally, the results of those experiments.

Flaws Found After Apparatus Fabrication

The first test done with the apparatus was the previously mentioned validation beam and was to better understand all of the components working together. This first test gave many insights into minor flaws in the system that affected the overall results. As mentioned in Chapter III, the first test did not have the ESC, transmitter, receiver, and the tensioning spring. During the first test, it was noticed on the load cell that the tension could not adequately be held. The load cell would rise to a selected value and instantly begin to lower significantly. This was thought to be caused by the synthetic rope that came with the winch, stretching, and the slack in the spool. To alleviate this issue, the synthetic rope was replaced with a steel cable. While the steel cable did help with the stretching issue, the slack issue on the spool was magnified due to the cable not being able to meet the bending radius of the spool. However, because the length of the steel cable did not need to be the total 10 ft. reducing the overall length of the cable to a point where it did not require as many

rotations around the spool helped significantly with the tension loss due to slack. Although with this change, the tension was held better, it was not yet adequate enough. Finally, to better resolve the tensioning issue, a spring was added between the winch and the load cell to keep a constant tension between the two. This can be viewed below with the tensioning spring linking the load cell and winch.

Figure 58: Tensioning Spring Applied To Apparatus

With the addition of the spring, it was able to nearly fully resolve the tensioning issue. Now when applying the force, the load could be kept in tension and did not drastically drop after reaching the selected value.

Next, with the tensioning issue solved, another flaw was found in that the remote control that was provided with the winch pulled at too high of a rate. This caused the load to jump very quickly on the order of 10-20 lbs. This was very unfavorable, so a new method needed to be investigated to alleviate this new issue. The first thought to reduce the rate of pull was to add a pulley to the system to halve the rate. However, after more thought, it was realized that what really needed to be minimized was the impulse from the winch imparted to the load cell. Therefore, while adding a pulley to the system would halve the pull rate, it would also double the force because it

would give the winch a mechanical advantage. Because impulse is a force multiplied by the change in time, the pulley would net no change in the impulse that needed to be lowered. The next idea to try was to add an ESC to the system that could then be connected to a potentiometer. The addition of the ESC worked to expectation and significantly slowed the rate of the winch to allow the load to only jump from 2-8 lbs. at a time. Now with the ESC proven to work, a new problem arose in that now the remote used initially was no longer usable. To control the winch remotely, it was decided to use the Flysky transmitter and receiver mentioned in Chapter III. This allowed remote control while still allowing fine controlling of the winch.

Procedures For Setting Up Apparatus For Testing

This section will go over the general procedures for setting up a test on the apparatus. If reference is needed for terminology, please refer to Figure 28, Figure 33, Figure 35, and Figure 36.

1) Decide what wing is being tested and what its attachment method is, i.e., top-mounted wing, bottom-mounted, or two-piece wing
2) Modify the top mounting plate to simulate the attachment method of the selected wing.

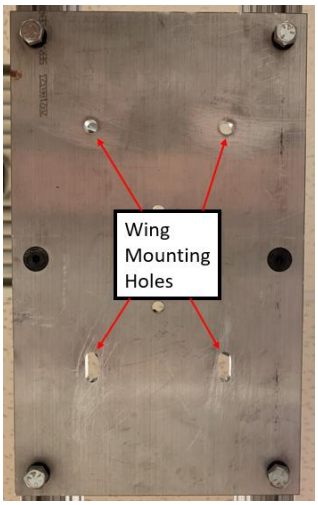

Figure 59: Top Mounting Plate Modified For Wing Attachment

3) Define and mark locations of where the point loads need to be located for simulating shear and moment on wing.

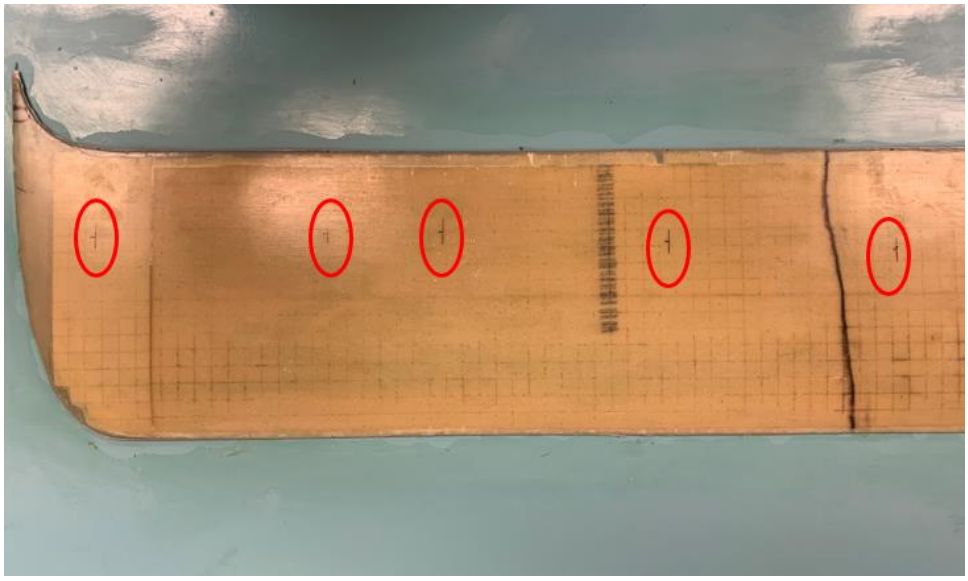

Figure 60: Wing Marked For Wing Clamp Placements

4) Adjust eyebolts on whiffletree tiers to appropriate locations for defined point loads from step 3.

5) Adjust eyebolts on wing clamps to the desired location along the chord.

Figure 61: Wing Clamps With Eyebolt Location

6) Cut foam insulation spacer for wing clamp via bandsaw, hotwire, or Exacto knife.

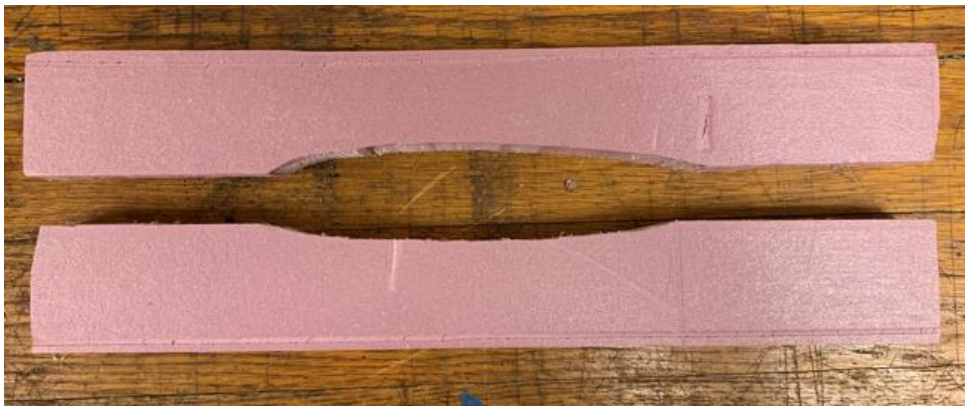

Figure 62: Wing Clamp Foam Insert For Wing

7) Move vertical structure into place for attachment of top mounting plate.

8) Attach the top mounting plate to the top structure.

9) Attach wing to top mounting plate.

Figure 63: Top Mounted Wing Attached To Top Mounting Plate

10) Align vertical ruler stands next to wingtips and record the height of wingtips from the ground. This is for setting the datum for measuring deflection.

11) Attach wing clamps onto the wing in their appropriate locations.

Figure 64: Applied Wing Clamps Front View

Figure 65: Applied Wing Clamp Side View

12) Verify that all wing clamps are placed in appropriate locations.

13) Attach Tier 1-3 of the whiffletree to the wing clamps via the connecting links. This allows the whiffletree assembly to be broken up into port and starboard sides so the tiers may be attached one side at a time and not both at once.

Figure 66: Applied Whiffletree For Tiers 1-3

14) Attach Tier 4 to the connecting links of Tier 3 to link both sides of the whiffletree together.

Figure 67: Tier 4 Applied To Whiffletree

15) Attach load cell to the bottom connecting link of Tier 4. This should now be approximately 30 lbs. of load distributed to the wing or sometimes referred to as the pre-load weight.
16) Ensure all connecting links are fully closed.
17) Loosen and move the mounting bottom plate to where the winch cable is in-line vertically with the whiffletree and load cell.
18) Define what tensioning spring is required for loading the wing. The tension spring should be engaged when the planned test load is reached.
19) Power on the load cell.
20) Attach tensioning spring to load cell. If the spring attachment point is too small for the load cell hook, add the spare connecting link that will fit between the load cell and tensioning spring.

Figure 68: Tension Spring

21) Attach winch cable to tensioning spring.

22) Turn on the transmitter and plug in the power supply. Ensure the ESC switch is on and the receiver is plugged in. Make sure to turn the transmitter on first before plugging in the power supply.
23) With everything powered, retreat to a safe distance from the apparatus.
24) Using the transmitter, begin turning the winch.
25) Use load cell to indicate load on test wing and load to the desired load or until wing reaches failure.

Experimental Setup

This section will overview the experiments being conducted and the experimental setup for each. There will be three experiments in total.

Experiment #1

The first experiment conducted was the previously mentioned aluminum beam deflection experiment in section 4.2 for validating the load transfer throughout the whiffletree. This was also done to prove repeatability in the system and to simulate proof loading tests for a wing. Because this experiment is to show repeatability and to prove its loading characteristics, multiple tests were conducted for this experiment. This experiment was conducted by loading the aluminum beam to 100 lbs. because the load of the whiffletree, or pre-load weight, is 30lbs, the load cell read roughly 70 lbs. The deflection of the beam was measured on both sides via vertically mounted rulers, shown in Figure 66. When setting the datum and measuring the deflection, the beam was measured at its neutral axis. This data was initially recorded through pictures and input into an Excel spreadsheet, but due to an apparent parallax error in the photos, data was recorded via notebook and then input into an Excel spreadsheet.

Experiment #2

The second experiment conducted after the deflection experiment was finished was to simulate a failure test using the aluminum beam. Because part of the apparatus's function was to be able to test wings to failure doing so on the aluminum beam was significant because of the known yield stress of the material. The setup was the same as in the first experiment, with the loads placed in the exact same locations, except now the load was applied to and past the allowable max bending moment of the beam. Once the theoretical value for the allowable max bending moment was found, it was used as a guide to know how much force was required to be applied to the beam. Because of the elastic properties of the aluminum beam, the only way to know when it had reached its yield point was to apply the load and then release the force and check if the beam had permanently deflected. To know if the beam had permanently deflected after applying a load, the vertical rulers from the first experiment were used to measure the deflection with the beam with the pre-load weight on the beam. Having the pre-load weight on the beam before setting the datum on the ruler was very important because after applying a load and checking for permanent deformation, the pre-load weight would still be attached to the beam. Removing the whiffletree to check for permanent deformation would be cumbersome and increase the potential of introducing errors in the experiment, and therefore setting the datum after attaching the whiffletree is more favorable. Just as in the first experiment, the datum and deflection measurements were evaluated at the neutral axis.

Experiment #3

Finally, the third experiment conducted was testing a composite wing to failure. The whiffletree configuration for testing the wing was moved 1 in. inboard of the previous tests on the aluminum beam. Now the point loads from the half-span of the wing are at a distance of 5 in., 11 in, 17 in., 20 in, and 26 in. The wing used in this experiment was exactly like the wing viewed in previous Solidworks models, except with a slightly smaller span. The overall dimensions and airfoil of the wing used in this experiment had a span of 55.5 in., a chord of 7.5 in., and used a NACA

2412 airfoil. This wing was designed and fabricated at OSU and is comprised of a fiberglass skin, carbon tow spar caps, cross-grain balsa shear web, and aircraft plywood ribs. Below, Figure 69, Figure 70, and Figure 71 display internal top and side views of the wing along with the actual fabricated wing used for testing.

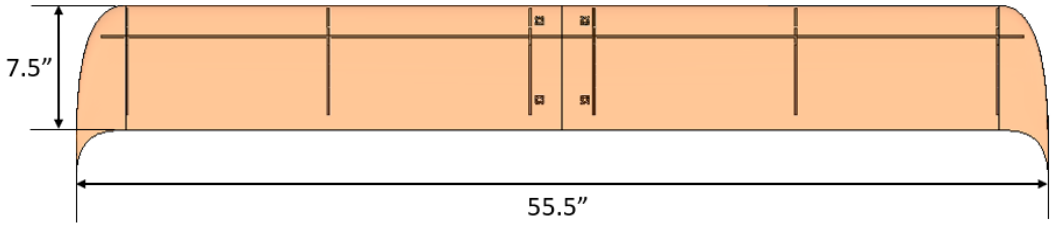

Figure 69: Experiment 3 Test Wing Internal Top-View

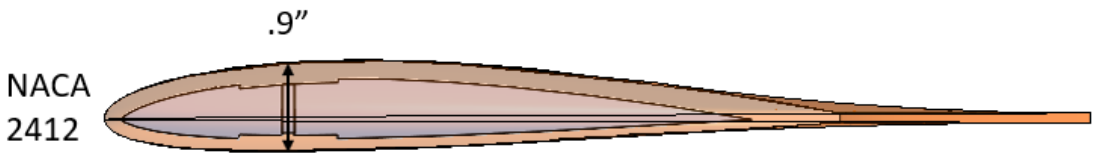

Figure 70: Experiment 3 Test Wing Side-View

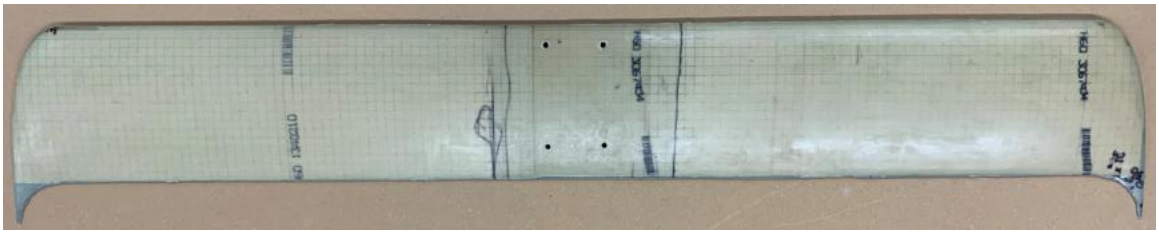

Figure 71: Fabricated Experiment 3 Test Wing

The wing’s skin has a layup of 90/45/Divinycell Foam/45/90. The divinycell foam, shear web, and ribs are each 1/8 in. thick. Before setting up the experiment, an estimated value needed to be estimated for when the composite wing would fail. To estimate this value, a Wing Spar analysis program that was developed at OSU’s composite aerospace assembly lab for designing composite wings was used to estimate the failure mode and value of failure. This program takes inputs for the geometry of the wing and I-beam spar along with the material properties for the spar caps and shear

web. Before calculating stress and strain on the spar, the spar is transformed into a homogenous material using the transform area method. To calculate the stress and strain on the spar, the program calculates the aerodynamic loads on the wing and applies these loads to the spar. Once the calculations are finished, the program outputs if the spar is within the limits of the flight envelope and will not fail or if it will fail in either pure shear, strain, compressive failure due to bending, tensile failure due to bending, or shear buckling. The inputs and results for the Wing Analysis program can be viewed below in Figure 72 and Figure 73.

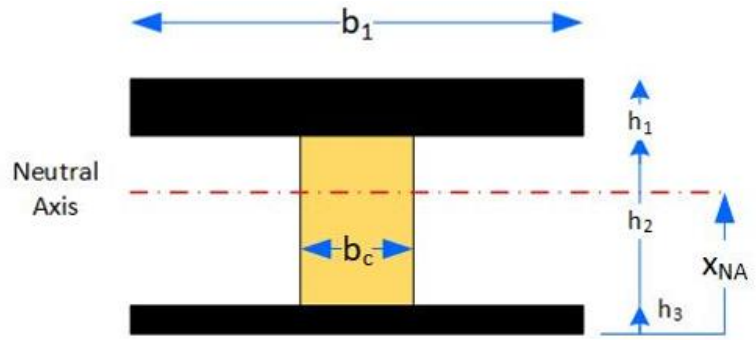

SPAR INPUTS

$h_1 \equiv 8 \cdot 0.005$ Spar cap thickness (compression) [in]

$h_3 \equiv 8 \cdot 0.005$ Spar cap thickness (tension) [in]

$b_1 \equiv 1$ cap width [in]

$b_c \equiv .125$ core width [in]

$E \equiv 135 \cdot 145 \cdot 1000 = 1.957 \times 10^7$ Youngs Modulus of spar cap material [psi]

$E_c \equiv 7116$ Youngs Modulus of core material [psi]

$\sigma_{ult\_c} \equiv 174000$ Ultimate compressive strength (cap) [psi]

$\sigma_{ult\_t} \equiv 217000$ Ultimate tensile strength (cap) [psi]

$\tau_{ult} \equiv 900$ Ultimate shear strength (core) [psi]

$V \equiv 227$ V Airspeed [ft/s]

$\alpha g \equiv 15$ Angle of attack

$W \equiv 7$ Weight of plane (if g load needed)

status = "SHEAR FAILURE !"

Figure 72: Wing Spar Analysis Spar Inputs

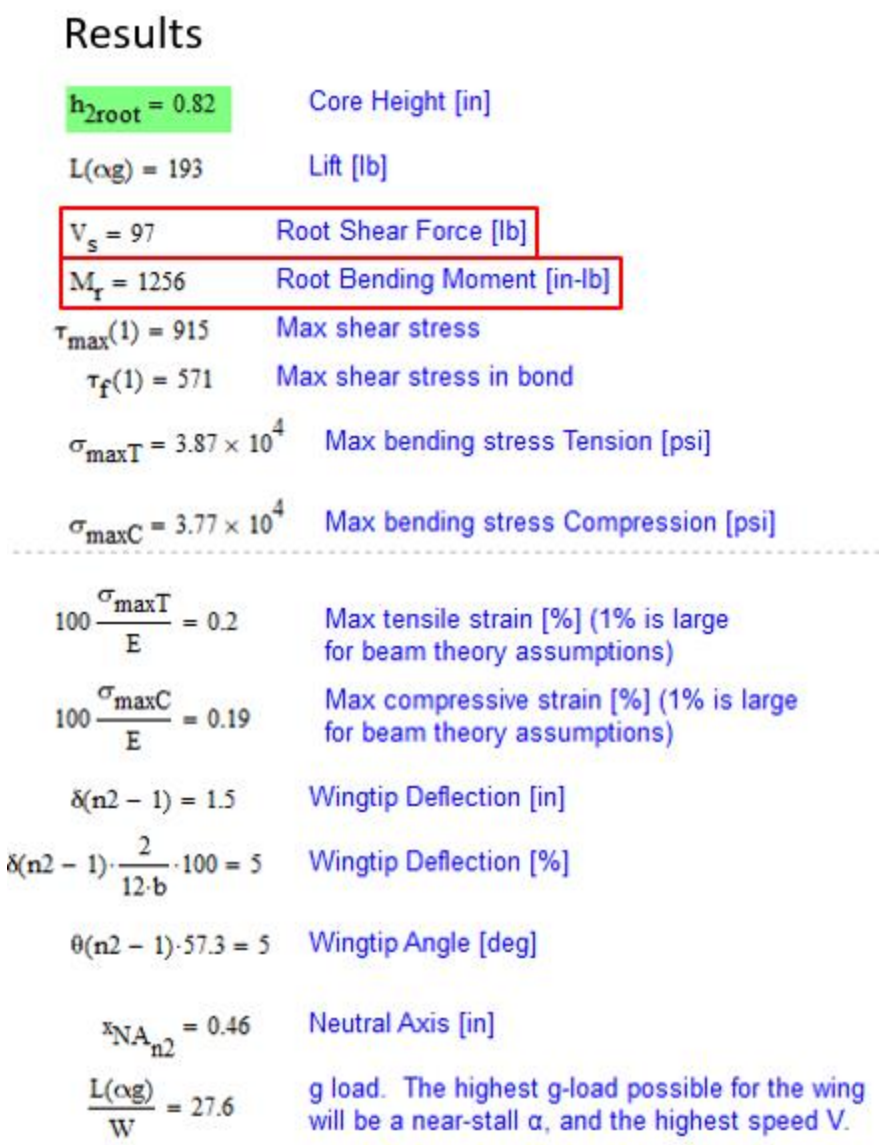

Figure 73: Wing Spar Analysis Results

As viewed above, the wing is expected to fail in shear at a root shear force of 97 lbs. The root shear force and bending moment were noted to be compared to the experimental data after testing was finished.

Setting up for this experiment, the procedures list from the previous section was used. Taking note of the wing's height with the vertical rulers before adding the pre-load weight was done to set the deflection datum. Because this is an experiment that tests the wing to failure, the test was recorded to know the exact value of failure and deflection of the beam. The sum of the

load cell's value at failure and the pre-load weight divided by two gives the maximum root shear. The sum is divided by two due to the attachment method (square four-bolt pattern); it fundamentally creates two cantilever beams. However, to get the maximum bending loading on the wing, a static analysis is required.

Results

Experiment #1

Figure 74: Aluminum Beam Deflection Experiment

In the first experiment with the aluminum beam, two beams were used with a total of 17 tests. After the fourth test, the first beam was noticeably yielded and was determined to be done so sometime between tests 3 and 4. As mentioned earlier, in the first test, the system had issues with holding tension, and because of that, it was concluded that it was the reasoning for the two sides to differ so much and to be so much lower than expected. However, before this conclusion was made, a theory that the twist of the beam was causing a stiffness difference from one side compared to the other. It was believed that the aluminum beam was work hardened when manufactured and possibly could've caused the beam to be stiffer. This is because work hardening decreases ductility and can increase the strength of the material; this at first seemed very plausible. However, after more research and consideration, the realization that stiffness and ductility are not related due to stiffness being directly related to the material's elastic properties, while ductility is directly related to the material's strength properties. While work hardening does change the material's strength properties, reducing ductility, it does not affect the material's elastic modulus and therefore does not affect the stiffness characteristics of the material. The consideration of the inertia being different on the more twisted side was also considered; however, due to the cross-section of the beam being symmetrical across the vertical and lateral axes, the inertia is the same in any rotated configuration.

As previously stated, there were a total of 17 tests conducted; however, there are 34 data points because the deflection of the beam was measured on both the left and right sides. Figure 75 displays the experimental data gathered from these tests.

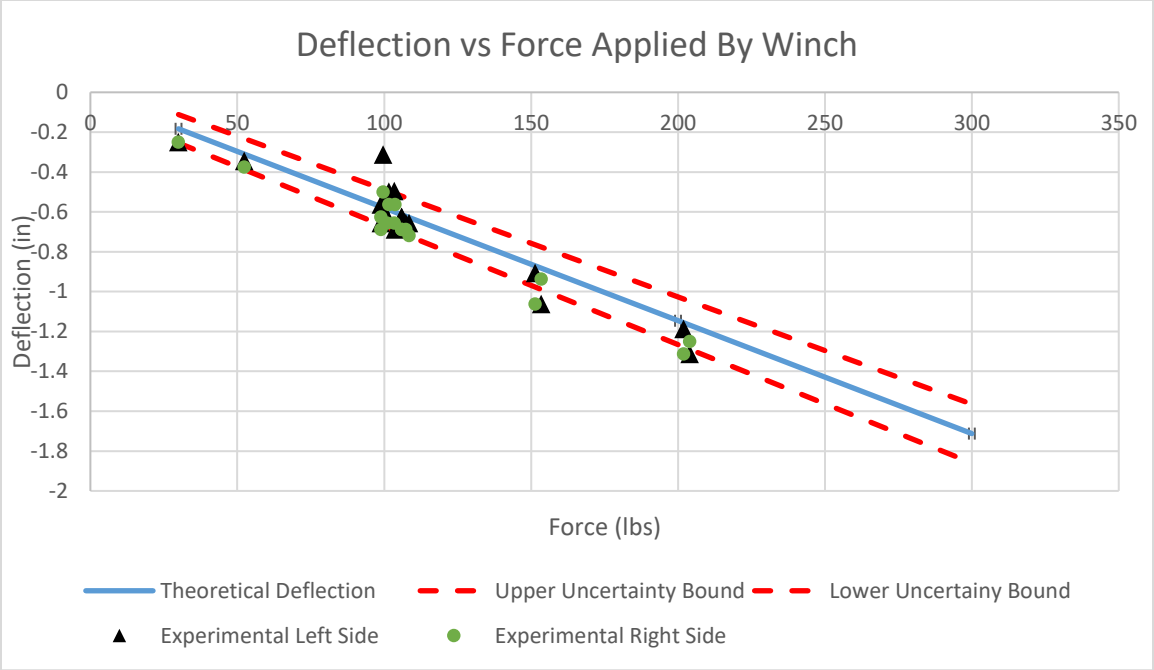

Figure 75: Experimental Deflection vs. Force Data

As shown above, the experimental data is plotted along with the theoretical deflection vs. the force applied from the winch. In this case, if the beam were a wing, the force would be the total lift created by the wing. The uncertainty bounds are also plotted on this chart. As mentioned earlier, the uncertainty for the deflection of the aluminum beam was ±5%. In this upper and lower bound case, it also accounts for the uncertainty of the measurement device (vertical ruler) used to physically measure the deflection of the beam. In this case, the vertical rulers, as seen in Figure 49, the uncertainty of the ruler is 1/16 of an inch, which is half the resolution of the ruler. Therefore, the uncertainty bounds graphed in Figure 75 were ±5% ±.0625 in., or ±15.7%. This ±15.7% does not apply to the shear and bending moment because those are measured by the load cell and are already accounted for in the full uncertainty analysis conducted earlier. The data above displays that the apparatus can repeatedly be predicted for a specific deflection and provides strong confidence that forces applied and distributed throughout the whiffletree are indeed transferring to the beam as expected.

Experiment #2

Figure 76: Aluminum Beam Yield Experiment

The deflection tests previously conducted not only were to prove the apparatus's accuracy and repeatability but also to simulate a wing being tested to an ultimate or proof load specification. While one of the apparatus's goals is to test wings to proof loads, as previously stated, it is also intended to test wings to failure and to assist in finding weaknesses in wing designs. With the deflection tests for the beam completed, a failure test for the aluminum beam could now be conducted. Using equation (5) to solve for the max allowable bending moment before yielding, it was calculated to be approximately 2414 lb.-in. With the same whiffletree configuration for the

beam deflection tests, it was calculated that the required load to reach the max allowable bending moment to begin yielding the beam was approximately 322 lbs. As mentioned in the experimental setup, in this experiment, the beam had to be loaded and then released to be checked for permanent deformation. Because the expected failure load was 322 lbs. the beam was first loaded up to 300 lbs. and then checked for permanent deformation. There were no signs of permanent deflection as the beam went back to the previously set datum. Next, the beam was loaded to 330 lbs. and checked again. This time the beam had indeed shown permanent deformation as both sides of the beam were permanently deflected by .125 in. To check and ensure the beam was indeed in its plastic zone, the beam was loaded to 390 lbs. and then evaluated for its new deflection. This gave a value of .5 in. for both sides of the beam and left no doubt that the beam had exceeded its yield point. Because there was no way to know the exact moment the beam yielded, it could be concluded that the beam did yield somewhere between 300 lbs. and 330 lbs., which gives a percent error range of 2.5% to 6.8%. Figure 77 displays the aluminum beam permanently deformed from this experiment.

Figure 77: Permanently Deformed Aluminum Beam

Experiment #3

Figure 78: Composite Wing Setup Before Testing

Finally, for the third experiment, the aforementioned Wing Spar analysis program was used to estimate the failure mode and value of failure. It estimated the failure mode to be a shear failure with a max root shear of 97 lbs. During the test at around 140 lbs. an initial bit of cracking could be heard followed by a few more around 180 lbs. until eventually reaching its catastrophic failure at 209 lbs. This would mean the wing experienced a root shear force of 119.5 lbs, recall; as mentioned in the experimental setup section, the root shear force is the sum of the load cell value and pre-load weight divided by two. By doing a static analysis, the experimental bending moment was calculated. Table 4 displays the theoretical root shear force and bending moment values calculated earlier, along with experimental results and the percent error of the results. The percent

error for the root shear and bending moment were 23% and 33%, respectively. This is not surprising that the wing was slightly stronger than the estimated failure due to the Wing Spar Analysis tool only calculating for the spar and not the other components of the wing. Figure 78 and Figure 79 display before and after photos of the wing test.

Table 4: Composite Wing Test Results

	Theoretical	Experimental	Percent Error
Root Shear Force (lbs.)	97	119.5	23%
Root Bending Moment(lb.-in.)	1256	1673	33%

Figure 79: Composite Wing After Reaching Failure

After the wing had reached failure, it was time to fully unload the wing and detach it from the apparatus to be investigated for its failure mode. The only visible failure was that the wing had opened at the seamline of the wing, which in the wings case is its camber line. However, once the force was released, it closed and was no longer visible. The only way to see the burst seem was to reapply a bending moment to the wing. With the wing known to have an apparent failure somewhere on the wing, it was time to investigate and inspect the wing.

The first step in investigating the wing was to ensure the insulation foam used in the wing clamps distributed the force well enough and did not crush the fiberglass skin of the wing. As hoped, the insulation foam worked adequately in distributing the loads while not creating any areas of stress concentrations that the skin couldn't withstand. There were also no signs of buckling failure anywhere on the outside. The outside of the wing was unchanged after the test in comparison to the wing before testing. With the outside of the wing showing no failures, it was time to investigate internally. To investigate the spar, a section was cut out of the bottom side of the wing and can be viewed below.

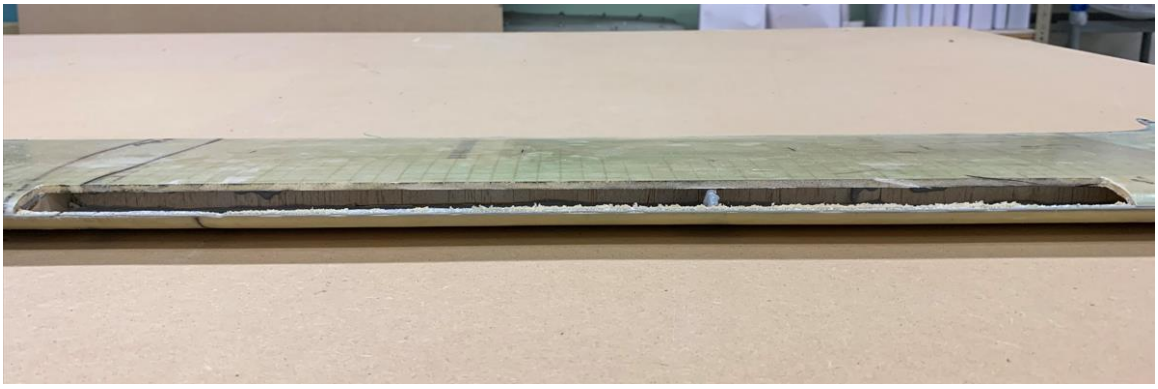

Figure 80: Wing With Cut Out Section

After cutting the wing open, it could be concluded that the wing failed in shear; however, it is uncertain if the wing failed from the shear in the shear web or the transverse shear going through the shear web and/or the epoxy bond of the shear web to the spar cap. Figure 81 and Figure 82 show a close-up of the wing's shear web at the root and at the quarter span of the wing.

Figure 81: Wing Shear Web At Wing Root

Figure 82: Wing Shear Web At Quarter Span

There is a clear shear failure at the root with a crack in the balsa that propagates vertically and then in the transverse direction along the epoxy bond line. Along with the crack at the root, another shear failure can be found at the quarter span. There is also clear debonding of the shear web from the epoxy, along with signs of debonding of the epoxy from the fiberglass skin. The break in the shear web at the quarter span is believed to have happened as a result of other failures beforehand. At the quarter span location, when the wing failed at 119.5 lbs. there was a clear large amount of torsion on the wing, which is believed to have caused the break at the quarter span. However, between the shear failure at the root or the debonding on the epoxy, there is no way to definitively say which happened first or if both happened simultaneously. This will require further investigation and tests that go beyond the scope of this research.

CHAPTER VI

SUMMARY AND FUTURE WORK

This chapter will wrap up all the knowledge gained from this research and the goals achieved from this thesis. Along with this, there will also be a section about future work this thesis could potentially lay the foundation for.

Summary

The motivation of this thesis was to develop a static structural testing apparatus for composite wings. In this thesis, the methods of static wing testing were expanded upon, an analytical approach to designing an experimental apparatus, to finally, testing and validating the design apparatus. This research conducted the design of an apparatus for testing small-scale UAS wings not commonly found in industry today and how difficult it can be to simulate the stresses lift creates on a wing structure. It also provided insight into how significant a proper uncertainty analysis is and must be considered for experiments using a similar testing method and or design. Finally, it provided questions about wing failure modes that can be studied in future research.

Goals Achieved

As previously stated in Chapter I, the goal of this thesis was to design an experimental apparatus for testing small-scale UAS wings, with the objectives of this research to reach this goal as follows.

1. Conduct an extensive literature review of how composite wings are currently being statically tested.
2. Design testing apparatus for static wing testing
    a. Be able to withstand simulating a wing loading for Group I and II UAS to at least 5 G's
    b. Have the ability to adjust load distribution for different wing planforms
    c. Be able to test large and small UAV wings
3. Manufacture and assemble testing apparatus
4. Conduct theoretical analysis to be compared to experimental data to validate the apparatus simulates loads as expected
5. Show how apparatus would be applied to different wing planforms

For this research to be considered successful, these objectives need to be met. Objective 1 was met addressed and met in Chapter II and led to the decision to use a whiffletree for the testing apparatus because of its superior ability to simulate the forces acting on a wing as opposed to other testing methods. Objectives 2 and 5 were met in Chapter III. Objective 2's sub-objectives were addressed by a thorough mechanical analysis of the highly modular 80/20 shafts used extensively throughout the design and sized for any Group I and Group II UAS to a loading of, at the very least, 5 G's. Finally, Objectives 3 and 4 were completed in Chapter IV. The deflection experiment chosen to validate that the loads were applied as expected was an experiment with a high figure of merit as it is used commonly in many mechanical behavior and material science courses as a fundamental way of comparing gathered experimental data to a theoretical analysis. This experiment not only validated the whiffletree applied and distributed loads as it was intended but also displayed the importance of a complete uncertainty analysis for all components of an experiment, including items bought "off the shelf." Finally, this research also meets a goal in the motivation section of Chapter I, in that OSU's composite aerospace assembly lab now has a better and more accurate way to proof load most UAVs produced in the lab for the long-term future of its work.

Future Work

While the research in this thesis is significant in better understanding the whiffletree and structural testing wings, there is much more future research that can be produced from this research. As mentioned in testing the composite wing to failure, there was no way of definitively knowing exactly how that wing had failed. Future research could be conducted in if the normal shear was the limiting factor or potentially the transverse shear. It could also be a case of poor surface preparation for bonding the components. With this apparatus fabricated and available at OSU, other failure modes outside of shear can be studied, such as root bending moment, compressive or tensile failure, and how the loads transfer through the wing when there is a control surface or cut open section in the wing. This research could be used to gather experimental data to be compared to theoretical analyses such as OSU's Wing Spar Analysis program or a finite element analysis. There are countless amounts of research that be helped from the research presented and could provide a greater understanding and knowledge of how composites fail and interact.

REFERENCES

[1] "OSU Aerospace Design," Oklahoma State University, [Online]. Available: https://aerodesign.okstate.edu/projects.html. [Accessed 21 March 2022].

[2] "AIAA," AIAA, [Online]. Available: https://www.aiaa.org/dbf. [Accessed 21 March 2022].

[3] Federal Acquisition Regulation, *14-CFR 23.307–Proof of Structure.*

[4] ASTM F3298–19, *Standard Specification for Design, Construction, and Verification of Lightweight Unmanned Aircraft Systems (UAS),* 2021.

[5] D. Pokhrel, "Aviation Nepal," 29 12 2019. [Online]. Available: https://www.aviationnepal.com/winglets-why-are-they-needed/. [Accessed 21 March 2022].

[6] "Sonex," 10 12 2010. [Online]. Available: https://www.sonexaircraft.com/onexarchive-121010/. [Accessed 21 March 2022].

[7] E. Stewart, "Kit Planes," Kit Planes, 21 March 2021. [Online]. Available: https://www.kitplanes.com/testing-testing/. [Accessed 21 March 2022].

[8] Y.-B. Park, K.-H. Nguyen, J.-H. Kweon, J.-H. Choi and J.-S. Han, "Structural Analysis of a Composite Target-drone," *Int'l J. of Aeronautical & Space Sci.,* vol. 12, pp. 84-91, 2011.

[9] "Ebrary," [Online]. Available: https://ebrary.net/59649/engineering/static_structural_testing. [Accessed 21 March 2022].

[10] "Elixir Aircraft," [Online]. Available: https://elixir-aircraft.com/en/news/wing-test. [Accessed 21 March 2022].

[11] G. Frulla and E. Cestino, "Design, manufacturing and testing of a HALE-UAV structural demonstrator," *Composite Structures,* vol. 83, pp. 143-153, 2008.

[12] N. Mufidatul Ula, A. Marta, Y. Giri Wijaya and M. Muksin, "Wing static test of LSU-02 NGLD aircraft using Whiffletree method," *AIP Conference Proceedings 2088,* 20119.

[13] M. J. Nicolas , R. W. Sullivan and L. W. Richards, "Large Scale Applications Using FBG Sensors:Determination of In-Flight Loads and Shape of a Composite Aircraft Wing," *Aerospace 2016,* vol. 3, no. 18, 2016.

[14] J. Paur, "Wired," 29 March 2010. [Online]. Available: https://www.wired.com/2010/03/boeing-787-passes-incredible-wing-flex-test/. [Accessed 21 March 2022].

[15] "Flight Global," [Online]. [Accessed 21 March 2022].

[16] W. A. Lokos, C. D. Olney, T. Chen, N. D. Crawford, R. Stauf and E. Y. Reichenbach, "Strain Gage Loads Calibration Testing of the Active Aeroelastic Wing F/A-18 Aircraft," NASA/TM-2002-210726, 2002.

[17] K. Yang, L. Zhang, S. Ji, Y. Yue and W. Ji, "STATIC TESTING AND ANALYSIS OF COMPOSITE WING OF A TWO-SEATER AIRCRAFT POWERED BY Li-ion BATTERY ELECTRIC PROPULSION," *Advanced Composites Letters,* vol. 25, no. 6, 2016.

[18] S. Chinvorarat1, B. Watjatrakul1, P. Nimdum1, T. Sangpet1, T. Soontornpasatch and P. Vallikul, "Static testing for composite wing of a two-seater seaplane," *IOP,* 2019.

[19] K. Yang, Y.-l. Guo, G. Ma, H. Geng, Q.-f. Li and J.-j. Xue, "Design and static testing of wing structure of a composite four-seater electric aircraft," *Sci Eng Compos Mater,* vol. 27, no. DE GRUYTER , pp. 258-263, 2020.

[20] B. Ramanaiah, H. Ramachandra, S. Sanjeev Kumar, . M. Kotresh, B. Varughese, R. Sundaram, G. Kamath and M. Subba Rao, "Challenges in Static Testing of Co-Cured Co-Bonded Composite Aircraft Structures," *National Conference on Scientific Achievements of SC & ST Scientists & Technologists,* pp. 69-82, 2009.

[21] J. Simsiriwong, "STRUCTURAL TESTING OF AN ULTRALIGHT UAV COMPOSITE WING AND FUSELAGE," Mississippi State University, Starkville, 2009.

[22] "80/20," 80/20, [Online]. Available: https://8020.net/. [Accessed 21 March 2022].

[23] "GlobalSecurity," GlobalSecurity, [Online]. Available: https://www.globalsecurity.org/intell/systems/uav-classes.htm. [Accessed 21 March 2022].

[24] Schrenk, "Technical Memorandum 948 - A Simple Approximation Method for Obtaining the Spanwise Lift Distribution," *NACA*, 1940.

[25] J. John D. Anderson, Fundamentals of AERODYNAMICS, FIFTH EDITION, New York: McGraw-Hill, 2007.

[26] R. G. Budynas and K. J. Nisbett, Shigley's Mechanical Engineering Design, Tenth Edition, New York: McGraw-Hill, 2015.

[27] E. ToolBox, "Euler's Column Formula," 2012. [Online]. Available: https://www.engineeringtoolbox.com/euler-column-formula-d_1813.html. [Accessed 21 March 2022].

[28] M. C. Niu, in *Composite Airframe Structures*, Conmilit Press Ltd. , 1992, pp. 494-496.

[29] L. William A, C. D. Olney, T. Chen, N. D. Crawford, R. Stauf and E. Y. Reichenbach, "STRAIN-GAUGE LOADS CALIBRATION TESTING OF THE ACTIVE AEROELASTIC WING F/A-18 AIRPLANE," NASA, 2002.

[30] R. Team, "Riding ATV," Riding ATV, 20 January 2021. [Online]. Available: https://ridingatv.com/how-many-amps-does-a-winch-draw/. [Accessed 21 March 2022].

[31] S. J. Kline, "The Purposes of Uncertainty Analysis," *Journal of Fluids Engineering*, vol. 107, no. 2, pp. 153-160, 1985.

[32] "Unmanned Systems Technology," EchoBlue Ltd., [Online]. Available: https://www.unmannedsystemstechnology.com/company/uav-factory/. [Accessed 21 March 2022].

APPENDICIES

Lift Distribution Calculations

$$\Gamma_0 = \frac{2V_\infty SC_L}{b\pi} \qquad L = \rho_\infty V_\infty \Gamma_0 \int_{-b/2}^{b/2} \left(1 - \frac{4y^2}{b^2}\right)^{1/2} dy$$

$r := 1.268$

$Cl := 1.268$

$\rho := .002378 \frac{slug}{ft^3}$ .002378

$V_0 := 200 \frac{ft}{s}$ $b := 55.5in = 4.625 \cdot ft$ $c := 7.5in$ $Span := b \cdot c = 2.891 \cdot ft^2$

$y := 0, 0 + .1ft .. \frac{b}{2}$ $Cl \cdot .5 \cdot \rho \cdot V_0^2 \cdot Span = 174.322 \cdot lbf$

$\Gamma_0 := \frac{2 \cdot V_0 \cdot Span \cdot Cl}{b \cdot \pi}$

$\Gamma(y) := \Gamma_0 \left[1 - \left(2\frac{y}{b}\right)^2\right]^{\frac{1}{2}}$

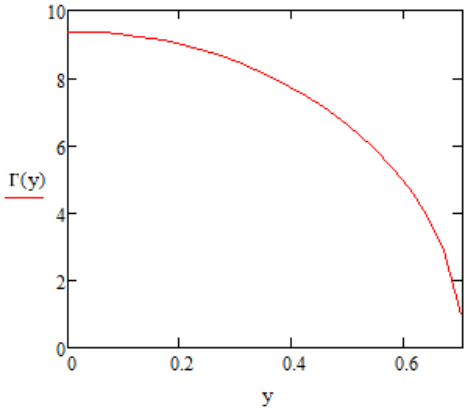

$lift_{prime}(y) := \rho \cdot V_0 \cdot \Gamma(y)$

$lift_{prime}(0) = 47.99 \cdot \frac{lbf}{ft}$

$lift_{prime}(25.6in) = 270.3 \frac{kg}{s^2}$

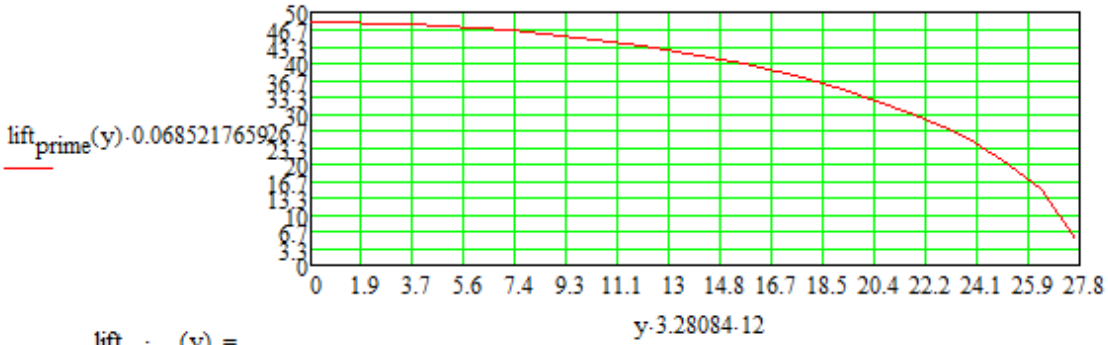

$lift_{prime}(y) =$

3.999	$\frac{lbf}{in}$
3.995	
3.984	
3.965	
3.939	
3.905	
3.862	
3.812	
3.752	
3.684	
3.606	
3.518	
3.419	
3.307	
3.183	
...	

$$Shear(y) := \int_0^y -lift_{prime}(y)\,dy + 87.2lbf$$

$Shear(0) = 87.2 \cdot lbf$

$Shear\left(\frac{b}{2}\right) = 0 \cdot lbf$ $\qquad \frac{b}{2} = 2.313 \cdot ft$

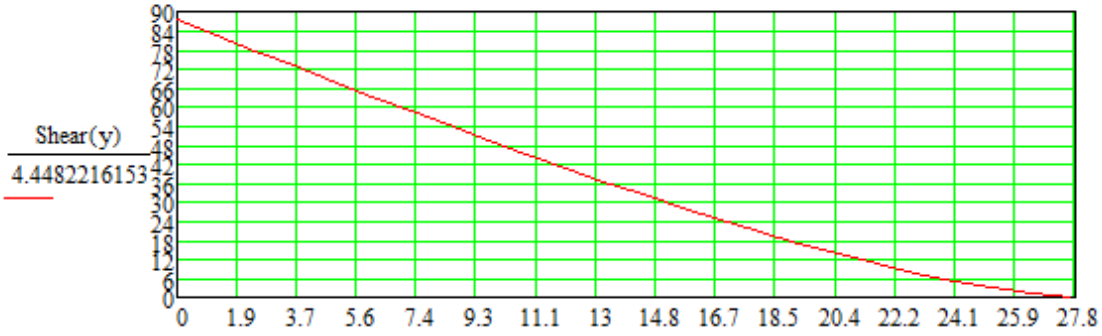

$Shear(y) =$ $\qquad y \cdot 3.28084 \cdot 12$ $\qquad y =$

87.2	·lbf	0 ·in
82.402		1.2
77.614		2.4
72.843		3.6
68.1		4.8
63.393		6
58.732		7.2
54.127		8.4
49.588		9.6
45.126		10.8
40.751		12
36.475		13.2
32.312		14.4
28.276		15.6
24.38		16.8
20.642		18
17.082		19.2
13.721		20.4
10.585		21.6
7.707		22.8
5.13		24
...		...

$$\text{Moment}(y) := -\left[\left(\int_0^y \text{Shear}(y)\,dy\right) - 85.635\,\text{lbf}\cdot\text{ft}\right]$$

$$\text{Moment}(0) = 1027.62\cdot\text{lbf}\cdot\text{in}$$

$$\text{Moment}\left(\frac{b}{2}\right) = 3.464\times 10^{-4}\cdot\text{lbf}\cdot\text{ft}$$

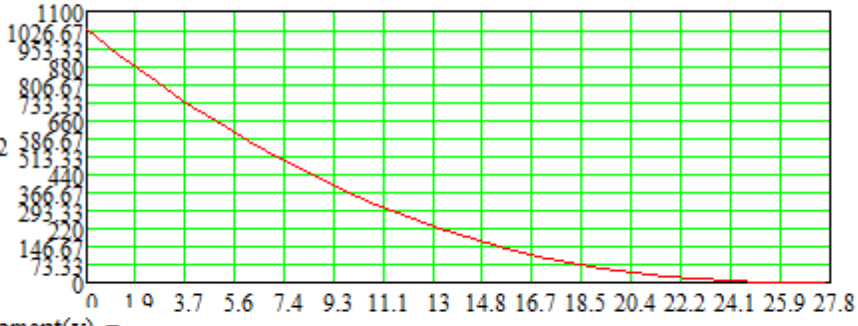

Moment(y)·0.73756·12

y =

0	·in
1.2	
2.4	
3.6	
4.8	
6	
7.2	
8.4	
9.6	
10.8	
12	
13.2	
14.4	
15.6	
16.8	
18	
19.2	
20.4	
21.6	
22.8	
24	
25.2	
26.4	
27.6	

Moment(y) =

1028	·lbf·in
926	
830	
740	
655	
576	
503	
435	
373	
316	
265	
218	
177	
141	
109	
82	
59	
41	
26	
16	
8	
...	

$$\text{Moment}(3\text{in}) = 783.999\cdot\text{lbf}\cdot\text{in}$$

Uncertainty Analysis

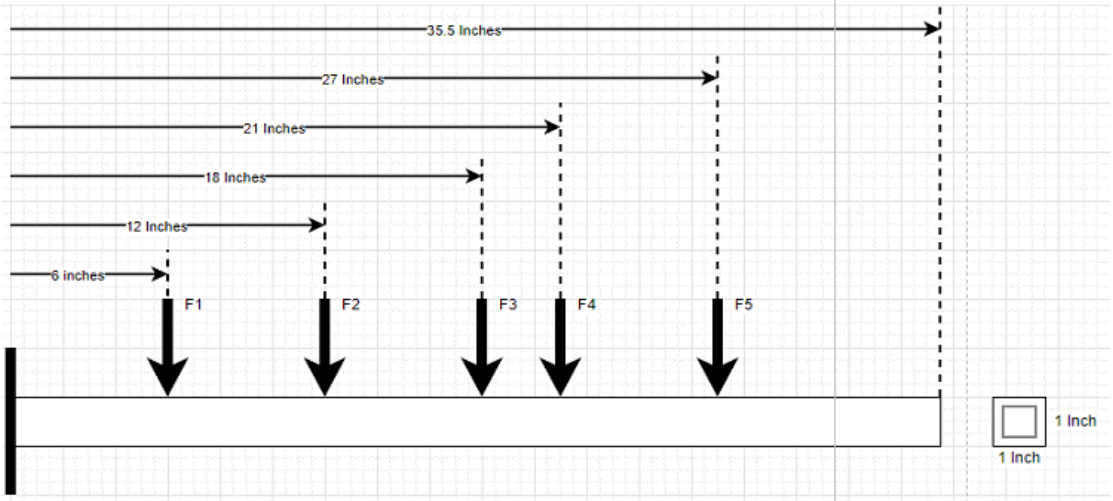

$$y_{max}(d1, d2, d3, d4, d5, d_{Self\_W}) := d1 + d2 + d3 + d4 + d5 + d_{Self\_W}$$ y has uncertainties in each term

$$y1(F1, a1, E, I_b, l_b) := \frac{F1 \cdot a1^2 \cdot (a1 - 3l_b)}{6 \cdot E \cdot I_b} \qquad y2(F1, a2, E, I_b, l_b) := \frac{F1 \cdot a2^2 \cdot (a2 - 3l_b)}{6 \cdot E \cdot I_b}$$

$$y4(F2, a4, E, I_b, l_b) := \frac{F2 \cdot a4^2 \cdot (a4 - 3l_b)}{6 \cdot E \cdot I_b} \qquad y5(F2, a5, E, I_b, l_b) := \frac{F2 \cdot a5^2 \cdot (a5 - 3l_b)}{6 \cdot E \cdot I_b}$$

F, a, I, lb, and w.self_w each have uncertainties

$$y3(F1, a3, E, I_b, l_b) := \frac{F1 \cdot a3^2 \cdot (a3 - 3l_b)}{6 \cdot E \cdot I_b} \qquad y_{Self\_W}(w_{Self\_Wb}, l_b, E, I_b) := \frac{-w_{Self\_Wb} \cdot l_b^4}{8 \cdot E \cdot I_b}$$

$$I(b, h, t) := \left(\frac{b \cdot h^3}{12}\right) - \left[\frac{[b - (2 \cdot t)][h - (2 \cdot t)]^3}{12}\right]$$ b, h, and t each have uncertainties

$$I_b := I(b, h, t) = 0.034 \cdot in^4$$

$$Self\_W(b, h, t, l_b) := \rho_{Al} \cdot \left[(b \cdot h \cdot l_b) - (b - 2 \cdot t)(h - 2 \cdot t)(l_b)\right]$$

$$Self\_W_b := Self\_W(b, h, t, l_b)$$

$$w_{Self\_W}(l_b, Self\_W_b) := \frac{Self\_W_b}{l_b}$$

$$w_{Self\_Wb} := w_{Self\_W}(l_b, Self\_W_b)$$

$$d1 := y1(F1, a1, E, I_b, l_b) = -0.022 \cdot in$$

$$d2 := y2(F1, a2, E, I_b, l_b) = -0.082 \cdot in$$

$$d3 := y3(F1, a3, E, I_b, l_b) = -0.173 \cdot in$$

$$d4 := y4(F2, a4, E, I_b, l_b) = -0.1139 \cdot in$$

$$d5 := y5(F2, a5, E, I_b, l_b) = -0.17506 \cdot in$$

$$d_{Self\_W} := y_{Self\_W}(w_{Self\_Wb}, l_b, E, I_b) = -0.0135\,in$$

$$Total_{Deflection} := d1 + d2 + d3 + d4 + d5 + d_{Self\_W} = -0.58\,in$$

$$U_I := \sqrt{\left[\frac{d}{db}[(I(b,h,t)) \cdot U_b]\right]^2 + \left[\frac{d}{dh}[(I(b,h,t)) \cdot U_h]\right]^2 + \left[\frac{d}{dt}[(I(b,h,t)) \cdot U_t]\right]^2} \qquad U_I = 0.003 \cdot in^4$$

$$U_{Self\_Wb} := \sqrt{\left[\frac{d}{db}[(Self\_W(b,h,t,l_b)) \cdot U_b]\right]^2 + \left[\frac{d}{dh}[(Self\_W(b,h,t,l_b)) \cdot U_h]\right]^2 + \left[\frac{d}{dt}[(Self\_W(b,h,t,l_b)) \cdot U_t]\right]^2 + \left[\frac{d}{dl_b}[(Self\_W(b,h,t,l_b)) \cdot U_{lb}]\right]^2} \qquad U_{Self\_Wb} = 0.087\,lbf$$

$$U_{wSelf\_Wb} := \sqrt{\left[\frac{d}{dl_b}[(w_{Self\_W}(l_b, Self\_W_b)) \cdot U_{lb}]\right]^2 + \left[\frac{d}{dSelf\_W_b}[(w_{Self\_W}(l_b, Self\_W_b)) \cdot U_{Self\_Wb}]\right]^2} \qquad U_{wSelf\_Wb} = 0.949 \frac{lb}{s^2}$$

$$U_{y1} := \sqrt{\left[\frac{d}{dF1}[(y1(F1,a1,E,I_b,l_b)) \cdot U_{F1}]\right]^2 + \left[\frac{d}{da1}[(y1(F1,a1,E,I_b,l_b)) \cdot U_{a1}]\right]^2 + \left[\frac{d}{dI_b}[(y1(F1,a1,E,I_b,l_b)) \cdot U_I]\right]^2 + \left[\frac{d}{dl_b}[(y1(F1,a1,E,I_b,l_b)) \cdot U_{lb}]\right]^2} \qquad U_{y1} = 0.002 \cdot in$$

$$U_{y2} := \sqrt{\left[\frac{d}{dF1}[(y2(F1,a2,E,I_b,l_b)) \cdot U_{F1}]\right]^2 + \left[\frac{d}{da2}[(y2(F1,a2,E,I_b,l_b)) \cdot U_{a2}]\right]^2 + \left[\frac{d}{dI_b}[(y2(F1,a2,E,I_b,l_b)) \cdot U_I]\right]^2 + \left[\frac{d}{dl_b}[(y2(F1,a2,E,I_b,l_b)) \cdot U_{lb}]\right]^2} \qquad U_{y2} = 0.008 \cdot in$$

$$U_{y3} := \sqrt{\left[\frac{d}{dF1}[(y3(F1,a3,E,I_b,l_b)) \cdot U_{F1}]\right]^2 + \left[\frac{d}{da3}[(y3(F1,a3,E,I_b,l_b)) \cdot U_{a3}]\right]^2 + \left[\frac{d}{dI_b}[(y3(F1,a3,E,I_b,l_b)) \cdot U_I]\right]^2 + \left[\frac{d}{dl_b}[(y3(F1,a3,E,I_b,l_b)) \cdot U_{lb}]\right]^2} \qquad U_{y3} = 0.017 \cdot in$$

$$U_{y4} := \sqrt{\left[\frac{d}{dF2}[(y4(F2,a4,E,I_b,l_b)) \cdot U_{F2}]\right]^2 + \left[\frac{d}{da4}[(y4(F2,a4,E,I_b,l_b)) \cdot U_{a4}]\right]^2 + \left[\frac{d}{dI_b}[(y4(F2,a4,E,I_b,l_b)) \cdot U_I]\right]^2 + \left[\frac{d}{dl_b}[(y4(F2,a4,E,I_b,l_b)) \cdot U_{lb}]\right]^2} \qquad U_{y4} = 0.011 \cdot in$$

$$U_{y5} := \sqrt{\left[\frac{d}{dF2}[(y5(F2,a5,E,I_b,l_b)) \cdot U_{F2}]\right]^2 + \left[\frac{d}{da5}[(y5(F2,a5,E,I_b,l_b)) \cdot U_{a5}]\right]^2 + \left[\frac{d}{dI_b}[(y5(F2,a5,E,I_b,l_b)) \cdot U_I]\right]^2 + \left[\frac{d}{dl_b}[(y5(F2,a5,E,I_b,l_b)) \cdot U_{lb}]\right]^2} \qquad U_{y5} = 0.018 \cdot in$$

$$U_{ySelf\_W} := \sqrt{\left[\frac{d}{dw_{Self\_Wb}}[(y_{Self\_W}(w_{Self\_Wb}, l_b, E, I_b)) \cdot U_{wSelf\_Wb}]\right]^2 + \left[\frac{d}{dl_b}[(y_{Self\_W}(w_{Self\_Wb}, l_b, E, I_b)) \cdot U_{lb}]\right]^2 + \left[\frac{d}{dl_b}[(y_{Self\_W}(w_{Self\_Wb}, l_b, E, I_b)) \cdot U_I]\right]^2} \qquad U_{ySelf\_W} = 0.002\,in$$

$$U_{ymax} := \sqrt{\left[\frac{d}{dd1}[(y_{max}(d1,d2,d3,d4,d5,d_{Self\_W})) \cdot U_{y1}]\right]^2 + \left[\frac{d}{dd2}[(y_{max}(d1,d2,d3,d4,d5,d_{Self\_W})) \cdot U_{y2}]\right]^2 + \left[\frac{d}{dd3}[(y_{max}(d1,d2,d3,d4,d5,d_{Self\_W})) \cdot U_{y3}]\right]^2 + \left[\frac{d}{dd4}[(y_{max}(d1,d2,d3,d4,d5,d_{Self\_W})) \cdot U_{y4}]\right]^2 + \left[\frac{d}{dd5}[(y_{max}(d1,d2,d3,d4,d5,d_{Self\_W})) \cdot U_{y5}]\right]^2 + \left[\frac{d}{dd_{Self\_W}}[(y_{max}(d1,d2,d3,d4,d5,d_{Self\_W})) \cdot U_{ySelf\_W}]\right]^2}$$

$U_{ymax} = 0.029\,in$

$Total_{Deflection} = -0.58\,in$

$Total\_Deflection\_Max := Total_{Deflection} - U_{ymax} = -0.608\,in$

$Total\_Deflection\_Min := Total_{Deflection} + U_{ymax} = -0.551\,in$

$$Percent\_Uncertainty := \frac{U_{ymax} \cdot 100}{Total_{Deflection}} = -4.925$$

$E \equiv 10000000 \frac{lbf}{in^2}$ $b \equiv 1in$ $h \equiv 1in$ $t \equiv .0625in$ $l_b \equiv 35.5in$ $\rho_{A1} \equiv .1 \frac{lbf}{in^3}$

$F_{Load\_Cell} \equiv 100lbf$ $F1 \equiv \frac{F_{Load\_Cell}}{8} = 12.5\,lbf$ $F2 \equiv \frac{F_{Load\_Cell}}{16} = 6.25\,lbf$

$a1 \equiv 6in$ $a2 \equiv 12in$ $a3 \equiv 18in$ $a4 \equiv 21in$ $a5 \equiv 27in$

$U_b \equiv .012in$ $U_h \equiv .012in$ $U_t \equiv .007in$ $U_{F1} \equiv .03 \cdot \frac{F_{Load\_Cell}}{8}$ $U_{F2} \equiv .03 \cdot \frac{F_{Load\_Cell}}{16}$

$U_{lb} \equiv \frac{1in}{64}$ $U_{a1} \equiv \frac{1in}{64}$ $U_{a2} \equiv \frac{1in}{64}$ $U_{a3} \equiv \frac{1in}{64}$ $U_{a4} \equiv \frac{1in}{64}$ $U_{a5} \equiv \frac{1in}{64}$

$$\left[\frac{d}{dF1}\left[\left(y3\left(F1, a3, E, I_b, l_b\right)\right)\cdot U_{F1}\right]\right]^2 = 2.701 \times 10^{-5}\,in^2$$

$$\left[\frac{d}{da3}\left[\left(y3\left(F1, a3, E, I_b, l_b\right)\right)\cdot U_{a3}\right]\right]^2 = 7.299 \times 10^{-8}\,in^2$$

$$\left[\frac{d}{dI_b}\left[\left(y3\left(F1, a3, E, I_b, l_b\right)\right)\cdot U_{I}\right]\right]^2 = 2.741 \times 10^{-4}\,in^2$$

$$\left[\frac{d}{dl_b}\left[\left(y3\left(F1, a3, E, I_b, l_b\right)\right)\cdot U_{lb}\right]\right]^2 = 8.418 \times 10^{-9}\,in^2$$

$$\left[\frac{d}{dd1}\left[\left(y_{max}\left(d1, d2, d3, d4, d5, d_{Self\_W}\right)\right)\cdot U_{y1}\right]\right]^2 = 4.806 \times 10^{-6}\,in^2$$

$$\left[\frac{d}{dd2}\left[\left(y_{max}\left(d1, d2, d3, d4, d5, d_{Self\_W}\right)\right)\cdot U_{y2}\right]\right]^2 = 6.786 \times 10^{-5}\,in^2$$

$$\left[\frac{d}{dd3}\left[\left(y_{max}\left(d1, d2, d3, d4, d5, d_{Self\_W}\right)\right)\cdot U_{y3}\right]\right]^2 = 3.012 \times 10^{-4}\,in^2$$

$$\left[\frac{d}{dd4}\left[\left(y_{max}\left(d1, d2, d3, d4, d5, d_{Self\_W}\right)\right)\cdot U_{y4}\right]\right]^2 = 1.302 \times 10^{-4}\,in^2$$

$$\left[\frac{d}{dd5}\left[\left(y_{max}\left(d1, d2, d3, d4, d5, d_{Self\_W}\right)\right)\cdot U_{y5}\right]\right]^2 = 3.076 \times 10^{-4}\,in^2$$

$$\left[\frac{d}{dd_{Self\_W}}\left[\left(y_{max}\left(d1, d2, d3, d4, d5, d_{Self\_W}\right)\right)\cdot U_{ySelf\_W}\right]\right]^2 = 3.668 \times 10^{-6}\,in^2$$

$$F_1(F_0, d_1, d_2) := \frac{F_0 \cdot d_1}{d_1 + d_2}$$

$$d_1 := 3\text{in} \qquad d_2 := 3\text{in}$$

$$F_0 \equiv 100\text{lbf} \qquad U_{d1} := \frac{1\text{in}}{8} \qquad U_{d2} := \frac{1\text{in}}{8}$$

$$U_{F1} := \sqrt{\left[\frac{d}{dF_0}\left[\left(F_1(F_0, d_1, d_2)\right)U_{F1}\right]\right]^2 + \left[\frac{d}{dd_1}\left[\left(F_1(F_0, d_1, d_2)\right)U_{d1}\right]\right]^2 + \left[\frac{d}{dd_2}\left[\left(F_1(F_0, d_1, d_2)\right)U_{d2}\right]\right]^2} = 1.485\,\text{lbf}$$

$$\frac{U_{F1} \cdot 100}{F_1(F_0, d_1, d_2)} = 2.97$$

$$\left[\frac{d}{dF_0}\left[\left(F_1(F_0, d_1, d_2)\right)U_{F1}\right]\right]^2 = 0.551\,\text{lbf}^2$$

$$\left[\frac{d}{dd_1}\left[\left(F_1(F_0, d_1, d_2)\right)U_{d1}\right]\right]^2 = 1.085\,\text{lbf}^2$$

$$\left[\frac{d}{dd_2}\left[\left(F_1(F_0, d_1, d_2)\right)U_{d2}\right]\right]^2 = 1.085\,\text{lbf}^2$$

Root Distance(in	Lprime(y) (lb/in)	Shear(lbs	Moment(lb*in)
0	4.00	93	1160
1.2	4.00	88	1052
2.4	3.99	83	949
3.6	3.97	78	852
4.8	3.95	74	761
6	3.92	69	676
7.2	3.88	64	596
8.4	3.83	60	522
9.6	3.78	55	453
10.8	3.72	50	390
12	3.65	46	332
13.2	3.58	42	279
14.4	3.49	37	232
15.6	3.39	33	190
16.8	3.29	29	152
18	3.17	25	119
19.2	3.04	22	91
20.4	2.89	18	67
21.6	2.72	15	47
22.8	2.54	12	31
24	2.33	9	19
25.2	2.08	6	10
26.4	1.79	4	5
27.6	1.41	2	1
28.8	0.87	0.4	0
29.5	0.00	0	0

	Load(lbs)		Moment(lb*in)	
Root Distance(in)	1	2	1	2
0	93	93	1395	697.5
0	93	46.5		
6	93	46.5	558	279
6	69.75	34.88		
12	69.75	34.88	418.5	209.25
12	46.5	23.25		
18	46.5	23.25	279	139.5
18	23.25	11.63		
21	23.25	11.63	69.75	34.875
21	11.625	5.813		
27	11.625	5.813	69.75	34.875

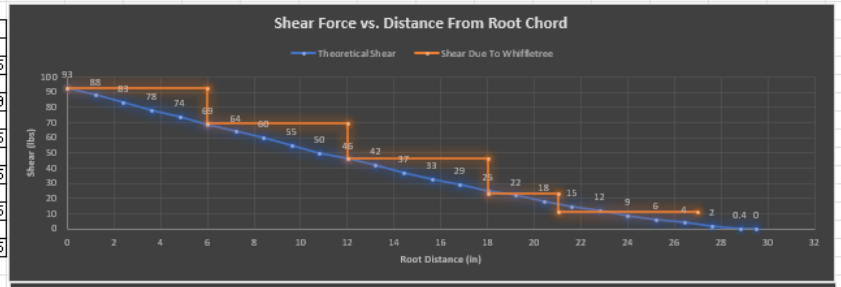

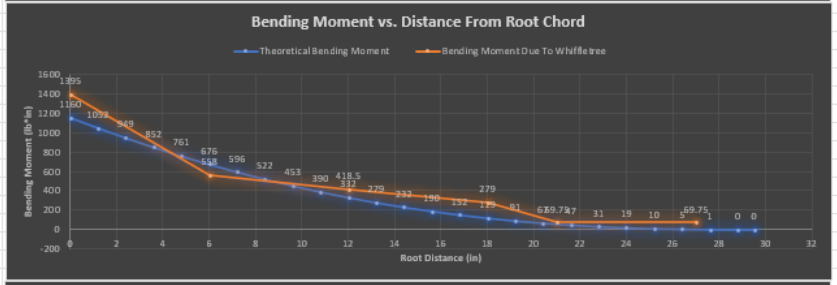

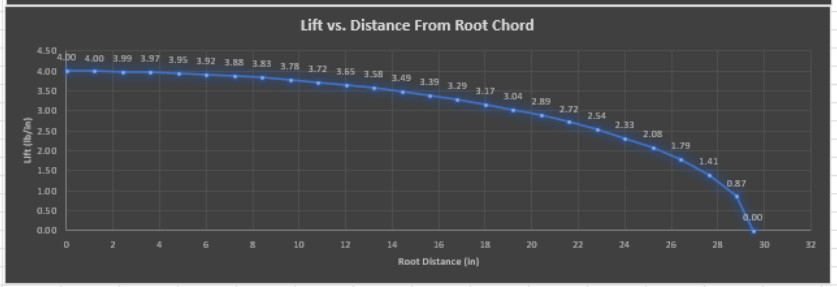

	103.25				
	GTOW OBSIDIAN	15			
	Wingspan(in)	53		0	15
				26.5	15
				26.5	0
	Vmax(lbs)	15			
	Mmax(lb*in)	-198.75			
	0	-198.75			
	26.5	0			

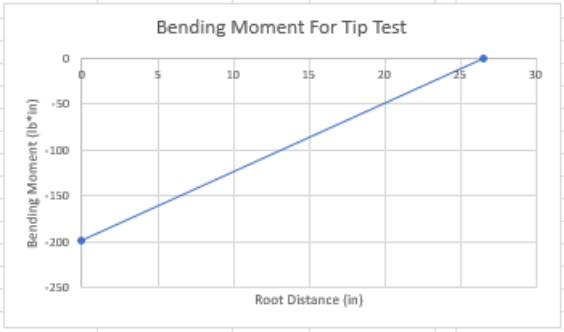

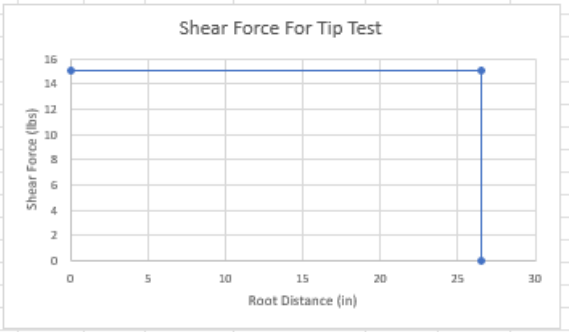

Root Distance(in	Lprime(y) (lb/in)	Shear(lbs	Moment(lb*in)
0	4.00	87.2	1028
1.2	4.00	82.402	926
2.4	3.98	77.614	830
3.6	3.97	72.843	740
4.8	3.94	68.1	655
6	3.91	63.393	576
7.2	3.86	58.732	503
8.4	3.81	54.127	435
9.6	3.75	49.588	373
10.8	3.68	45.126	316
12	3.61	40.751	265
13.2	3.52	36.475	218
14.4	3.42	32.312	177
15.6	3.31	28.276	141
16.8	3.18	24.38	109
18	3.04	20.642	82
19.2	2.89	17.082	59
20.4	2.71	13.721	41
21.6	2.51	10.585	26
22.8	2.28	7.707	16
24	2.01	5.13	8
25.2	1.68	2.913	3
26.4	1.23	1.153	1
27.6	0.42	0.08	0

	Load(lbs)		Moment(lb*in)	
Root Distance(in)	1	2	1	2
0	87.2	93	1220.8	651
0	87.2	46.5		
5	87.2	46.5	523.2	279
5	65.4	34.88		
11	65.4	34.88	392.4	209.25
11	43.6	23.25		
17	43.6	23.25	261.6	139.5
17	21.8	11.63		
20	21.8	11.63	65.4	34.875
20	10.9	5.813		
26	10.9	5.813	65.4	34.875

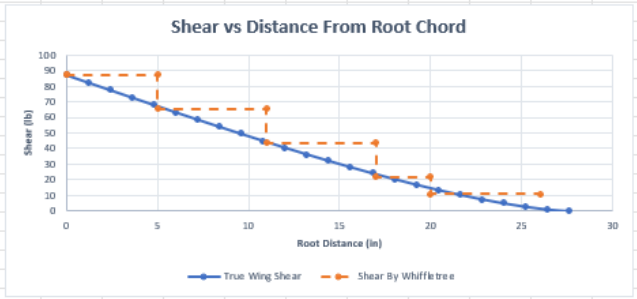

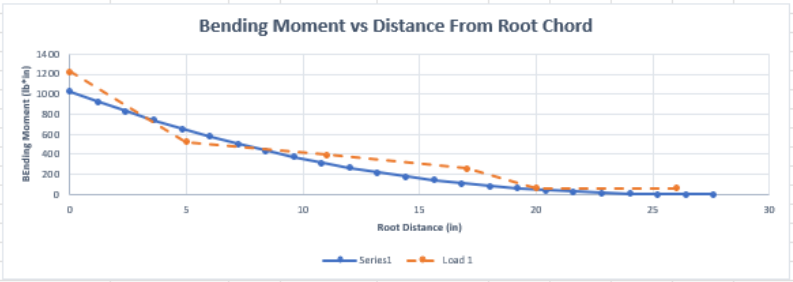

E(psi)	10200000
I (in^4)	0.042587

II 25-2550	
I (in^4)	0.292421

Tier	Length	Force	Deflection(in)	Max Moment (lb*in)
4	61	550	5.99	8388
3	23.5	275	0.17	1616
2	11	137.5	0.01	378
1	11	68.75	0.00	189

Deflection(in)	Max Moment (lb*in)
0.9	8388

Allowable Load Before Buckling	
n	4
L(in)	60
F	4763.59088
Over 4 legs	1190.89772

$F = n\,\pi^2\,E\,I\,/\,L^2$ (1)

where

F = allowable load (lb, N)

n = factor accounting for the end conditions

E = modulus of elastisity (lb/in^2, $Pa\ (N/m^2)$)

L = length of column (in, m)

I = Moment of inertia (in^4, m^4)

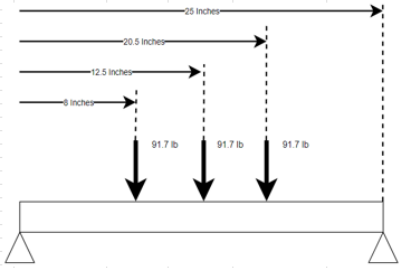

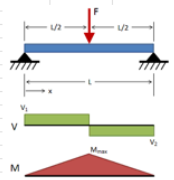

Deflection:

$$\delta = -\frac{Fx}{48EI}\left(3L^2 - 4x^2\right) \quad (0 \le x \le L/2)$$

$$\delta_{max} = \frac{FL^3}{48EI} \quad @\,x = L/2$$

Slope:

$$\theta = -\frac{F}{16EI}\left(L^2 - 4x^2\right) \quad (0 \le x \le L/2)$$

$$\theta_1 = -\frac{FL^2}{16EI} \quad @\,x = 0$$

$$\theta_2 = +\frac{FL^3}{16EI} \quad @\,x = L$$

Shear:

$$V_1 = +F/2 \quad (0 \le x \le L/2)$$

$$V_2 = -F/2 \quad (L/2 \le x \le L)$$

Moment:

$$M_{max} = FL/4 \quad @\,x = L/2$$

Mmax(lb*in)	2981
Mmax(lb*in)	10235
Mmax(lb*in)	31352

0.8958

E(psi)	10200000
I (in^4)	0.292421
Length (in)	25
Force (lbs)	91.66666667
	Deflection (in)
x1 & x3 (in)	8
x2 (in)	12.5
	0.02516244

E(psi)	10200000	Vertical Distance From Winch and	10.85
I (in^4)	0.042587		
Length (in)	25		
Force (lbs)	91.66666667		
		Deflection (in)	
x1 & x3 (in)	9.065	-0.013995493	
x2 (in)	0	0	
		-0.027990987	
max moment	830.9583333	% of Vertical Dista	0.3%

Tier	Length (in	Force (lbs	Deflection(in	Max Moment (lb*in)
4	61	550	5.99	8388
3	23.5	275	0.17	1616
2	11	137.5	0.01	378
1	11	68.75	0.00	189

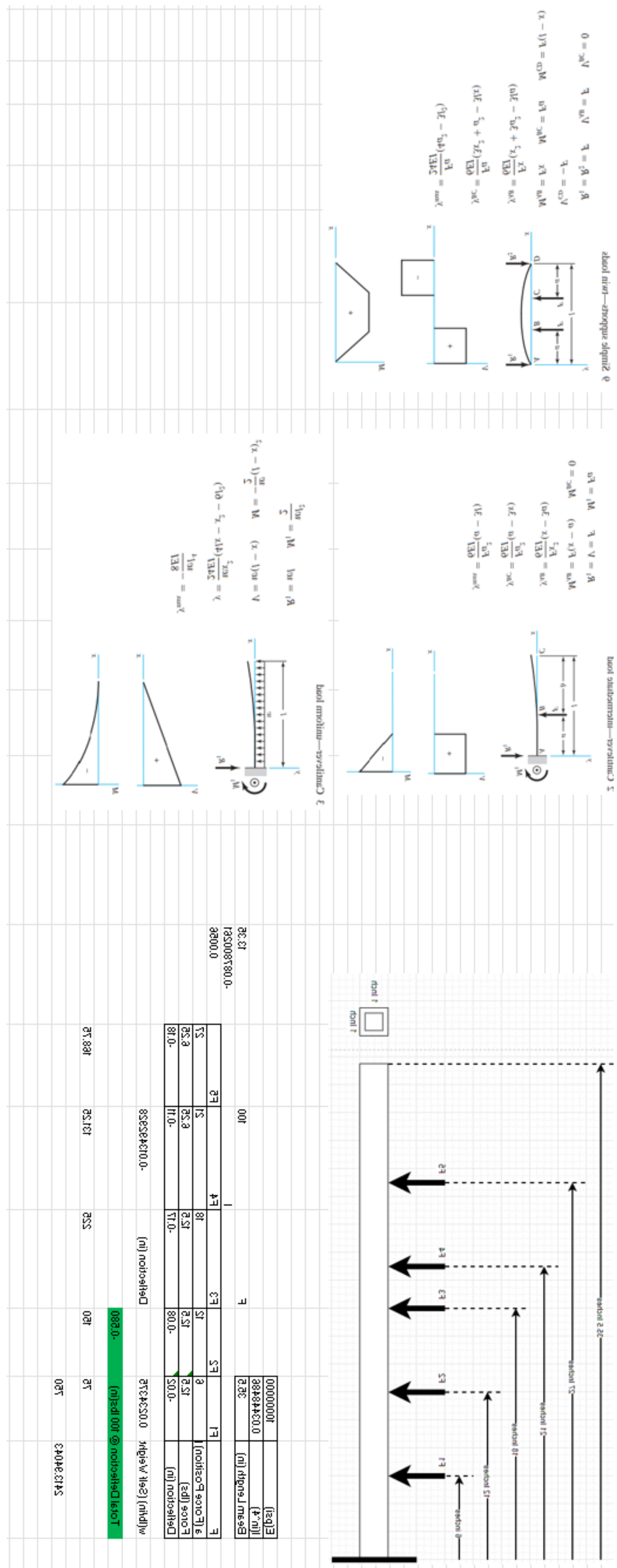

Force	104	153	201.5	255
L1	12.45	18.14	23.84	30.04
L2	13.35	19.85	26.6	34.12
L3	12.95	19.53	26.3	34
L4	12.79	18.49	24.08	30.24
Theoretical	13	19.125	25.1875	31.875

Values taken by using statics and assumes distance from top eyebolts is 6 inches. The values below are what the distance the bottom needs

F2	2.87	2.85	2.84	2.83
F3	3.08	3.11	3.17	3.21
F2	2.99	3.06	3.13	3.20
F3	2.95	2.90	2.87	2.85

Force	104	153	201.5	255
Theoretical Def	-0.108	-0.159	-0.210	-0.265
Exp Def L1 & L2	-0.105	-0.154	-0.203	-0.257
Exp Def L3 & L4	-0.107	-0.156	-0.204	-0.258

Difference From Theoretical				
Exp Def L1 & L2	-0.003	-0.005	-0.006	-0.008
Exp Def L3 & L4	-0.001	-0.003	-0.005	-0.007

Difference	104	153	201.5	255
L1 and L2	0.9	1.71	2.76	4.08
L3 and L4	0.16	1.04	2.22	3.76

Sum on Each Memb	104	153	201.5	255
L1 and L2	25.8	37.99	50.44	64.16
L3 and L4	25.74	38.02	50.38	64.24
Theoretical	26	38.25	50.375	63.75

% Difference of Sum	104	153	201.5	255
L1 and L2	-1%	-1%	0%	1%
L3 and L4	-1%	-1%	0%	1%

Percent Error	104	153	201.5	255	Average Error
L1	4%	5%	5%	6%	5%
L2	3%	4%	6%	7%	5%
L3	0%	2%	4%	7%	3%
L4	2%	3%	4%	5%	4%
Average	2%	4%	5%	6%	4%

Theoretical	3	% Error
Experimental	2.85	5%
Average	3.14	-5%
	3.10	-3%
	2.89	4%

Uncertainty	Uncertainty Upper	Uncertainty Lower
0.008	-0.100	-0.116
0.012	-0.147	-0.171
0.016	-0.194	-0.226
0.020	-0.245	-0.285

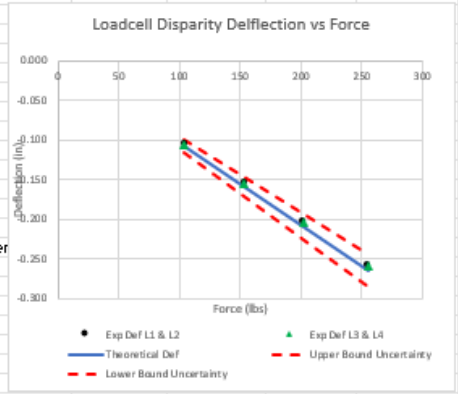

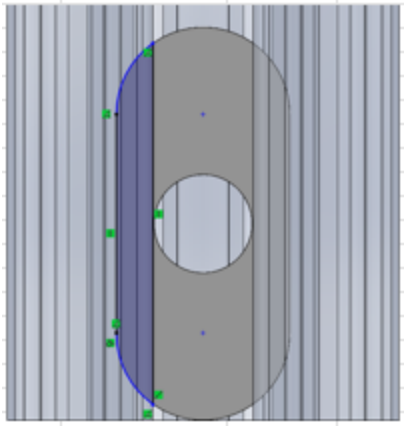

Area(in^2)		0.160	
YS(psi)		35000	
Force(lbs)		Stress(lbs/in^2)	FS
0		0	
200		1250	28.0
400		2500	14.0
550		3438	10.2
600		3750	9.3
800		5000	7.0
1000		6250	5.6
1200		7500	4.7
1400		8750	4.0
1600		10000	3.5
1800		11250	3.1
2000		12500	2.8
2200		13750	2.5
2400		15000	2.3
2600		16250	2.2
2800		17500	2.0
3000		18750	1.9
3200		20000	1.8
5600		35000	1.0

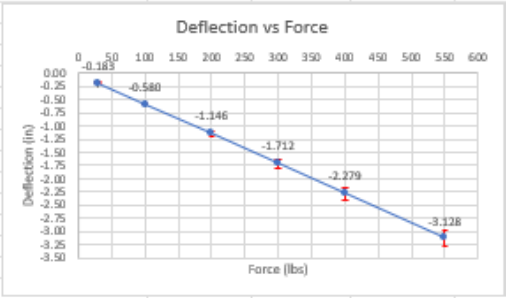

Force (lbs)	Deflection(in)	Uncertainty	Max. Def Valu	Min. Def Value	Percent ofDef
30	-0.183	0.009	-0.174	-0.192	4.9%
100	-0.580	0.029	-0.551	-0.609	5.0%
200	-1.146	0.057	-1.089	-1.203	5.0%
300	-1.712	0.085	-1.627	-1.797	5.0%
400	-2.279	0.114	-2.165	-2.393	5.0%
550	-3.128	0.157	-2.971	-3.285	5.0%

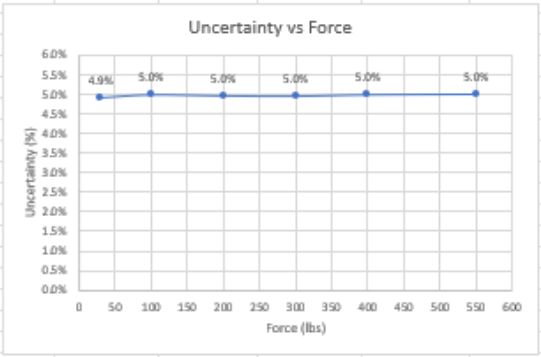

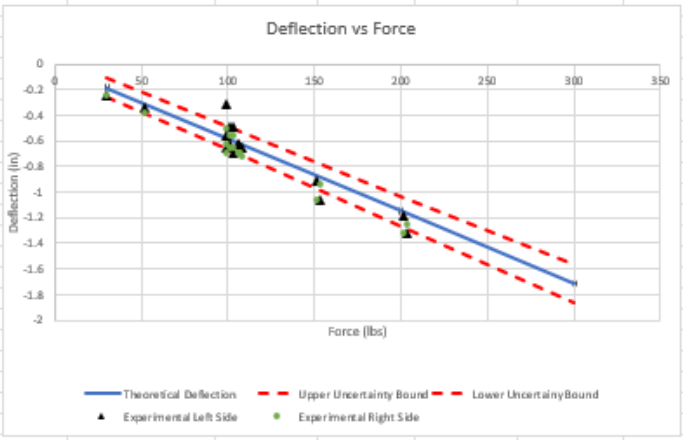

Force (lbs)	Deflection(in)	Uncertainty	Max. Def Valu	Min. Def Value	Percent ofDef
30	-0.183	0.009	-0.174	-0.192	4.9%
100	-0.580	0.029	-0.551	-0.609	5.0%
200	-1.146	0.057	-1.089	-1.203	5.0%
300	-1.712	0.085	-1.627	-1.797	5.0%
400	-2.279	0.114	-2.165	-2.393	5.0%
550	-3.128	0.157	-2.971	-3.285	5.0%

Upper Uncertainty	Lower Uncertainty
-0.1115	-0.2545
-0.488246804	-0.671246804
-1.02650068	-1.26550068
-1.564754556	-1.859754556
-2.102008432	-2.455008432
-2.908389247	-3.347389247

	Theoretical	Experimental	% Error
Root Shear (lbs)	97	119.5	23%
Root Bending Moment(lb*in)	1256	1673	33%

				Left (Facing the Apparatus)			Right (Facing the Apparatus)		
Date	Test	Force	Notes	Initial	Final	Difference	Initial	Final	Difference
1/4/2022	1	99.6	First Beam, heavily twisted. One side deflected much than the other and could be due to the more twist on the one side. Don't think load is accurate due to the sythentic rope not keeping tension. Before adding	59.78125	59.46875	-0.3125	60.09375	59.59375	-0.5
1/20/2022	2	101.6	First Beam, seems less twisted than before? Before Spring addition. Tension is better than before but still not good enough and still large	60	59.5	-0.5	60.1875	59.625	-0.5625
1/23/2022	3	103.6	First Beam, seems less twisted than before? Spring added also swapped the beam ends	60.15625	59.46875	-0.6875	60.34375	59.78125	-0.5625
1/25/2022	4	98.9	First Beam, Noticeably yielded and not sure when	60	59.34375	-0.65625	60.46875	59.78125	-0.6875
2/5/2022	5	98.9	Second Beam	13.4375	12.875	-0.5625	59.875	59.25	-0.625
2/8/2022	6	103.4	Second Beam, Picture is at a noticeable angle on Left so not good. Paralax	12.71875	13.21375	-0.495	59.78125	59.125	-0.65625
2/9/2022	7	105.9	Second Beam	12.5625	13.1875	-0.625	59.9375	59.25	-0.6875
2/11/2022	8	100.9	Second Beam	12.6875	13.3125	-0.625	59.90625	59.25	-0.65625
2/11/2022	9	105.9	Second Beam	12.6875	13.3125	-0.625	59.90625	59.21875	-0.6875
2/12/2022	10	108.4	Second Beam	12.59375	13.25	-0.65625	59.90625	59.1875	-0.71875
3/6/2022	11	29.9	Second Beam, Beam seemed more twisted than before. More Twisted on left side	12.5	12.75	-0.25	59.875	59.625	-0.25
3/6/2022	12	52.4	Second Beam	12.5	12.84375	-0.34375	59.875	59.5	-0.375
3/6/2022	13	107.4	Second Beam	12.5	13.15625	-0.65625	59.875	59.1875	-0.6875
3/6/2022	14	151.4	Second Beam	12.5	13.40625	-0.90625	59.875	58.8125	-1.0625
3/6/2022	15	201.9	Second Beam	12.5	13.6875	-1.1875	59.875	58.5625	-1.3125
3/6/2022	16	153.4	Second Beam, the beam swapped side vs the last test to show theres not a bias to the right side. Not sure why one side is weaker	12.4375	13.5	-1.0625	59.875	58.9375	-0.9375
3/6/2022	17	203.9	Second Beam, the beam swapped side vs the last test to show theres not a bias to the right side. Not sure why one side is weaker	12.4375	13.75	-1.3125	59.875	58.625	-1.25

VITA

Randy Phuc Ho

Candidate for the Degree of

Master of Science

Thesis: DEVELOPMENT OF AN EXPERIMENTAL APPARATUS WITH THE CAPABILITY TO TEST SEMI-MONOCOQUE UAS WINGS

Major Field: Mechanical and Aerospace Engineering

Biographical:

Education:

Completed the requirements for the Master of Science in Mechanical and Aerospace Engineering at Oklahoma State University, Stillwater, Oklahoma in May, 2022.

Completed the requirements for the Bachelor of Science in Aerospace Engineering at Oklahoma State University, Stillwater, Oklahoma in 2020.

Completed the requirements for the Bachelor of Science in Mechanical Engineering at Oklahoma State University, Stillwater, Oklahoma in 2020.

Professional Memberships:

AIAA